α-ketoglutaric acid stimulates muscle hypertrophy and fat loss through OXGR1-dependent adrenal activation

Yexian Yuan[1, 8], Pingwen Xu[3, 8], Qingyan Jiang[1, 2, 8], Xingcai Cai[1], Tao Wang[1], Wentong Peng[1], Jiajie Sun[1], Canjun Zhu[1], Cha Zhang[1], Dong Yue[1], Zhihui He[1], Jinping Yang[1], Yuxian Zeng[1], Man Du[1], Fenglin Zhang[1], Lucas Ibrahimi[3], Sarah Schaul[3], Yuwei Jiang[4], Jiqiu Wang[5], Jia Sun[6], Qiaoping Wang[7], Songbo Wang[1], Lina Wang[1], Xiaotong Zhu[1], Ping Gao[1], Qianyun Xi[1], Cong Yin[1], Fan Li[1], Guli Xu[1], Yongliang Zhang[1], Gang Shu[1, 2, *,†]

[1]Guangdong Province Key Laboratory of Animal Nutritional Regulation, College of Animal Science, South China Agricultural University, 483 Wushan Road, Tianhe District, Guangzhou, Guangdong 510642, China

[2]National Engineering Research Center for Breeding Swine Industry, College of Animal Science, South China Agricultural University, 483 Wushan Road, Tianhe District, Guangzhou, Guangdong 510642, China

[3]Division of Endocrinology, Department of Medicine, The University of Illinois at Chicago, Chicago, Illinois, 60612, USA

[4]Department of Physiology and Biophysics, The University of Illinois at Chicago, Chicago, Illinois, 60612, USA

[5]Ruijin Hospital, Shanghai Jiao Tong University School of Medicine, 200240, China

[6]Zhujiang Hospital, Southern Medical University, 510280, China

[7]School of Pharmaceutical Sciences (Shenzhen), Sun Yat-Sen University Guangzhou, 510275, China

[8]Co-first author

†Lead contact

*Correspondence should be addressed to:

Gang Shu (Lead contact)

483 Wushan Road, Tianhe District, Guangzhou, Guangdong 510642, China

E-mail: **shugang@scau.edu.cn**

Telephone: +86-20-85284901

Fax: +86-20-85284901

Running title: α-ketoglutaric acid stimulates lipolysis through OXGR1

Conflict of interest statement

The authors have declared that no conflict of interest exists.

Summary: Beneficial effects of resistance exercise on metabolic health and particularly muscle hypertrophy and fat loss are well established, but the underlying chemical and physiological mechanisms are not fully understood. Here we identified a myometabolite-mediated metabolic pathway that is essential for the beneficial metabolic effects of resistance exercise *in vivo*. We showed that substantial accumulation of the tricarboxylic acid cycle intermediate α-ketoglutaric acid (AKG) is a metabolic signature of resistance exercise performance. Interestingly, human plasma AKG level is also negatively correlated with BMI. Pharmacological elevation of circulating AKG induces muscle hypertrophy, brown adipose tissue (BAT) thermogenesis, and white adipose tissue (WAT) lipolysis *in vivo*. We further found that AKG stimulates the adrenal release of adrenaline through 2-oxoglutarate receptor 1 (OXGR1) expressed in adrenal glands. Finally, by using both loss-of-function and gain-of-function mouse models, we showed that OXGR1 is essential for AKG-mediated exercise-induced beneficial metabolic effects. These findings reveal an unappreciated mechanism for the salutary effects of resistance exercise, using AKG as a systemically-derived molecule for adrenal stimulation of muscle hypertrophy and fat loss.

Keywords: AKG/lipolysis /obesity/OXGR1/thermogenesis.

Introduction

Obesity is recognized as a global epidemic, and there is an urgent need to control obesity and obesity-related metabolic diseases (Gungor, 2014). Among diverse promising strategies for preventing obesity, physical exercise is considered to be one of the most effective ways of controlling body weight. Numerous intervention studies have evaluated the role of exercise in the attainment and maintenance of healthy body weight, as well as additional beneficial effects on metabolic, respiratory and cardiovascular function independent of weight loss (DiPietro & Stachenfeld, 2000; Strasser, 2013). However, exercise presents variations in duration and intensity that promote different mechanical and metabolic stimuli, which result in distinct beneficial effects on cardiovascular function, whole-body metabolism, and glucose homeostasis.

Among the various classifications of exercise, endurance (aerobic) and resistance (nonaerobic) exercise are highlighted. Specifically, endurance exercise is a low-intensity and long-duration format of training, while resistance exercise is characterized by a high-intensity and short-duration (Patel et al, 2017). Endurance exercise is widely considered to increase endurance and cardiac health, while resistance exercise presents stimulatory effects on fat loss and muscle hypertrophy (Kilani, 2010). Although both endurance and resistance exercise lead to fat loss (Benito et al, 2015), resistance but not endurance exercise increases muscle mass and resting metabolic rate (Dolezal & Potteiger, 1998; Hunter et al, 2000; Poehlman et al, 2002; Poehlman et al, 1991), providing better weight loss maintenance in long-term observation. There have been numerous analyses of plasma metabolites following acute endurance exercise in both clinic and animal models (Aguer et al, 2017; Duft et al, 2017; Huffman et al, 2014; Lewis et al, 2010; Sato et al, 2019; Starnes et al, 2017), which has generated a number of metabolomics “signatures” in the circulation. These plasmas metabolic profiles

provide signatures of endurance exercise performance and cardiovascular disease susceptibility, and also identify molecular pathways that may modulate the salutary effects on cardiovascular function. However, very few metabolomics data is available for resistance exercise (Berton et al, 2017; Li et al, 2012), and the underlying chemical and physiological mechanisms for the stimulatory effects of resistance exercise on fat loss and muscle hypertrophy are not fully understood. Our goal is to identify the essential mediator for the beneficial metabolic effects of resistance exercise and provide potential therapeutic strategies to mimic the health effects of resistance exercise to combat obesity.

Emerging evidence has identified skeletal muscle as secretory organs in regulating energy homeostasis and obesity progression in other tissues (Ibrahim et al, 2017; Rai & Demontis, 2016). Exercise can induce systemic metabolic effects either via changes in the mass and metabolic demand of muscle or via the release of muscle-derived cytokines (myokines) and metabolites (myometabolites) to target different downstream tissues (Schnyder & Handschin, 2015). Many myokines secreted in response to exercise improve glucose homeostasis and protect against obesity, such as irisin (Bostrom et al, 2012), Interleukin-15 (IL-15) (Barra et al, 2014), Meteorin-like (METRNL) (Rao et al, 2014). Similarly, myometabolites can mediate exercise-induced metabolic functions. For example, β-aminoisobutyric acid (BAIBA), a novel exercise-induced muscle factor, attenuates insulin resistance, improves glucose tolerance, and promotes the browning of white adipose tissue (WAT) and hepatic β-oxidation (Jung et al, 2015; Roberts et al, 2014). In addition to their roles as metabolic substrates for gluconeogenesis, alanine and glutamine, the major amino acids released by skeletal muscle, can also act as hormone secretagogues and regulate the release of insulin, insulin-like growth factor 1, glucagon, and growth hormone (Nair & Short, 2005). Lactate, another prominent myometabolite

released during exercise, has been proposed as a systemic modulator of metabolic homeostasis and the redox state (Brosnan & Letto, 1991; Corkey & Shirihai, 2012; Finsterer, 2012; Salgueiro et al, 2014). While metabolite therapies for obesity are emerging, metabolite-induced beneficial effects on improvement of obesity continue to face a serious challenge of low long-term therapeutic efficiency. Here we aim to identify the essential exercise-induced myometabolites, which may mimic the long-term potent anti-obesity effects of regular physical exercise.

In the present study, we first applied a comparative metabolomics approach and demonstrated that substantial accumulation of a tricarboxylic acid cycle (TCA) cycle intermediate, α-ketoglutaric acid (AKG), is a serum metabolic signature of acute resistance exercise in mice. We also found human plasma AKG is negatively correlated with BMI. We then systematically characterized the metabolic effects of AKG treatment in mice fed on chow or high-fat diet (HFD). Further, we used both loss-of-function and gain-of-function mouse models to determine whether AKG receptor OXGR1, expressed by the adrenal glands, is required for the anti-obesity effects of AKG. Finally, we tested whether OXGR1 is essential for resistance exercise-induced metabolic beneficial effects. Collectively, these results support the notion that AKG is an essential mediator of resistance exercise-induced beneficial metabolic effects. Notably, these data suggest that pharmacologically targeting the AKG-OXGR1 pathway may mimic some of the benefits of resistance exercise to improve metabolic health *in vivo*.

Results

Exercise induces the enrichment of AKG

Consistent with the previous observation that physical exercise can effectively decrease fat deposition (Maillard et al, 2018), we found that both ladder-climbing (resistance) and treadmill (endurance) exercise had similar effects of inhibiting HFD-induced body weight gain (Fig. 1A). However, resistance exercise showed better beneficial metabolic effects compared with endurance exercise, as indicated by the higher lean-to-fat ratio (Fig. 1B) and lower gonadal adipose tissue (gWAT) index (Fig. 1C). To search for the essential mediators of resistance exercise-induced metabolic salutary effects, we assessed the relative changes in serum metabolites in response to resistance exercise by using mass spectrometry to measure metabolites after resistance exercise in male mice. We obtained peripheral blood samples from both unexercised control mice and mice after acute resistance exercise (40 min at the conclusion of ladder-climbing exercise with 10% of bodyweight resistance). These training parameters had been shown to significantly increase serum lactate, a commonly used biomarker for peripheral muscle fatigue, indicating a successful resistance-training program (Fig. EV1G). We found that fifty-six metabolites changed significantly at peak exercise compared to the unexercised group (Fig. 1D). Most of the decreased metabolites are amino acids, while most of the increased metabolites are fatty acids (Fig. 1D-E). Interestingly, several well-established accumulation signatures of succinate, malate, hypoxanthine, and xanthine induced by endurance exercise (Lewis et al, 2010) were found to be decreased by endurance exercise (Fig. 1D and EV1A-D).

Additionally, the observed changes in plasma metabolites immediately after cessation of exercise reflect rapid up-regulation of the TCA cycle intermediates/AKG-related metabolites (Fig. 1F).

151 Notably, AKG concentration in human plasma exhibited a statistically significant inverse relationship
152 with several metabolic risk factors (Table 1), including body mass index (BMI, R = -0.59, P<0.001,
153 Fig. 1G), hip circumference (HCF), waist circumference (WCF), fat mass, and body weight (Fig. EV1H),
154 suggesting an essential role of AKG in body weight control. We also showed that acute resistant
155 exercise induced a time-dependent rapid increase of serum AKG in both chow- or HFD-fed mice (Fig.
156 1H). Peak serum concentration was reached within 2 hrs after exercise and was 1.6 or 1.9 times higher
157 than the physiological dose in non-exercise chow mice (105.41 ± 4.78 vs. 64.11 ± 3.23 μmol/L) or
158 non-exercise HFD mice (94.93 ± 3.8 vs. 50.13 ± 3.3 μmol/L). Consistently, we found that a modest
159 but significant increase of AKG was induced by wheel-running (endurance) exercise in chow-fed
160 mice (91.327 ± 3.73 vs. 69.801 ± 2.82 μmol/L, Fig. 1I). Importantly, resistant exercise induced a
161 much higher increase of serum AKG level compared to wheel-running exercise (112.22 ± 3.16 vs.
162 91.327 ± 3.73 μmol/L, Fig. 1I), suggesting an exercise type-dependent increase of serum AKG
163 induced by exercise. Additionally, we found serum AKG level is not associated with running distance
164 in wheel-running exercise (Fig. EV1E), suggesting that exercise type instead of intensity plays a
165 major role in the stimulation on serum AKG.
166
167 We further showed that AKG levels were consistently increased in different muscles from mice doing
168 resistance exercise (Fig. 1J). This result prompted us to examine whether exercise changes the
169 activities of essential enzymes for AKG synthesis or degradation in the muscle. We tested several
170 enzymes, including glutamate dehydrogenase (GDH), which converts glutamate to AKG;
171 α-ketoglutaric acid dehydrogenase (α-KGDH), which catalyzes the conversion of AKG to
172 succinyl-CoA; isocitrate dehydrogenase (ICDHm), which catalyzes the oxidative decarboxylation of

173 isocitrate, producing AKG and CO_2 (He et al, 2015; Xiao et al, 2016). We found both wheel-running
174 and resistance exercise significantly enhanced the activities of all three enzymes in the tibialis anterior,
175 gastrocnemius and soleus (Fig. 1K-1M), suggesting that resistance exercise enhances AKG synthesis
176 and release. This point of view is further supported by our observations that *in vivo* electrical
177 stimulation of gastrocnemius muscle (hind limb) increased serum AKG (Fig. EV1F). Thus, our
178 observations indicate that exercise increases muscle AKG synthesis and blood AKG level, suggesting
179 a physiological role of AKG in exercise-induced response.
180
181 **AKG mimics exercise-induced metabolic beneficial effects**
182 If AKG plays a physiological role in exercise-induced beneficial effects, AKG supplementation will
183 mimic some of the metabolic effects of exercise. Water supplementation of AKG is well tolerated
184 (Chen et al, 2017). Moreover, we confirmed that acute oral administration resulted in increased
185 circulating AKG (Fig. 2A). On this basis, we systematically characterized the metabolic effects of 2%
186 AKG supplementation in water in both male and female C57BL/6 mice fed on regular chow. We
187 found that AKG significantly increased body weight gain in both male and female mice when fed
188 chow (Fig. EV2A and EV2G). We also found increased food intake in both male and female
189 AKG-treated mice (Fig. EV2B and EV2H). Notably, male or female AKG-treated mice started to gain
190 more body weight than their controls at 1 or 2 weeks after treatment, whereas food intake differences
191 began at 2 or 6 weeks after treatment (Fig. EV2A-B and EV2G-H), indicating that the hyperphagia
192 phenotypes could be secondary to the bodyweight increase induced by AKG. These weight
193 differences induced by AKG in both sexes were due to the increases in muscle size indicated by
194 upregulated lean mass (Fig. EV2C and EV2I) and gastrocnemius and soleus weight (Fig. EV2D and

195 EV2J). This is consistent with our previous observations that AKG promotes skeletal muscle
196 hypertrophy and protein synthesis (Cai et al, 2016) while inhibits skeletal muscle protein degradation
197 and muscle atrophy (Cai et al, 2018).
198
199 Interestingly, opposite to the stimulatory effects on muscle mass, we found that AKG significantly
200 decreased fat mass, weights of gWAT and inguinal white adipose tissue (iWAT), and adipocyte sizes
201 of gWAT in both male and female mice (Fig. EV3D-F and EV3J-L). Consistent with decreased
202 adiposity, we observed increased mRNA expression of thermogenic genes including uncoupling
203 protein 1 (UCP1), iodothyronine deiodinase 2 (Dio2), and cell death-inducing DNA fragmentation
204 factor-alpha-like effector A (Cidea) in brown adipose tissue (BAT) of AKG-treated male mice (Fig.
205 EV2M). Similarly, AKG-induced upregulation of UCP1 in the BAT was also suggested by both
206 western blot and immunohistochemistry (IHC) analyses of the UCP1 protein (Fig. EV2N-P). These
207 results suggest a role of AKG in BAT thermogenesis, which encourages us to examine if AKG
208 regulates thermogenesis-related hormones. We found that AKG significantly increased serum
209 epinephrine (E) and decreased non-esterified fatty acids (NEFA), but showed no effect on
210 norepinephrine (NE), thyroxine (T4), or triiodothyronine (T3) in males (Fig. EV2Q-U), implying an
211 increased adrenergic stimulation induced by AKG. Thus, our observations indicate that AKG
212 increases muscle mass and body weight, while at the same time decreasing WAT expansion and
213 stimulating BAT thermogenesis of chow-fed mice.
214
215 To investigate whether AKG supplementation also produces beneficial metabolic effects in the
216 diet-induced obesity (DIO) model, we characterized AKG's effects on energy homeostasis of male

and female mice that were fed on HFD. Unexpectedly, in both sexes, AKG-treated mice showed increased water intake (Fig. 2B and 2M), decreased body weight gain (Fig. 2D and 2O), and comparable food intake (Fig. 2C and 2N). Notably, both AKG-treated male and female mice still showed increased lean mass as we observed in chow-fed mice (Fig. 2E-F and 2P-Q). The inhibitory effect of AKG on HFD-induced body weight gain was solely due to a decrease in fat mass, more specifically gWAT and iWAT but not BAT (Fig. 2G-I and 2R-T). Consistently, in both sexes, the average adipocyte sizes of both gWAT and iWAT were significantly smaller in AKG-treated mice than in control mice (Fig. 2K-L and 2U-V). Additionally, we found that 11-weeks of AKG water supplementation increased serum AKG level up to a dose comparable to that observed in HFD-fed mice receiving resistance exercise (increased from 58.77 ± 3.2 to 80.38 ± 3.3 μmol/L, Fig. 2J vs. 94.93 ± 3.9 μmol/L, Fig. 1H), suggesting a physiological boost of circulating AKG level. These data suggest a physiological role of AKG in preventing HFD-induced weight gain and expansion of adipose tissue in both sexes.

To determine the mechanisms underlying the protective effects of AKG on DIO, male control and AKG-treated mice were adapted into an indirect calorimetry system. AKG-treated mice showed significantly higher energy expenditure in both light, and dark cycles (Fig. 3A-B) compared to control mice. The enhanced energy expenditure was associated with increases of both core body temperature (Fig. 3E) and cold-induced BAT temperature (Fig. 3F-G), indicating an increase of thermogenesis. Consistently, AKG dramatically increased the mRNA expression of thermogenic genes, including UCP1, Dio2, and Cidea (Fig. 3M), and the protein expression of UCP1 (Fig. 3N-O) in the BAT. This AKG-induced BAT thermogenesis is further supported by the decreased serum NEFA in AKG-treated

239 males (Fig. 3Q), suggesting a higher metabolism and oxidation rate of NEFA as an energy source.
240 Notably, AKG also effectively increased the mRNA expression of beige markers in the iWAT,
241 including Tumor Necrosis Factor Receptor Superfamily Member 9 (CD137), Tumor Necrosis Factor
242 Receptor Superfamily Member 5 (CD40), T-box transcription factor 1 (TBX1), Transmembrane
243 protein 26 (TMEM26), Cbp/P300 Interacting Transactivator With Glu/Asp Rich Carboxy-Terminal
244 Domain 1 (CITED1) and Solute Carrier Family 27 Member 1 (slc27a1) in iWAT (Fig. 3P). Combining
245 our observation that AKG failed to affect cumulative HFD intake (Fig. 2C) and calorie absorption
246 (Fig. EV3A), our data suggest that AKG prevents DIO by increasing thermogenesis and energy
247 expenditure without affecting energy intake.
248
249 Additionally, AKG also decreased the respiratory exchange ratio (RER) (Fig. 3C-D), suggesting
250 AKG-treated mice used more fat as a fuel source compared to control mice. Consistently, the
251 increased RER was associated with enhanced lipolysis in the WATs, as indicated by increased
252 phosphorylation of hormone-sensitive lipase (p-HSL), and protein expression of adipocyte
253 triglyceride lipase (ATGL) in the WAT (Fig. 3I-3L), both of which are the key lipases in adipocytes.
254 Notably, a normal lipogenesis in WATs was indicated by unchanged mRNA expression of lipogenic
255 genes (Fig. 3H), including peroxisome proliferator-activated receptor gamma (PPARγ), fatty acid
256 synthase (FASN), and acetyl-CoA carboxylase (ACC). Both BAT thermogenesis and WAT lipolysis
257 are under coordinated control by metabolic hormones. Similar to what we observed in chow-fed mice,
258 we found AKG significantly increased serum E, but not NE, T4, or T3 in males (Fig. 3R-3U),
259 implying increased adrenergic stimulation induced by AKG. In summary, our results indicate that
260 AKG stimulates BAT thermogenesis and fat metabolism, and by doing so to promote energy

expenditure and prevent DIO.

It has been shown that AKG lowered mice body weight through influencing intestinal microbiota (Chen et al, 2017), suggesting another alternative mechanism for anti-obesity effects of AKG. On this basis, we used 16S DNA sequencing to analyze the microbial composition in the feces from HFD-fed male mice after 1 or 4 weeks of AKG supplementation. Surprisingly, we found that AKG supplementation had no effect on microbial composition at both the phylum- (Fig. EV3B) or genus-level (Fig. EV3C) analyzed by the Anosim and Adonis methods (Fig. EV3D). These suggest that microbial composition may not be the primary mediator for the inhibitory effects of AKG on HFD-induce obesity.

Metabolic effects of AKG are mediated by adrenergic stimulation of adipose tissue thermogenesis and lipolysis

We next examined if acute AKG treatment would produce similar beneficial metabolic effects as we observed in the mice receiving long-term supplementation of AKG. Specifically, male C57BL/6 mice were intraperitoneal (i.p.) injected with AKG at a dose of 10 mg/kg. We found that this dose of AKG effectively increased blood AKG concentration up to a physiological level observed in resistance exercise mice within 2 hrs (Fig. 4A). AKG acute treatment increased not only the temperature (Fig. 4B-C) but also the expression of thermogenic genes, i.e., UCP1, Dio2 and Cidea (Fig. EV4C-D) in the BAT 3 hrs after injection. Additionally, AKG also enhanced protein expression of ATGL and p-HSL in gWAT (Fig. 4D) and decreased serum NEFA level (Fig. EV4B). These results indicate that similar to long-term supplementation, acute i.p. injection of AKG also stimulates BAT thermogenesis and WAT

lipolysis.

To explore the mechanism in which AKG promotes BAT thermogenesis, we examine the direct effects of AKG in *in vitro* or *ex vivo* models of BAT. We found that *in vitro* AKG treatment failed to affect mitochondrial function (Fig. EV5A-B) and p-AMPKα or p-FoxO1 protein expression (Fig. EV5I-J) of primary brown adipocyte. Consistently, we found that *ex vivo* AKG treatment failed to affect oxygen consumption rate (OCR) of BAT and NEFA levels in the culture medium (Fig. EV5K-L), suggesting an indirect regulatory role of AKG in BAT metabolism. To further identify this indirect pathway, we evaluated the mitochondrial responses to AKG treatment in *in vitro* models of other metabolic organs, including chromaffin (adrenal gland), C2C12 (skeletal muscle) and HepG2 (liver) cell lines. We found that AKG decreased ATP production in all models (Fig. EV5C-H), which is consistent with a previous observation that AKG extends lifespan by inhibiting the ATP synthase (Chin et al, 2014). Additionally, AKG also decreased the basal respiration of C2C12 cells (Fig. EV5E-F), suggesting an autocrine regulatory role of AKG in muscle metabolism, which is consistent with our previous findings (Cai et al, 2018; Cai et al, 2016). Importantly, AKG dramatically decreased basal respiration and enhanced spare respiratory capacity (SRC) of adrenal chromaffin cells (Fig. EV5C-D), which enables cells to overcome various stresses including HFD-induced oxidation stress, suggesting a direct effect of AKG on the adrenal gland.

In supporting this view, AKG stimulated the release of instantaneous intracellular calcium from chromaffin cells (Fig. EV5P), and this stimulatory effect is dose-dependent (Fig. EV5Q), suggesting AKG-induced direct activation of intracellular calcium-dependent signaling pathways. Importantly,

304 we also found AKG dose-dependently increased the release of E, but not NE, from chromaffin cells
305 (Fig. EV5R-S), indicating activation of adrenal medulla function. The same stimulatory effects were
306 consistently observed in *ex vivo* adrenal gland model. Specifically, we found AKG increased the
307 concentration of E, but not NE, in the medium from organ cultures of adrenal glands (Fig. EV5M-N).
308 Additionally, the protein expression of phospholipase C-β (PLCβ), one of the intracellular calcium
309 signaling effectors, was enhanced in the adrenal gland by *ex vivo* AKG treatment (Fig. EV5O).
310 Therefore, our data suggest that AKG directly acts on adrenal medullary chromaffin cells to increase
311 E release.
312
313 This view is further supported by the evidence from *in vivo* mouse model. Specifically, we found that
314 protein expression of PLCβ and phosphorylation of extracellular-signal-regulated kinase (p-Erk) in
315 the adrenal glands were upregulated by acute AKG treatment (Fig. EV4E). The Erk pathway is
316 involved in directing cellular responses to extracellular stimuli (Roberts, 2012). The upregulation of
317 both PLCβ and p-Erk indicates enhanced adrenal activation. Notably, serum catecholamine (E but not
318 NE) was significantly increased by both acute and long-term AKG treatments (Fig. 3R-3S, 4E and
319 EV4A), suggesting an AKG-induced activation of the adrenal medulla. Consistently, AKG treatment
320 also increased heart rate (Fig. EV4H-I) and blood pressure (Fig. EV4J-L), both of which are direct
321 physiologic and behavioral responses induced by adrenal gland E. However, no obvious difference
322 was observed in locomotor activity (Fig. EV4F-G). Taken together, both *in vitro* and *in vivo* evidence
323 supports that AKG directly acts on the adrenal gland to increase the release of E.
324
325 It is well-established that catecholamines are an essential driver of BAT thermogenesis by stimulating

the UCP1 signaling pathway (Sharara-Chami et al, 2010). Importantly, catecholamines also induce WAT lipolysis to promote the release of fatty acids, which are used as the principal substrate for BAT thermogenesis (Bartelt et al, 2011). Therefore, increased serum E may mediate the stimulatory effects of AKG on BAT thermogenesis and WAT lipolysis. Consistent with this speculation, we found that while acute AKG treatment significantly increased oxygen consumption and decreased RER, both regulatory effects were abolished by co-injection of SR59230A, a beta-3 adrenergic receptor (ADRB3) inhibitor (Fig. 4F-4I). ADRB3 is the key mediator for the stimulatory effects of catecholamines on WAT lipolysis and BAT thermogenesis (Claustre et al, 2008; Jiang et al, 2017). These results suggest a mediating role of E in the anti-obesity effects of AKG.

To provide further evidence to support this hypothesis, we investigated the metabolic effects of AKG in adrenalectomized male mice. Interestingly, we found that the anti-obesity effects of AKG were abolished by adrenalectomy (Fig. 4J-U). Specifically, not only the inhibition on body weight (Fig. 4J), fat mass (Fig. 4L), iWAT and gWAT weight (Fig. 4M) and serum NEFA (Fig. 4N), but also the stimulation on lean mass (Fig. 4L), cold-induced BAT thermogenesis (Fig. 4O-P), mRNA expression of thermogenic genes in the BAT (Fig. 4Q), protein expression of ATGL and p-HSL in the iWAT (Fig. 4R-4S) and UCP1 protein expression in the BAT (Fig. 4T-4U) were diminished by adrenalectomy. These results suggest a mediating role of adrenal stimulation in AKG-induced adipose tissue lipolysis and thermogenesis.

2-oxoglutarate receptor 1 in the adrenal gland ($OXGR1^{AG}$) is required for the stimulatory effects of AKG on adipose tissue thermogenesis and lipolysis

As an endogenous intermediate metabolite in the TCA cycle, AKG is traditionally known as an energy donor or a precursor in amino acid biosynthesis (Wu et al, 2016). However, recent studies have shown that AKG also functions as a signaling molecule, and acts as a regulator of epigenetic processes and cellular signaling, via protein binding with many different AKG sensors (Zdzisinska et al, 2017). These AKG sensors include hypoxia-inducible factor prolyl-hydroxylases (PHDs), ten-eleven translocations (TETs), lysine demethylase 6B (JMJD3), octamer-binding transcription factor 4 (OCT4), ankyrin repeat, SAM and basic leucine zipper domain containing 1 (ASZ1), WAP four-disulfide core domain 15A (wdfc15a), depleted in azoospermia-like (Dazl) and its endogenous G protein-coupled receptor (OXGR1) (Zdzisinska et al, 2017). We postulate that the stimulatory effect of AKG on adrenal E secretion is mediated by one of these AKG sensors. Notably, we found that OXGR1 has the highest absolute mRNA expression level in the adrenal gland among different AKG sensors (Fig. 5A). Adrenal OXGR1 absolute mRNA expression is also much higher than the expression in other tissues, except the testis (Fig. 5B). Additionally, immunofluorescence staining (IF) of OXGR1 showed strong signals in the adrenal inner medulla instead of the outer cortex (Fig. 5C). Interestingly, acute AKG treatment or resistant exercise both increased the mRNA expression of OXGR1 in the adrenal gland (Fig. 5D). These results suggest a possible role of $OXGR1^{AG}$ in the direct stimulatory effects of AKG on adrenal E release.

To test this point of view, we first generated a loss-of-function *in vitro* chromaffin cell model by using siRNA to target OXGR1 specifically. We found OXGR1 siRNA treated chromaffin cells showed significantly less protein expression of OXGR1 compared to control siRNA treated cells (Fig. 5E), which validated our OXGR1 knockdown chromaffin cell model. By using this model, we showed that

370 the knockdown of OXGR1 abolished the stimulatory effects of AKG on the secretion of E (Fig. 5F)
371 and release of instantaneous intracellular calcium (Fig. 5G), suggesting a mediating role of $OXGR1^{AG}$
372 in AKG-induced E release.
373
374 To further determine the role of OXGR1 in AKG's metabolic effects *in vivo*, we generated an OXGR1
375 global knock-out mouse model (OXGR1KO) by using the Clustered Regularly Interspaced Short
376 Palindromic Repeats (CRISPR) method (Fig. EV6A-B). We found OXGR1KO mice showed
377 completely abolished OXGR1 mRNA expression compared to WT control mice (Fig. EV6C), which
378 validates our knockout model. Surprisingly, we failed to found any metabolic phenotypes in
379 OXGR1KO mouse when fed on chow (Fig. EV6D-O). However, consistent with *in vitro* chromaffin
380 cell model, when HFD-fed mice were supplemented with AKG, OXGR1KO abolished AKG-induced
381 release of serum E (Fig. EV7A) as well as the inhibitory effects of AKG on HFD-induced increases of
382 body weight (Fig. 5H) and fat mass (Fig. 5J-K), specifically iWAT (Fig. 5L) and gWAT (Fig. 5M).
383 Similarly, OXGR1KO also diminished AKG-induced inhibition on adipocyte size in both gWAT and
384 iWAT (Fig. EV7C-D) and stimulation on lean mass (Fig. 5J-K). These results suggest an essential role
385 of OXGR1 in the inhibitory effects of AKG on HFD-induced obesity.
386
387 The key mediating role of OXGR1 is further supported by our results from the indirect calorimetry
388 system. We found that while AKG did not change food intake in both WT and OXGR1KO mice (Fig.
389 5I), AKG increased oxygen consumption and decreased RER in WT but not OXGR1KO mice (Fig.
390 5P-S). These results suggest that OXGR1 mediates the stimulatory effects of AKG on energy
391 expenditure and fat burning. Consistently, in WT but not OXGR1KO mice, AKG increased ATGL

392 protein in the gWAT (Fig. 5N-O), the phosphorylation of HSL in both iWAT and gWAT (Fig. 5N-O
393 and EV7E-F), and UCP1 protein in the BAT (Fig. EV7B). Thus, these data further provide *in vivo*
394 evidence to support that OXGR1 is a key mediator for the AKG supplementation-induced lipolysis
395 and thermogenesis.
396
397 To assess if $OXGR1^{AG}$ is sufficient to mediate the anti-obesity effects of AKG, we generated an
398 OXGR1 adrenal-selective reexpression ($OXGR1RE^{AG}$) mouse model by delivering
399 HBAAV2/9-OXGR1 virus into the adrenal gland of OXGR1KO mice. In this model, adrenal OXGR1
400 expression and the stimulatory effects of AKG on serum E levels were both successfully rescued
401 compared to control OXGR1KO mice (Fig. EV7G-H), suggesting an $OXGR1^{AG}$-mediated E-releasing
402 effect of AKG. AKG showed no effects on food intake in both OXGR1KO and $OXGR1RE^{AG}$ mice
403 (Fig. 6B). Similar to what we observed before, in the control OXGR1KO mice, AKG failed to induce
404 metabolic phenotypes (Fig. 6A-L). On the other hand, we showed similar anti-obesity effects of AKG
405 in $OXGR1RE^{AG}$ mice as what we observed in WT mice. These AKG-induced anti-obesity effects
406 include decreases in body weight gain (Fig. 6A), fat mass (Fig 6C-D), gWAT and iWAT weight (Fig.
407 6E-F), adipocyte size of gWAT and iWAT (Fig. EV7J-K), and RER (Fig. 6K-L), as well as increases
408 in lean mass (Fig. 6C-D), oxygen consumption (Fig. 6I-J), ATGL protein in gWAT (Fig. 6G-H),
409 phosphorylation of HSL in both iWAT and gWAT (Fig. 6G-H and EV7L-M), and UCP1 protein in
410 BAT (Fig. EV7I). These results indicate $OXGR1^{AG}$ is sufficient to mediate the anti-obesity effects of
411 AKG.
412
413 Consistent with this point of view, we found enhanced anti-obesity effects of AKG in the OXGR1

adrenal-specific overexpression mouse model (GRP99OE^{AG}). In this model, the HBAAV2/9-OXGR1 virus was delivered into the adrenal gland of WT mice. The mRNA of OXGR1 was successfully overexpressed in the adrenal gland of GRP99OE^{AG} mice compared to WT mice injected with HBAAV2/9-GFP control virus (Fig. EV8A). We found that adrenal overexpression of OXGR1 enhanced the anti-obesity effects of AKG. For example, GRP99OE^{AG} enhanced AKG's inhibitory effects on body weight gain (Fig. EV8B), fat mass (Fig. EV8D-E), gWAT and iWAT weight (Fig. EV8F-G), adipocyte size of gWAT and iWAT (Fig. EV8P-Q), and RER (Fig. EV8N-O), as well as stimulatory effects on serum E levels (Fig. EV8K), lean mass (Fig. EV8D-E), oxygen consumption (Fig. EV8L-M), ATGL protein in gWAT (Fig. EV8H-I), phosphorylation of HSL in both iWAT and gWAT (Fig. EV8H-I and EV8R-S), and UCP1 protein in BAT (Fig. EV8J). Additionally, AKG showed no effect on food intake in both WT control and GRP99OE^{AG} mice (Fig. EV8C). Thus, the results from both loss-of-function and gain-of-function models demonstrate that OXGR1^{AG} mediates the AKG supplementation-induced adipose tissue thermogenesis and lipolysis and in turn preventing DIO.

OXGR1 is required for beneficial metabolic effects of exercise

Our data suggest that exercise increases AKG and OXGR1 mediates anti-obesity effects of AKG supplementation. Based on these observations, we tested whether OXGR1 is required for exercise-induced beneficial metabolic effects by comparing the salutary effects of two-week resistance exercise in OXGR1KO and WT mice. As we observed in WT mice, exercise induced a similar increase of serum AKG level in OXGR1KO mice (Fig. 7H). We found exercise did not change food intake in both WT and OXGR1KO mice (Fig. 7D), consistent with the previous observations in

436 the adult and aged male mice following the same ladder-climbing resistance exercise (Kim et al,
437 2016). Exercise effectively decreased body weight gain in WT control mice, while deletion of
438 OXGR1 attenuated the bodyweight decrease induced by resistance exercise (Fig. 7A-B). Although
439 resistance exercise significantly decreased fat mass (Fig. 7G), specifically gWAT and iWAT weight
440 (Fig. 7E-F) in both OXGR1KO and WT control mice, these resistance exercise-induced decreases
441 were higher in WT than OXGR1KO mice (Fig. 7C and 7E-G). Similar attenuations were found in
442 resistance exercise-induced increases of lean mass (Fig. 7G), serum E levels (Fig. 7I), UPC1 mRNA
443 expression in BAT (Fig. 7J), ATGL and HSL mRNA expression in gWAT (Fig. 7K) and oxygen
444 consumption (Fig. 7L-M), as well as decrease of RER (Fig. 7N-O). These data collectively support a
445 model in which resistance exercise increases AKG secretion from muscle tissues to bind with adrenal
446 OXGR1, and by doing so to increase adipose tissue lipolysis and thermogenesis and prevent DIO.
447
448 **The p65/NF-κB inflammatory pathway is required for the stimulatory effects of AKG on E**
449 **release from chromaffin cells *in vitro*.**
450 To explore the intracellular mechanism of AKG-induced E release, we investigated the transcriptomic
451 alteration induced by AKG treatment in *in vitro* adrenal chromaffin cells by RNA sequencing.
452 Ingenuity pathway analysis (IPA) was used for functional annotation of the genes differentially
453 expressed between the control and AKG treatment group. Unexpectedly, we found that AKG activated
454 the inflammatory responses, especially the cytokine interleukin (IL) pathways (Fig. 8A). It is
455 well-known that the expression of inflammatory genes and pro-inflammatory cytokines is mainly
456 regulated by nuclear factor kappa B (NF-κB) family of transcription factors (Hu et al, 2005; Karin et
457 al, 2004). Here, we showed that AKG effectively increased the phosphorylation of IκB kinase (IKK,

458 an upstream activator for NF-κB) and nuclear factor of kappa light polypeptide gene enhancer in
459 B-cells inhibitor, alpha (IκBα, an inhibitor of NF-κB, Fig. 8B-C), suggesting an AKG-induced NF-κB
460 activation. We speculate that AKG activates IKK to phosphorylate the inhibitory IκBα protein, which
461 leads to the dissociation of IκBα from NF-κB and subsequent nuclear shuttling and activation of
462 NF-κB. In support of this view, we found AKG increased the expression of p65, a subunit of NF-κB
463 transcription complex, in the nucleus protein extraction, while decreased P65 in the cytoplasm (Fig.
464 8B-C). The same nucleus NF-κB (p65) translocation was also observed by IF staining (Fig. 8D).
465 These results indicated that AKG activates NF-κB inflammatory pathway in *in vitro* adrenal
466 chromaffin cells.
467
468 To directly test if OXGR1 is required for the stimulatory effects of AKG on the NF-κB pathway, an
469 OXGR1-knockdown chromaffin cell model was generated by using siOXGR1. We found OXGR1
470 knockdown significantly decreased protein expression of OXGR1 (Fig. 8B-C), which validated our
471 loss-of-function model. By using this model, we showed that the knockdown of OXGR1 abolished the
472 stimulatory effects of AKG on OXGR1 protein expression and NF-κB signal transduction cascade
473 (Fig. 8B-D), suggesting a mediating role of OXGR1 in mediating AKG-induced NF-κB signaling
474 activation. It has been previously shown that circulating cytokines affect chromaffin cell secretory
475 function through NF-κB activation (Ait-Ali et al, 2008; Bunn et al, 2012; Douglas et al, 2010). NF-κB
476 signaling activation may play a role in AKG-induced E secretion. Consistent with this speculation, we
477 found that while AKG treatment increased the release of E and activated NF-κB signaling, both
478 stimulatory effects were abolished by co-treatment of IKK16, an IKK inhibitor (Fig. 8E-G). These
479 results suggest a mediating role of NF-κB activation in the stimulatory effects of AKG on E release in

480 *in vitro*.

481

482 **Discussion**

483 The major finding of our study is that exercise responsive myometabolite, AKG, prevents
484 HFD-induced body weight gain and adiposity in both male and female mice. Systemic
485 characterization revealed normal food intake, but robust increases in energy expenditure, BAT
486 thermogenesis, and WAT lipolysis induced by AKG. We further provided both *in vitro* and *in vivo*
487 evidence supporting that the anti-obesity effect of AKG is mediated by adrenergic stimulation of
488 adipose tissue thermogenesis and lipolysis. By using both loss-of-function and gain-of-function
489 mouse models, we showed that AKG receptor OXGR1, expressed by adrenal glands, is essential for
490 the stimulatory effects of AKG on thermogenesis and lipolysis. Importantly, we demonstrated that
491 OXGR1 is required for exercise-induced weight loss and fat reduction. We also provided *in vitro*
492 evidence supporting that the adrenal activation of p65/NF-κB inflammatory pathway is required for
493 the stimulatory effects of AKG on E release. These findings implicate myometabolite AKG in the
494 physiological mechanism underlying exercise-induced weight loss and demonstrate that AKG acts as
495 a previously unappreciated systemic adrenergic signal, and exerts profound effects on whole-body
496 metabolism.

497

498 The comprehensive serum metabolite signatures induced by acute resistance exercise include
499 decreased amino acids and increased fatty acids. These findings are consistent with previous
500 observations that the oxidation and catabolism of amino acids, especially branched-chain amino acids
501 (BCAA), are promoted by exercise (Qun et al, 2014), while the mobilization of free fatty acids from

depots and efflux of plasma free fatty acids are increased by exercise (Friedberg et al, 1963; Shimomura et al, 2004). Importantly, the metabolites of valine, i.e., alpha-ketoisovaleric acid (α-keval) and 2-hydroxy-3-methylbutyric acid (2H3MA), as well as a metabolite of alanine, pyruvic acid (Pyr), were also increased after acute exercise. All these three metabolites can be converted into acetyl-CoA or succinyl-CoA, which is the main input or important intermediate for TCA oxidation (Li et al, 2017). Consistently, AKG, another essential intermediate in the TCA cycle, was found to be upregulated by exercise.

We successfully identified several rapid response metabolites (pyruvate, lactate, malate, succinate, AKG, xanthine, and hypoxanthine) induced by resistance exercise. In line with other literature (Berton et al, 2017; Yde et al, 2013), we found resistance exercise induced a rapid accumulation of pyruvate and lactate, reflecting anaerobic metabolism and muscle damage (Gorostiaga et al, 2014). The increase of pyruvate is due to the limited ability of mitochondria to oxidase pyruvate during anaerobic exercise. To fulfill the high energy demand required by resistance exercise, pyruvate is converted to lactate in muscle and then transported through the bloodstream to the liver, where lactate can be converted into glucose by gluconeogenesis. The increased levels of pyruvate and lactate validate our resistance exercise model.

Interestingly, opposite to well-established accumulation signatures of malate, succinate, hypoxanthine, and xanthine following endurance exercise (Aguer et al, 2017; Lewis et al, 2010), our metabolomics analyses found these metabolites decreased following acute resistance exercise. The same trend was consistently demonstrated by LC-MS/MS analyses comparing the metabolic response following

524 endurance and resistance exercise, suggesting an exercise type-specific metabolic response. Notably,
525 succinate was found to be increased shortly after resistance exercise (bilateral leg extension exercises)
526 in humans (Berton et al, 2017). This discrepancy may be attributed to the different forms of resistance
527 exercise (i.e., bilateral leg extension vs. ladder climbing), the time points taken into consideration in
528 the studies (i.e., 5 min after vs. immediately after), as well as the research subjects (i.e., moderately
529 trained humans vs. untrained mice).
530
531 Consistent with a previous report (Leibowitz et al, 2012), we found AKG significantly increased in
532 the blood following resistance exercise. Interestingly, we also found resistance exercise decreased
533 circulating glutamate and leucine, both of which can be metabolized into AKG. The observed
534 elevation in AKG levels may be attributed to glutamate and leucine degradation. Consistent with this
535 point of view, both leucine degradation (Pechlivanis et al, 2010) and glutamate breakdown (Leibowitz
536 et al, 2012) were found to increase the circulating AKG. Considering the critical role of AKG in the
537 TCA cycle, it is likely that amino acid metabolism (leucine degradation) and muscle glutamate
538 content depletion contribute to the energy supply during resistance exercise.
539
540 AKG is an important biological molecule with pleiotropic activity, and has been shown to have broad
541 therapeutic potentials, such as decreasing risk of cancer (Mullen et al, 2014), maintaining intestinal
542 health (Hou et al, 2011), promoting muscle growth (Cai et al, 2016) and orchestrating macrophage
543 activation through epigenetic alteration (Liu et al, 2017; Zdzisinska et al, 2017). Notably, a potential
544 role of AKG in energy homeostasis has also been suggested by our observations. When fed on chow,
545 AKG-treated mice showed upregulation of lean muscle mass and body weight gain. These results are

546 consistent with our previous observations that AKG increases muscle protein synthesis (Cai et al,
547 2016) while decreasing muscle protein degradation (Cai et al, 2018). On the other hand, we found
548 AKG treatment increases BAT thermogenesis and decrease fat mass, which is consistent with the
549 previous report that AKG increases BAT adipogenesis and thermogenesis via an epigenetic way (Yang
550 et al, 2016). These metabolic changes induced by AKG resemble several key metabolic responses
551 induced by resistance exercise, i.e., enhanced thermogenesis, increased muscle mass, and decreased
552 fat pads (Allen et al, 2001; Stanford & Goodyear, 2016). Additionally, oral administration of AKG has
553 been previously shown to decrease adiposity in a DIO rat model (Tekwe et al, 2012). Based on these
554 observations, we postulated that AKG might have similar beneficial metabolic effects on DIO as
555 resistance exercise.
556
557 Consistent with this, we found AKG prevented body weight gain induced by HFD, which is
558 associated with increased energy expenditure but not food intake. Notably, decreased body weight
559 gain is due to a superior portion of fat mass loss compared to lean mass gain. As we observed in
560 chow-fed mice, AKG increased BAT expression of thermogenic genes including UCP1, Dio-2, and
561 Cidea, suggesting upregulation of BAT thermogenesis. Similar AKG-induced WAT lipolysis was also
562 indicated by upregulated RER and increased expression of ATGL and pHSL, the main enzymes
563 catalyzing lipolysis in WAT (Bolsoni-Lopes & Alonso-Vale, 2015). These results suggest that the
564 water supplement of AKG prevents DIO by increasing BAT thermogenesis and WAT lipolysis.
565
566 Exercise-induced myometabolites cause physiological changes in target tissues either directly or
567 indirectly by affecting the secretion of endogenous hormones. As an exercise-induced metabolite

(Leibowitz et al, 2012), AKG has been shown to exert direct regulatory effects on the muscle development (Cai et al, 2016), liver injury and repair (Wang et al, 2015), and intestinal immune protection (Hou et al, 2011). It is unknown whether AKG directly acts on the BAT or indirectly act through other tissues to increase thermogenesis. To test the direct effects of AKG on BAT, we used both *ex vivo* BAT tissue or *in vitro* primary brown adipocyte culture models. We found that direct treatment of AKG failed to affect dissolved oxygen, NEFA levels, or calcium signaling in both models, suggesting an alternative indirect effect of AKG. Importantly, AKG supplementation has been shown to mediate the stimulatory effects of dietary restriction on lifespan by inhibiting ATP synthase and rapamycin (TOR) signaling (Chin et al, 2014). It is possible that AKG acts on ATP synthase and TOR signaling to regulate BAT thermogenesis. However, AKG treatment also failed to regulate ATP production or protein expression of p-AMPKα and p-FoxO1. These results indicate an indirectly regulatory role of AKG in BAT metabolism.

Both BAT thermogenesis and WAT lipolysis are under coordinated control by metabolic hormones. For example, thyroid hormones T4 and its active form, T3, as well as type 2 deiodinase (D2), an essential enzyme activating T4 to T3, are required for adaptive thermogenesis in BAT (de Jesus et al, 2001; Mullur et al, 2014). E and NE, the catecholamines secreted from the adrenal glands, have been shown to activate triglyceride lipase and induce lipolysis in WAT (Bartness et al, 2014; Jocken & Blaak, 2008), and also upregulate UCP1 and stimulate BAT thermogenesis (Collins et al, 2010; Sharara-Chami et al, 2010). Here, we found that AKG increased the mRNA expression of Dio-2, the gene coding D2 protein, in the BAT, suggesting an increase of conversion from T4 to T3. However, we failed to observe any changes in serum T3 and T4 levels.

590

591 Interestingly, we found AKG significantly stimulated the release of E, the main hormone secreted by
592 the adrenal medulla. Considering the stimulatory effects of E on both BAT thermogenesis and WAT
593 lipolysis, it is likely that AKG promoted BAT thermogenesis and WAT lipolysis through stimulating
594 the release of E from the adrenal medulla. In supporting this view, we found that the acute stimulatory
595 effects of AKG on energy expenditure and fat burning (indicated by oxygen consumption and RER)
596 were abolished by the systemic blockage of ADRB3. More importantly, the adrenalectomized male
597 mice showed no metabolic responses to water supplementation of AKG. These findings indicate an
598 indirect stimulation of AKG on adipose tissue thermogenesis and lipolysis through adrenal released E.

599

600 One important issue to be considered is the direct effects of E on the behavior of the mice. Consistent
601 with the well-established functions of circulating E (Tank & Lee Wong, 2015), we found that acute
602 AKG treatment increased both heart rate and blood pressure but not physical activity. These cardiac
603 changes are consistent with the increased demand for higher blood glucose and free fatty acids during
604 exercise, suggesting a possible role of AKG in exercise. The release of E from the adrenal gland is
605 tightly controlled by SNS (Grassi & Ram, 2016) and AKG may increase the adrenal release of E by
606 increasing SNS input to the adrenal gland. However, we found AKG treatment increases PLCβ protein,
607 and releases of calcium ion and E from *ex vivo* adrenal gland and *in vitro* adrenal medullary
608 chromaffin cells. These findings suggest that AKG may directly act on the adrenal gland to increase
609 instantaneous intracellular calcium, and by doing so, promote the release of E.

610

611 To investigate how AKG interacts with the adrenal medulla to increase the release of E, we examined

612 adrenal expression levels of different AKG sensors, which have been previously shown to interact
613 with AKG to exert physiological functions. These include the classical sensors of AKG, i.e., JMJDs,
614 TETs, PHDs, and GPRs. Among these different AKG sensors, OXGR1, a verified AKG receptor, was
615 found to have the highest expression in the adrenal gland. OXGR1 is an orphan G protein-coupled
616 receptor first discovered in 2002, and later was identified as the receptor for AKG and renamed as
617 2-Oxoglutarate receptor 1 (He et al, 2004; Wittenberger et al, 2002). It has been shown that the
618 half-maximal effective concentration (EC50) for OXGR1 to AKG is ~70 μM (He et al, 2004), which
619 is equal to the concentration of circulating AKG at rest condition (69.8 ± 2.8 μM, Fig. 1H), suggesting
620 a baseline activation of OXGR1. Notably, both wheel-running and ladder-climbing significantly
621 increase circulating AKG (91.3 ± 3.7 μM vs. 112.2 ± 3.2 μM, Fig. 1I), indicating an enhanced
622 OXGR1 activation induced by exercise. Previous studies have indicated that OXGR1 plays an
623 important role in mucin regulation in otitis (Kerschner et al, 2013) and cardiac hypertrophy (Omede et
624 al, 2016). However, there is no known role of OXGR1's effects on fat thermogenesis and lipolysis.
625 We found that while OXGR1 is widely expressed in many tissues, adrenal glands, testes, and brain
626 have the highest expression of GRP99, which is consistent with a previous report (Diehl et al, 2016).
627 Importantly, OXGR1 is highly expressed inside the adrenal gland medulla but not adrenal cortex, the
628 main region that releases E. These results suggest a possible mediating role of OXGR1 in the
629 stimulatory effects of AKG on E release.
630
631 To directly test if OXGR1 mediates the anti-obesity effects of AKG, we used CRISPR gene-editing
632 technology to generate a global OXGR1KO mouse line. The single-guide RNA (sgRNA) was
633 designed to target the exon 4 of OXGR1 locus, and OXGR1 expression is effectively disrupted in the

OXGR1KO model. We found AKG showed no effects on serum E levels in OXGR1KO mice. Interestingly, AKG also failed to promote lipolysis or prevent DIO in these OXGR1KO mice, suggesting a key role of OXGR1 in mediating the metabolic effects of AKG. These attenuations are not a result of CRISPR-mediated off-site mutagenesis, as virus-mediated selective reexpression of OXGR1 in the adrenal gland of OXGR1KO mice rescued AKG's effects on body weight, energy expenditure, fat thermogenesis, and lipolysis. Consistently, selective overexpression of OXGR1 in the adrenal gland of WT mice enhanced these effects of AKG. These findings demonstrate that OXGR1 expressed in the adrenal gland has a major role in the anti-obesity effects of AKG. However, we cannot exclude the potential roles of OXGR1 expressed in other tissues. There is a possibility that AKG acts through the central nervous system (CNS) to increase sympathetic input to fat tissue, and by doing so to prevent DIO. Consistent with this view is that OXGR1 has high mRNA expression in the hypothalamus, which has been reported to regulate fat thermogenesis and lipolysis through SNS (Contreras et al, 2017). Interestingly, in our OXGR1RE^{AG} model, adrenal reexpression of OXGR1 cannot fully rescue the anti-obesity effects of AKG, suggesting that other OXGR1 pathways may be involved. Our lab is currently exploring if the metabolic effects of AKG are partially mediated by central OXGR1.

Although the beneficial metabolic effects of AKG supplementation were blocked in HFD-fed OXGR1KO mice, we failed to observe any metabolic phenotypes of OXGR1KO mice when fed on chow diet. These results suggest that OXGR1 is not required for energy homeostasis regulation and body weight control on chow when circulating AKG is at a baseline level (no AKG supplementation or exercise). It appears that OXGR1 only exert beneficial effects on metabolic health and particularly

656 muscle hypertrophy and fat loss when circulating AKG is high. Interestingly, our data indicate that
657 resistance exercise effectively increases serum AKG level in both chow and HFD fed mice. These
658 raise the possibility that AKG/OXGR1 signaling mediates the salutary effects of anaerobic exercise.
659 Consistent with this view, we found exercise-induced metabolic beneficial effects, including
660 bodyweight loss, lipolysis, and fat mass reduction, were largely attenuated in OXGR1KO mice.
661 Importantly, in OXGR1KO mice, resistance exercise effectively increased serum AKG up to the level
662 we observed after AKG water supplementation, while baseline AKG level is still normal, suggesting a
663 normal AKG response induced by resistance exercise. Take all these together, our data support a key
664 role of AKG/OXGR1 signaling in beneficial metabolic effects induced by resistance exercise.
665
666 Another interesting phenotype we observed in OXGR1KO mice is muscle hypotrophy and body
667 weight loss when fed on HFD, suggesting a potential protective effect of OXGR1 on HFD-induced
668 muscle loss. Notably, we showed that HFD significantly decreased baseline circulating AKG level in
669 mice and serum AKG level is negatively correctly with BMI in humans. So OXGR1 protects
670 HFD-induced muscle loss when circulating AKG is low, which is independent of resistance exercise.
671 The protective effect of OXGR1 is possibly mediated by directly increasing muscle protein synthesis
672 (Cai et al, 2016) and decreasing muscle protein degradation (Cai et al, 2018). Of course, it is also
673 possible that other indirect pathways are involved. DIO has been shown to lead to skeletal muscle
674 atrophy, associated with upregulation of muscle-specific ubiquitin ligases, oxidative stress,
675 myonuclear apoptosis, and autophagy (Abrigo et al, 2016). So OXGR1-mediated protection is also
676 possible due to the compensatory response to the other physiological changes induced by OXGR1KO,
677 e.g., cardiac hypertrophy (Omede et al, 2016) or impaired acid-base homeostasis (Tokonami et al,

2013).

In conclusion, we found that exercise-induced metabolic benefits are mediated through a systemic increase in the TCA cycle intermediate AKG. AKG exerts acute and chronic control over adipose tissue thermogenesis and lipolysis by stimulating the release of E through OXGR1, an AKG sensor expressed by the adrenal gland. Thus, our findings identify AKG as an exercise-responsive myometabolite with essential salutary metabolic effects, acting as a previously unappreciated systemic pathway for activation of adipocyte thermogenesis and lipolysis.

Materials and method

Animals

Mice were housed in a temperature/humidity-controlled environment (23°C ± 3°C/70% ± 10%) on a 12-hr light/12-hr dark cycle (6 am and 6 pm). Unless otherwise stated, the mice were maintained ad libitum on standard mouse chow (Protein 18.0%, Fat 4.5%, and Carbohydrate 58%, Guangdong Medical Science Experiment Center, Guangzhou, Guangdong, China) and water. All groups within one experiment contain individual mouse with the same strain and sex, showing similar in body weight and age. All used mice aged between 10 to 20 weeks at the time when they were sacrificed. C57BL/6 mice were purchased from the Animal Experiment Center of Guangdong Province (Guangzhou, Guangdong, China). C57BL/6 mice were used for acute or long-term experiments to study AKG's metabolic effects. The OXGR1KO mice (Shanghai Research Center for Model Organisms, Shanghai, China) were generated and maintained on a C57BL/6 background. They were used to study the metabolic effects of long-term AKG supplementation.

Adrenal chromaffin cell culture and primary tissue culture of adult adrenal gland and BAT

Mouse adrenal chromaffin cell line (cbr1301321, BIOSH Biotechnology Company, Shanghai, China), and adrenal gland or BAT obtained from 10-12 weeks old C57BL/6 mice were cultured in high glucose DMEM (11965175, Thermo Fisher Scientific, Carlsbad, CA, USA) at 37 °C in a humidified atmosphere that contained 5% CO_2. The DMEM was supplemented with 10% Fetal Bovine Serum (16000044, Thermo Fisher Scientific), 100000 units/L of penicillin sodium, and 100 mg/L of streptomycin sulfate (11860038, Thermo Fisher Scientific).

722 **Metabolic signatures of exercise in mouse serum**

723 Ten-week-old C57BL/6 male mice were divided into four groups: resistance exercise group,
724 endurance exercise group, running wheel exercise group, or a control group without exercise. For
725 resistance exercise group, resistance ladder-climbing exercise was performed as described previously
726 (Kim et al, 2016). Ladder climbing exercise was conducted by using a 1 m ladder with 1.5 cm grids.
727 The ladder was set to attain an 80-degree angle with the ground. Three days adaptation was conducted
728 by letting mice to climb up the ladder without any resistance. The mice were positioned at the very
729 bottom of a 1-meter ladder and motivated to climb up the ladder. When mice reached the very top of
730 the ladder, a 2-min rest was given before the next trail of ladder climbing. Mice first received
731 resistance training adaptations without a load attached to the tail for 1 week with 1h ladder-climbing
732 per day. After the adaptation, resistance at 10% of body weight was given to the mice by adding
733 weight on the tail. The loads were increased gradually as the exercise sessions preceded. To
734 progressively increase exercise intensity, 2 g of additional weights were applied after four successful
735 trails. After about 40 mins of resistance exercise, mice were exhausted and then anesthetized. Blood
736 samples were collected by retro-orbital bleeding. The serum was separated and used for metabolomics
737 analysis. Muscle samples, including tibialis anterior, forelimbs, gastrocnemius, pectineus, soleus,
738 dorsal muscle and pectoralis, were collected for AKG assay and AKG-related enzyme activity test.
739 For endurance exercise group, mice were forced running on a treadmill (47300 TREADMILL, Ugo
740 Basile, Italy) as described previously (Lewis et al, 2010). Mice were first acclimated for 5 minutes a
741 day for three days, at a low rate of 14 meters/min and no incline. On the fourth day, the treadmill was
742 set to a constant 10% incline and started at 10 meters/minute. Every two minutes, the speed was then
743 increased by 2 meters/minute, and the mice were forced to run to exhaustion. Exhaustion was

744 determined by the unwillingness of mice to keep running on the treadmill, despite stimulus by a small
745 electric shock on the stationary platform of the treadmill. Once determined to be exhausted, mice were
746 euthanized. For running wheel exercise group, mice were singly housed and given free access to home
747 cage running wheel for 1 day. For the control group, mice were singly housed and maintained on
748 normal chow. Serum and muscle samples were collected from both running wheel and control groups
749 as described in the resistance exercise group.
750
751 In another separate experiment, male C57BL/6 mice at 8 weeks of age were switched to HFD and
752 continuously fed with HFD for 12 weeks to induce DIO. At 20 weeks of age, mice received about
753 40-min resistance exercise as described above. Serums were collected at 0, 1, 2, 4, and 6 hrs after
754 exercise.
755
756 **Metabolomics analysis**
757 Serum samples from mice receiving resistance exercise and control mice were used for metabolic
758 signature analysis. The untargeted metabolomics profiling was performed on XploreMET platform
759 (Metabo-Profile, Shanghai, China) by Metabo-Profile Biotechnology Co., Ltd (Shanghai, China). The
760 sample preparation procedures are referred to in the previously published methods with minor
761 modifications (Qiu et al, 2009). Briefly, the serum samples were thawed on ice-bath and centrifuged
762 for 5 min at 4℃ and 3,000 g (Microfuge 20R, Beckman Coulter, Inc., Indianapolis, IN, USA) to
763 separate debris or a lipid layer. Each sample aliquot of 50 μL was mixed with ten μL of internal
764 standard and 175 μL of pre-chilled methanol/chloroform (v/v=3/1). After incubation at 20℃ for 20
765 min, the mixture was centrifuged at 14,000 g for 20 min at 4℃. The supernatant was transferred to an

autosampler vial (Agilent Technologies, Foster City, CA, USA). All the samples in autosampler vials were evaporated briefly to remove chloroform using a CentriVap vacuum concentrator (Labconco, Kansas City, MO, USA), and further lyophilized with a FreeZone free dryer equipped with a stopping tray dryer (Labconco). The sample derivatization and injection were performed by a robotic multipurpose sample MPS2 with dual heads (Gerstel, Muehlheim, Germany). Briefly, the dried sample was derivatized with 50 μL of methoxyamine (20 mg/mL in pyridine) at 30 ℃ for two hrs, followed by the addition of 50 μL of MSTFA (1% TMCS) containing FAMEs as retention indices. The mixture was further incubated at 37.5 ℃ for another one hr using the sample preparation head. In parallel, the derivatized samples were injected with the sample injection head after derivatization.

The GC-TOFMS raw data processing, peak deconvolution, compound annotation, statistical analysis, and pathway analysis were processed using XploreMET software (v3.0, Metabo-Profile, Shanghai, China) as described in a previous publication (Ni et al, 2016). Compound identification for GC–TOFMS was performed by comparing the mass fragments with JiaLib mass spectral databases. Principal component analysis (PCA) and orthogonal partial least squares discriminant analysis (OPLS-DA) was also performed with XploreMET. The Student t-test was used for further differentiating variables selection and validation ($P < 0.05$). The Z-score indicates how many standard deviations an observation is above or below the mean of the control group (Fig.1D). The calculated fold change of 1.5 or p-value of 0.05 is chosen for statistical significance. The V-plot that integrates the fold change and p-values is used for depicting the significantly different metabolites (Fig.1E).

Association between plasma AKG level and body mass index (BMI) in Chinese adults

This observational study was conducted in Zhujiang Hospital of South Medical University, between August 2018 and November 2018. A set of 45 Chinese volunteers aged from 24 to 75 (10 males and 35 females) were recruited from Zhujiang Hospital of South Medical University. One week before the start of the study, participants were asked to complete a self-administered form, including gender, age, and symptoms of heart disease and bone or joint problem. Individuals with previous history, signs, and symptoms, or self-declaration, of coronary heart disease, cardiovascular disease and kidney disease were excluded from the study. At the study day, height and body weight were obtained with participants wearing light clothing without shoes. BMI was calculated using equation BMI = kg/m^2, where kg is a participant's weight in kilograms, and m^2 is the height in meter squared. Blood samples were collected from each participant and stored in EDTA tubes. Samples were subsequently centrifuged (4000 × g for 20 min at 4°C), and plasmas were stored in -80°C. The plasma AKG levels were measured by LC-MS/MS analysis (Uplc1290-6470A QQQ Liquid chromatography-mass spectrometry instrument, Agilent technologies). The study was reviewed and approved by the Human Subjects Ethics committee of Zhujiang Hospital of South Medical University and written informed consent was obtained from each participant.

Long-term effects of AKG on energy homeostasis

To investigate the metabolic effects of AKG when mice fed on chow, both male and female C57BL/6 mice at 12 weeks of age were singly housed and randomly assigned to receive water or water supplemented with 2% AKG (α-Ketoglutaric acid disodium salt, A610289, Sangon Biotech (Guangzhou) Co., Ltd). Bodyweight and food intake were monitored weekly for 6 or 11 weeks. At the end of the experiment, mice from both sexes were deeply anesthetized and euthanized. Gastrocnemius

muscle and gWAT were isolated and weighted. An aliquot of gWAT was collected for HE staining and adipocyte size analysis. Additionally, serum and BAT were also collected in males. Serum was used to test the levels of NEFA, E, NE, T3, and T4. BAT was used to determine the mRNA and protein expression of UCP1, Dio2, and Cidea.

To investigate the metabolic effects of AKG in the DIO model, both male and female C57BL/6 mice at 12 weeks of age were singly housed and switched to HFD (D12492, Guangdong Medical Science Experiment Center). The mice were weighed and randomly assigned to receive water or water supplemented with 2% AKG. Bodyweight and food intake were continuously monitored weekly for 11 weeks. At the end of the experiment, body composition was determined using a nuclear magnetic resonance system (Body Composition Analyzer MiniQMR23-060H-I, Niumag Corporation, Shanghai, China). In females, mice were euthanized to collect and weigh BAT, gWAT, and iWAT. An aliquot of gWAT or iWAT was used for adipocyte size analysis. In males, core body temperature was measured using a RET-3 rectal probe (Kent Scientific, Torrington, CT, USA). Then mice were adapted into Promethion Metabolic Screening Systems (Sable Systems International, North Las Vegas, NV, USA). After adaptation for five days, O_2 consumption and RER were monitored for 3 days. O_2 consumption was normalized by body weight to represent energy expenditure. Subsequently, male mice were exposed to cold stress at 4℃ for 6 hrs. BAT surface temperatures were recorded using a FLIR E60 thermal imaging camera (FLIR Systems, Wilsonville, OR, USA). Then mice were euthanized to collect and weigh BAT, gWAT, and iWAT. An aliquot of gWAT or iWAT was used for adipocyte size analysis. Another aliquot of gWAT or iWAT was used to determine the mRNA expression of PPARγ, FASN, and ACC or protein expression of p-HSL and ATGL. BAT was used to determine the mRNA

and protein expression of UCP1, Dio2, and Cidea. Serum was also collected to test the levels of AKG, NNEFA, E, NE, T3, and T4.

Acute effects of AKG on energy homeostasis

To examine the acute effects of AKG on BAT thermogenesis and WAT lipolysis, 12-week-old C57BL/6 male mice were weighed and randomly divided into two groups to receive i.p. injection of either saline or 10 mg/kg AKG, respectively. Immediately after i.p. injection, mice were exposed to cold stress at 4℃. After 6-hr cold exposure, BAT surface temperatures were recorded as described before. One week after cold exposure, mice were concordantly i.p. injected with saline or 10 mg/kg AKG. Three hours after injection, the mice were euthanized to collect serum, iWAT, BAT, and adrenal gland. An aliquot of iWAT was used to determine the protein expression of ATGL and p-HSL. Serum was used to test E, NE, and NEFA levels. BAT was used to determine the mRNA and protein expression of UCP1, Dio-2, and Cidea. The adrenal gland was used to determine the protein expression of PLCβ and p-Erk.

To examine the acute effects of AKG on physical activity and heart rate, another cohort of 12-week-old C57BL/6 male mice was used. Under anesthesia, a telemetric Mini Mitter probe (G2 HR E-Mitter, Starr Life Science, Oakmont, PA, USA) was implanted into the abdominal cavity according to the manufacturer's instruction. Two weeks after recovery, mice were adapted into Promethion Metabolic Screening Systems. After adaptation for five days, mice were weighed and randomly divided into two groups to receive i.p. injection of saline or 10 mg/kg AKG at 7:00 am. The physical activity and heart rate were monitored real-time for 24h by Promethion Metabolic Screening Systems.

To examine if ADRB3 mediates the metabolic effects of AKG, 10-week-old male C57BL/6 mice were singly housed and adapted into Promethion Metabolic Screening Systems. After five days of adaptation, mice were weighed and randomly divided into four groups receiving i.p. injected of saline, 10 mg/kg AKG, 1 mg/kg SR59230A (S8688, Sigma Aldrich) or AKG + SR59230A at 7:00 am. O_2 consumption and RER were continuously recorded for 24 hrs after injection as described above.

AKG's effects in adrenalectomized mice

Eight-week-old C57BL/6 male mice were anesthetized with inhaled isoflurane. As described before (Makimura et al, 2003; Makimura et al, 2000), these mice received bilateral adrenalectomy or sham surgery. To compensate for the lass of mineralocorticoids, drinking water was supplemented with 0.9% NaCl. Two weeks after the surgery, when all mice recovered from body weight loss induced by surgery stress, mice from each surgery group were weighed and further divided into two groups receiving either water or water supplemented with 2% AKG. Bodyweight and food intake were continuously monitored weekly for ten weeks. At the end of the experiment, cold-induced BAT thermogenesis was tested as described before. Body composition and weighs of iWAT and gWAT were determined. An aliquot of iWAT was used to determine protein expression of p-HSL and ATGL. BAT was used to determine the mRNA and protein expression of UCP1, Dio2, and Cidea. Serum was also collected to test the levels of NEFA.

AKG response in *ex vivo* cultured BAT

AKG's effects on oxygen consumption rate (OCR) was determined in *ex vivo* cultured BAT. Briefly, the dissolved oxygen rate was measured by Micro 4 Oxygen meter (Presens Precision Sensing GmbH,

Regensburg, Germany) at 0, 5, 15, 25, 35, 45, and 55 mins after vehicle, 50 μM AKG, 100 μM AKG, or 10 μM NE treatment. The differences in dissolved oxygen rate between sessions represent OCR. In another separate trial, NEFA was measured in the supernatant medium from BAT after 30 min of *ex vivo* treatment with vehicle, 50 μM AKG, 100 μM AKG, or 10 μM NE.

AKG response in chromaffin cells *in vitro* and adrenal glands *ex vivo*

To determine the effects of AKG on adrenal E release, adrenal gland were *ex vivo* cultured and treated with 0, or 100 μM AKG for 30 mins. The supernatant medium was collected to test the levels of E and NE, while adrenal gland was collected for western-blot analysis of PLCβ protein expression. Similarly, chromaffin cells were treated with 0, 5 μM, 50 μM, 60 μM, 80 μM, 100 μM AKG for 30 mins. The supernatant medium was collected to test the levels of E and NE.

In another separate trial, the effects of AKG on intracellular calcium concentration were tested in chromaffin cells. Intracellular calcium was measured by calcium fluorometry following the manufacturer's instructions of fluo-8 AM kit (AAT Bioquest, Sunnyvale, CA, USA). Briefly, chromaffin cells were washed twice with Hank's Balanced Salt Solution (HBSS, pH=7.2–7.4) containing 8 g/L NaCl, 0.4 g/L KCl, 0.1 g/L $MgSO_4.7H_2O$, 0.1 g/L $MgCl_2.6H_2O$, 0.06 g/L $Na_2HPO_4.2H_2O$, 0.06 g/L KH_2PO_4, 1 g/L glucose, 0.14 g/L $CaCl_2$, and 0.35 g/L $NaHCO_3$ and incubated with 10 μ M fluo-8-AM at 37 °C for 1 h. After incubation, cells were washed twice again with HBSS and incubated with vehicle, 100 μM AKG, 100 μM succinate or 100 μM glutamate. Nikon Eclipse Ti-s microscopy was used to observe fluorescence which was initiated by AKG, succinate or glutamate we added. Fluorometric data were acquired at excitation and emission wavelengths of 490

and 525 nm (490/525 nm) every 2 s over a 180 s period.

Expression mapping of AKG sensors

Twelve-week-old male C57BL/6 mice were euthanized to collect adrenal gland, testis, hypothalamus, cortex, BAT, iWAT, gWAT, gastrocnemius muscle, soleus muscle, and liver. The mRNA expressions of OXGR1, PHD1, PHD2, PHD3, TET1, TET2, JMJD3, OCT4, ASZ1, wdfc15a, and Dazl in these tissues were tested by absolute RT-PCR. An aliquot of adrenal gland was fixed in 4% paraformaldehyde and cut into 8 μm sections. Sections will then be subjected to immunofluorescent staining of OXGR1.

OXGR1 knock-down in chromaffin cell

The OXGR1 siRNA and negative control siRNA was purchased from GenePharma Co., Ltd. (Shanghai, China) and transfected into chromaffin cells using Lipofectamine reagents (Invitrogen, Carlsbad, CA, USA) by manufacturer's instructions. The sequences of siRNA targeting OXGR1 are 5'-CCGACGAGCAAAUCUCAUUTT-3' (sense) and 5'-AAUGAGAUUUGCUCGUCGGTT-3' (anti-sense). The sequences of negative control siRNA are 5'-UUCUCCGAACGUGUCACGUTT-3' (sense) and 5'-ACGUGACACGUUCGGAGAATT-3' (anti-sense). An aliquot of transfected cells was collected to determine OXGR1 protein expression. Another aliquot of transfected cells was treated with 0, or 100 μM AKG for 30 mins. The supernatant medium was collected to test the levels of E. The last aliquot of transfected cells was used for fluo-8 AM assay to test AKG's effect on calcium flux as described above.

OXGR1 knockout (KO) mouse model

OXGR1KO mouse model was generated by Shanghai Model Organisms Center, Inc. The guide RNAs targeting exon 4 of OXGR1 gene were designed using CRISPR/Cas9 strategy as shown in a specific scheme (Fig. EV4A). The Cas9 mRNA was *in vitro* transcribed using mMESSAGE mMACHINE T7 Ultra Kit (Ambion, TX, USA) according to the manufacturer's instructions. Two sgRNAs were designed to delete the OXGR1 protein-coding region using the online designer (http://crispr.mit.edu/). The target sequences of two sgRNAs were 5'-GTTTAACCTCTAACTTCCAC-3' and 5'-TTAAAGGCTCGAAGGCTAAC-3'. The sgRNAs were *in vitro* transcribed using the MEGAshortscript Kit (ThermoFisher, USA) and subsequently purified using MEGAclearTM Kit (Ambion, Life Technologies). The mixture of Cas9 mRNA and sgRNAs were co-injected into zygotes of C57BL/6 mouse by microinjection. F0 mice were genotyped by PCR, using primer pairs: Forward: 5'-TATACCAGCTGTTTTTCTTGTTGC-3'; Reverse：5'-GATGCGTGGCTGTTTATGTCA-3'. The genotype of positive F0 was confirmed by sequencing. The positive F0 mice were chosen and crossed with C57BL/6 mice to produce F1 mice. The genotype of F1 mice was identified by PCR and confirmed by sequencing (Fig. EV6B). The mRNA expression of OXGR1 was also compared between WT and OXGR1KO mice. F1 mice with protein-coding region deletion in the exon four were used to intercrossed to obtain the homozygous OXGR1KO mice.

To determine if OXGR1 mediates the metabolic effects of AKG, male OXGR1KO and WT control mice at 12 weeks of age were singly housed and switched to HFD. These mice were weighted and further divided into two groups, receiving water or water supplemented with 2% AKG. Body weight was continuously monitored weekly for 13 weeks. At the end of the experiment, body composition was measured by QMR, while food intake, O_2 consumption, and RER were monitored by Promethion

Metabolic Screening Systems as described before. Then mice were euthanized to collect and weigh gWAT and iWAT. An aliquot of gWAT or iWAT was used for adipocyte size analysis by HE staining. Another aliquot of both gWAT or iWAT was used to determine protein expression of p-HSL and ATGL. BAT was collected to determine the protein expression of UCP1. Serum was also collected to test the levels of E.

To determine if OXGR1 is required for the anti-obesity effects of exercise, exercise-induced metabolic beneficial effects were compared between WT and OXGR1KO mice. Specifically, male C57BL/6 WT control or OXGR1KO mice were switched to HFD at eight weeks of old. After 12 weeks of HFD feeding, mice were further divided into two groups, receiving non-exercise or resistance exercise. For resistance exercise group, mice first received 3 days of adaption and then 11 days of resistance training. Adaptation and resistance training was conducted as described before. Bodyweight and food intake of all groups were monitored every day. Body composition was measured at 0, 4, 8, and 14 days after exercise. At the end of the 14-day exercise, O_2 consumption and RER were monitored by Promethion Metabolic Screening Systems as described before. Then mice were euthanized to collect and weigh gWAT and iWAT. An aliquot of iWAT was used to determine the mRNA expression of p-HSL and ATGL. BAT was collected to determine the mRNA expression of UCP1. Serum was also collected to test the levels of E. In a separate experiment, another cohort of male OXGR1KO mice (10 weeks) received 40-min resistant exercise as described before. Serums were collected before and immediately after exercise.

Adrenal-specific reexpression or overexpression of OXGR1

For the generation of OXGR1 overexpression HBAAV2/9-OXGR1 and control HBAAV2/9-GFP strains, OXGR1 coding region or GFP cassette was subcloned into the backbone of a pHBAAV-CMH-MCS-3flag-EF1-ZsGreen expression plasmid (Hanbio Biotechnology, Shanghai, China). Following DNA sequencing screening, the AAV plasmid was packaged into AAV serotype 2/9 virus by Hanbio Biotechnology. To specifically test if adrenal OXGR1 mediates the metabolic effects of AKG, OXGR1 adrenal-specific reexpression mouse model ($GRPRE^{AG}$) was generated by selectively delivering HBAAV2/9-OXGR1 into the adrenal gland of OXGR1KO mice. Briefly, 8-week-old male OXGR1KO mice were anesthetized with inhaled isoflurane. Bilateral incisions were made through the shaved skin of the abdominal wall just ventral to the kidney. Two μL HBAAV2/9-OXGR1 (1.1×10^{12} VG/mL) or control HBAAV2/9-GFP (1.4×10^{12} GC/mL) was bilaterally injected into the exposed adrenal glands. After two weeks of surgery recovery, mice were switched to HFD and further divided into two groups, receiving water or water supplemented with 2% AKG for 12 weeks (n = 8 per group). The long-term effects of AKG on body weight gain, food intake, energy expenditure, RER, body composition, and lipolysis and thermogenesis of fat tissues were investigated as described in the OXGR1KO model. Adrenal glands were also collected to test the mRNA expression of OXGR1. Similarly, an adrenal-specific overexpression mouse model ($OXGR1OE^{AG}$) was generated by selectively delivering HBAAV2/9-OXGR1 into the adrenal gland of C57BL/6 WT mice. The metabolic effects of long-term AKG supplementation were compared between $OXGR1OE^{AG}$ and control mice with an adrenal-specific injection of HBAAV2/9-GFP following the same experimental procedures as in the OXGR1RE studies.

HE staining

HE staining was performed as described before (Zhu et al, 2017). Briefly, an aliquot of iWAT and gWAT were fixed with 10% formalin and embedded with paraffin. Then fixed iWAT and gWAT were sectioned and stained with hematoxylin and eosin (HE). Pictures of stained adipose tissue were obtained in the same location with up to six fields of view. Adipocyte sizes of thirty adipocytes were analyzed per section. Data from 5 mice were averaged for each group.

Western blot analysis

Western blot analysis was performed as described before (Zhu et al, 2017). Briefly, total protein lysates (20 μg) were immunoblotted with rabbit-anti-OXGR1 antibody (1:2000, LS-A1865, LifeSpan BioSciences, Inc., Seattle, WA, USA), rabbit-anti-p-HSL (Ser563) (1:1000, #4139, Cell Signaling), rabbit-anti-HSL (1:500, sc-17194, Santa Cruz Biotechnology, Inc., Dallas, TX, USA), rabbit-anti-ATGL (1:1000, #2138, Cell Signaling), rabbit-anti-UCP1 (1:1000, #14670, Cell Signaling), rabbit-anti-p-Erk (1:1000, #4370, Cell Signaling), rabbit-anti-Erk (1:1000, #9102, Cell Signaling), rabbit-anti-PLCβ (1:500, Santa Cruz), rabbit-anti-p-AMPKα (Ser 485)(1:1000, #AP0116, ABclonal), rabbit-anti-AMPKα (1:2000, #A17290, ABclonal), rabbit-anti-FoXO1 (1:1000, #9454, Cell Signaling), rabbit-anti-p-FoXO1 (Ser 256) (1:1000, #9461, Cell Signaling), rabbit-anti-p-IKK (Ser 176) (1:1000, #2078, Cell Signaling), rabbit-anti-IKK (1:1000, #2682, Cell Signaling), rabbit-anti-NF-κB (p65) (1:1000, #8242, Cell Signaling), rabbit-anti-p-IκB (Ser32) (1:1000, #2859, Cell Signaling), rabbit-anti-IκB (1:1000, #4812, Cell Signaling), rabbit-anti-β-Tubulin (1:50000, AP0064, Bioworld Technology, Inc., St. Louis Park, MN, USA), followed by donkey-anti-goat HRP conjugated secondary antibody or goat-anti-rabbit HRP conjugated secondary antibody (1:50000, bs-0294D or bs-0295G, Bioss, Woburn, MA, USA). The levels of Tubulin served as the loading

1008 control.

1009

1010 **Relative quantitative PCR analysis**

1011 Real Time PCR assay was performed as described before (Cai et al, 2016). Briefly, total mRNA was
1012 extracted and digested with DNase I. The total mRNA (1 μg) was reverse-transcribed to cDNA using
1013 oligo (dT) 18 primer. SYBR Green relative quantitative real-time PCR was performed according to
1014 published protocols (Bookout & Mangelsdorf, 2003). Results were normalized by the expression of
1015 house-keeping gene β-actin. The primer sequences are shown as follows: β-actin, S: 5'-
1016 CCACTGGCATCGTGATGGACTCC -3', A: 5'-GCCGTGGTGGTGAAGCTGTAGC -3'; UCP1, S:
1017 5'-ACTGCCACACCTCCAGTCATT-3', A: 5'-CTTTGCCTCACTCAGGATTGG-3'; Cidea, S:
1018 5'-TGCTCTTCTGTATCGCCCAGT-3', A: 5'-GCCGTGTTAAGGAATCTGCTG-3'; Dio2, S:
1019 5'-AATTATGCCTCGGAGAAGACCG-3', A: 5'-GGCAGTTGCCTAGTGAAAGGT-3'; ATGL, S:
1020 5'-ACACCAGCATCCAGTTCAACCTTC-3', A: 5'-GACATCAGGCAGCCACTCCAAC-3', HSL, S:
1021 5'-CTCCTCATGGCTCAACTCC-3', A: 5'-ACTCCTGCGCATAGACTCC-3'; PPARγ, S:
1022 5'-GGAAGACCACTCGCATTCCTT-3', A: 5'-GTAATCAGCAACCATTGGGTCA-3'; FASN, S:
1023 5'-CTCCAAGCAGGCGAACACG-3', A: 5'-CGAAGGGAAGCAGGGTTGAT-3'; ACC, S:
1024 5'-TGATTCTCAGTTCGGGCACT-3', A: 5'-CTCTGCCTGCACTTTCTCTG-3'; CD137, S: 5'-
1025 CACGGAGCTCATCTCTTGGT-3', A: 5'-GTCCACCTATGCTGGAGAAGG-3'; TBX1, S:
1026 5'-TGGGACGAGTTCAATCAGCT-3', A: 5'-CACAAAGTCCATCAGCAGCA-3'; TMEM26,
1027 S:5'-ACCCTGTCATCCCACAGAG-3', A: 5'-TGTTTGGTGGAGTCCTAAGGTC-3'; slc27a1, S:
1028 5'-CGCTTTCTGCGTATCGTCTG-3', A: 5'-GATGCACGGGATCGTGTCT-3'; CD40, S:
1029 5'-TTGTTGACAGCGGTCCATCTA-3', A: 5'-CCATCGTGGAGGTACTGTTTG-3'; CITED1, S: 5'-

GAGGCCTGCACTTGATGTC-3', A: 5'-CACGGAGCTCATCTCTTGGT-3';

Absolute quantitative PCR analysis

The absolute quantitative RT-PCR assay was performed according to published protocols (Chini et al, 2007). Briefly, the cDNA samples of mouse tissues were first generated as described in relative quantitative RT-PCR analyses. The cDNA was then used as the template to amply target genes using primers listed as follows: JMJD3, S: 5'-CACCCCAGCAAACCATATTATGC-3', A: 5'-CACACAGCCATGCAGGGATT-3'; OXGR1, S: 5'-CTGCCTGCCATTGGTGATAGTGAC-3', A: 5'-TGCCTGCTGGAAGTTATTGCTGAC-3'; PHD1, S: 5'-TGTCACTGTGGTGTTTGGCTAC -3', A: 5'-GCATTTATCAGGATGGGAAGG-3'; PHD2, S: 5'-CCTGCCATTGGTGATAGTGAC-3', A: 5'-GGGTGGAAGGGTAAGAAACAT-3'; PHD3, S: 5'-TCAAGGCTGTGAGGTAGTCT-3', A: 5'-CTTGCATGGGAGGCTCATC-3'. OCT4, S: 5'-GAGGAGTCCCAGGACATGAA-3', A: 5'-AGATGGTGGTCTGGCTGAAC-3'; ASZ1, S: 5'-CTTTGGCGGAGGTGCTAGAT-3', A: 5'-TGCGACTACAGAGGTTCGTG-3'; Wfdc15a, S: 5'-TGAAGCCAAGCAGCCTCCTA-3', A: 5'-AGGTTGTCCAGGGTTCCACA-3'; TET1, S: 5'-CCCGGGCTCCAAAGTTGTG-3', A: 5'-GCAGGAAACAGAGTCATT-3'; TET2, S: 5'-TGTGTGGCACTAGATTTCAT-3', A: 5'-AGTCTCTGAAGCCTGTTGAT-3'; TET3, S: 5'-CAGTGGCTTCTTGGAGTCACCTC-3', A: 5'-GGATGGCTTTCCCCTTCTCTCC-3'; Dazl, S: 5'-TGCAGCCTCCAACCATGATGAATC-3', A: 5'-CACTGTCTGTATGCTTCGGTCCAC-3'; UTX, S: 5'-AAGGCTGTTCGCTGCTACG-3', A: 5'-GGATCGACATAAAGCACCTCC-3'. The Ct value of each gene was obtained for further analysis. To generate a standard curve for each gene, the specific PCR amplification product was purified by electrophoresis and gel extraction using Agarose Gel Recovery kit (D2111-02, Magen BioSciences,

Waltham, MA, USA). The DNA concentration of each product was measured by NanoDrop (2000c, ThermoFisher Scientific). The absolute copy number of each sample was calculated according to the following formula: $C=A/B \times 6.02 \times 10^{14}$. Where A is the concentration obtained by OD260 analysis (ng/μL), B is the molecular weight of the synthesized DNA (Daltons), and C is the copy number of the synthesized DNA (copies/μL). Subsequently, eight-fold serial dilution was carried out on each purified PCR product 12 times. The dilutions of each product were used as the templates for SYBR Green quantitative real-time PCR to target gene using above-mentioned primers amply. The Ct value of each dilution was obtained. The standard curve of each gene was plotted as a linear regression of the Ct values versus the log of the copy number. The final quantification data of each gene in different tissues were obtained by interpolating Ct value into the standard curve.

Immunofluorescence staining (IF)

Adrenal gland sections were incubated with the primary rabbit-anti-OXGR1 antibody (1:1000, LS-A1865, LSBio) at room temperature overnight, followed by goat-anti-rabbit FITC conjugated secondary antibody (1:1000, bs-0295G, Bioss) for one hr. Sections were mounted on slides and coverslipped with Mounting Medium with DAPI (H-1200, Vector Laboratories, Burlington, ON, Canada). Fluorescent images were obtained using Nikon Eclipse Ti-s microscopy (Nikon Instruments, Tokyo, Japan).

NF-κB translocation

Adrenal gland chromaffin cell was cultured in six well plates with an adhesive coverslip. About 50% coverage of coverslip, the cell was treated with 0, or 100 μM AKG for 3 hr. OXGR1 was interfered

with siOXGR1 as described above. IKK was inhibited by IKK inhibitor IKK16 (S2882, Selleck, USA) for 3 hr. IKK signaling pathway was further tested by western blot. Cell-climbing slices were rinsed 3 times in PBS, fixed in paraformaldehyde for 10 min and washed in 0.4% Triton X-100 (T9284, Sigma) for 30 min. After 1 hr of blockage in 3% goat serum at room temperature, the slices were incubated overnight in rabbit anti-NF-κB (p65) (1:1000) at room temperature. The next day, the slices were rinsed 3 times in PBS and incubated in goat-anti-rabbit FITC conjugated secondary antibody (1:1000, bs-0295G, Bioss). Then the slices were coverslipped with Mounting Medium with DAPI (H-1200, Vector Laboratories, Burlington, ON, Canada). Fluorescent images were obtained using Nikon Eclipse Ti-s microscopy (Nikon Instruments, Tokyo, Japan).

Immunohistochemical staining (IHC)

Adipose tissue IHC staining was performed as described before (Bal et al, 2017). Mice adipose tissues (brown and white adipose tissue) were fixed with 10% formalin, embedded with paraffin and sliced into 10 μm sections. The sections were mounted on slides and dehydrated with sequential alcohol gradient (0%, 50%, 70%, 80%, 90% and 100%). Antigen retrieval was performed by incubating with EDTA reagent at 90℃ for 10 min. The sections were then incubated with 0.3% H_2O_2 for 30 min, followed by blocking solution buffer for one hr at room temperature. Subsequently, the sections were incubated in rabbit anti-phospho-HSL (1:1000) or rabbit-anti-UCP1 (1:1000) overnight, followed by Biotin-SP-AffiniPure Goat Anti-Rabbit IgG (111-065-003, Jackson ImmunoResearch, West Grove, PA, USA) for one hr at room temperature. The sections were then visualized by incubation with the ABC kit (PK-4000, Vector Laboratories, Burlingame, CA, USA) according to manufacturer's instructions. Sections were then treated with diaminobenzidine (D12384, Sigma) for five mins,

followed by dehydration in a graded ethanol series from 50% to 100% and a final wash in xylene. Images were obtained using Upright microscopes, and Image-Pro Plus software was used to quantify grayscale. Up to six fields of view were captured from the same location within each adipose tissue.

Hormone, metabolite and enzyme activity assay

Serum levels of epinephrine (E), norepinephrine (NE), thyroxine (T4), triiodothyronine (T3), and non-esterified fatty acid (NEFA), as well as the enzyme activity of alpha-ketoglutarate dehydrogenase (OGDH), isocitrate dehydrogenase (ICDHm), and glutamate dehydrogenase (GDH) in different muscle tissues were measured using commercial available kits according to manufacturer's instructions (Nanjing Jiancheng Bioengineering Institute, Nan Jing, China).

Muscle contraction experiment *in vivo*

The method was described as previously (Ato et al, 2016; Park et al, 2012). For *in vivo* gastrocnemius electric stimulation, 10-weeks C57BL/6 male mice were anesthetized by isoflurane, and the gastrocnemius muscles were surgically exposed. The soleus muscle was removed. Subsequently, the mice were positioned with their right foot on a footplate. The gastrocnemius muscle was connected to an electrical stimulator with an isolator. The insulation pad was adjusted to 37 °C to cover the muscle during the whole experimental period of time. Physiological solution (2.5 mM Ca^{2+} Tyrode solution:, 5 mM KCl, 140 mM NaCl, 10 mM HEPES, 2 mM $MgCl_2$, 2.5 mM $CaCl_2$ and 10 mM glucose) was used to infiltrate muscle. Supramaximal electricity with a pulse width of 1 ms was delivered to muscles by a pair of platinum electrodes placed in parallel. Set the stimulation parameters, the wave width was 1 ms, the delay was 100 ms, the single continuous stimulus was used, the stimulation

frequency was 50 Hz, and the stimulation intensity gradually increases from zero under the condition of continuous single stimulation. Electric stimulate in unilateral gastrocnemius for 40 min (10 times, each time for 4 min, rest for 2 min between stimulates). The effect of temperature on muscle contraction characteristics can be effectively controlled during the experiment to prevent muscle inactivation. The contractile performance was assessed by measuring half relaxation time (the time required for the force to decrease 50% from the peak value at the end of stimulation). The *in vivo* contractility experiment was set up using the BL-420F biological signal acquisition and analysis system (Chengdu Taimeng software Co., Ltd. China). After stimulation, the mice were sacrificed, and plasma was collected to analyze the enrichment of AKG.

Primary brown adipocyte preparation and differentiation

The interscapular brown adipose stromal vascular fraction was obtained from 6 weeks C57BL/6 male mice as described previously (Mills et al, 2018). In brief, interscapular brown adipose tissue was dissected, and washed in PBS. Then it was minced and digested for 45 min at 37 °C in PBS (1.5 mg mL^{-1} collagenase B, 123 mM NaCl, 5 mM KCl, 1.3 mM $CaCl_2$, 5 mM glucose, 100 mM HEPES, and 4% essentially fatty-acid-free BSA). The obtained tissue suspension was filtered through a 40 μm cell strainer and then centrifuged at 600g for 5 min to pellet the SVF. After centrifugation, the upper layer of liquid (grease layer) was gently blotted dry; then the medium layer was blotted dry, so as not to affect the underlying precipitate (red cells on the pellet), then add 10 ml of SVF (10% FBS) medium. The 10 mL pipette was blown up and down 5-10 times, and the precipitate was blown off, then passed through a 40 μm filter sieve, mixed with 3 volumes of SVF (10% FBS) medium, and centrifuged at 600 g for 5 min. Poured off the culture solution and retained the precipitate. Cells were resuspended in

8-10 mL SVF (10% FBS) medium. The dish was evenly blown, inoculated into a 10 cm^2 petri dish to inoculate the cells uniformly. The cell pellet was resuspended in brown adipocyte culture medium and plated evenly. Cells were maintained at 37 °C in 10% CO_2. (The above operations are all started in the afternoon or evening within 90 min). The next morning (about 12 h), remove the culture medium of the culture dish, wash the cells 4 times in warm PBS (4 mL) (fast cross shake for 5-10 s). The amount of impurities was determined whether to continue washing (normal cells are adherent spindles, angular, transparent and floating cells are not), and after washing, 10 ml of SVF (10% FBS) medium was added. The following morning, brown pre-adipocytes were induced to differentiate with an adipogenic cocktail (0.5 mmol/L isobutylmethylxanthine, 5 mmol/L dexamethasone, 320 nmol/L insulin, 1 nmol/L triiodothyronine and 0.125 mmol/L indomethacin) in the adipocyte culture medium. Two days after induction, cells were re-fed every 48 h with adipocyte culture medium containing 1 μM rosiglitazone, 1 nM T3, and 0.5 μg mL^{-1} insulin. Cells were fully differentiated by day 7 after induction.

OCR

Cellular OCR was determined using an Agilent Seahorse XFp analyzer (S7802A, Agilent technologies). The culture of C2C12 and HepG2 cell were described as previously (Cai et al, 2018; Xu et al, 2018). C2C12 (China Infrastructure of Cell Line Researcher, China) and primary brown adipocytes were plated and differentiated in Seahorse XFp cell culture miniplates (103022100, Agilent technologies). Adrenal gland medulla cell and HepG2 cell were plated and differentiated in Seahorse XFp cell culture miniplates. Prepare assay medium by supplementing Agilent Seahorse XF Base Medium (102353-100, 103193-100, 103334-100, Agilent technologies). Agilent Seahorse

recommends 1 mM pyruvate (S8636, Sigma), 2 mM glutamine (G8540, Sigma), and 10 mM glucose (G8769, Sigma) as a starting point. Before analysis, the adipocyte culture medium was changed to respiration medium consisting of DMEM lacking $NaHCO_3$ (Sigma), NaCl (1.85 g/L), phenol red (3 mg/L), 2% fatty-acid-free BSA, and sodium pyruvate (1 mM), adjust pH to 7.4. Basal respiration was determined to be the OCR in the presence of substrate (1 mM sodium pyruvate) alone. Warm the assay medium to 37 °C. Adjust pH to 7.4 with 0.1 N NaOH. Oligomycin inhibits ATP synthase (complex V), and the decrease in OCR relates to the mitochondrial respiration associated with cellular ATP production after injection of oligomycin (1 μM). Spare respiratory capacity, defined as the difference between maximaland basal respiration, can be calculated by the Carbonyl cyanide-4 (trifluoromethoxy) phenylhydrazone (FCCP) (2 μM)-stimulated OCR. The combination of complex I inhibitor-Rotenone (0.5 μM) and complex III inhibitor-antimycin A (0.5 μM)canshut down mitochondrial respiration and enable the calculation of nonmitochondrial respiration driven by processes outside the mitochondria. The Agilent Seahorse XF Cell Mito Stress Test Report Generator automatically calculates the Agilent Seahorse XFp Cell Mito Stress Test parameters from Wave data.

Bomb calorimetry of feces.

Calorimetry was conducted using a calorimeter (IKA C200, Germany) as described previously (Mills et al, 2018). C57BL/6 male mice were fed HFD and fecal specimens were collected over a 48-h period. Collected fecal samples were baked at 60 °C for 24 h to remove water content. Fecal samples were combusted, and the energy content of the fecal matter was measured as the heat of combustion (kJ/g).

Blood pressure test

Mice blood pressure was tested by a non-invasive blood pressure measurement system with the biological signal acquisition and analysis system (BP300A, Chengdu Taimeng software Co., Ltd. China). The mice were restrained on a fixed frame and placed on a 37 °C thermostat pad. After 10-mins acclimation, the blood pressure sensor was placed on the root of the mice tail. Then the systolic and diastolic blood pressure of the mice was monitored and recorded in real-time.

16S rDNA sequencing

Fresh feces of mice were collected at 9:00 a.m. and frozen rapidly at -80 °C. 16S sequencing was carried out at Beijing Novogene Co., Ltd. The experimental method was referred to the previous literature (Chen et al, 2017). Total genome DNA from samples was extracted using the CTAB/SDS method and the concentration and purity were monitored by 1% agarose gels. Diluted the processed DNA to 1 ng/μL by sterile water. Amplicon Generation 16S rRNA/18S rRNA/ITS genes of distinct regions (16S V3-V4, 18S V4, ITS1 / ITS2, Arc V4, et al.) were amplified by specific primer (e.g. 16S V3-V4: 341F-806R, 18S V4: 528F-706R, et al.) with the barcode. The PCR reactions were carried out in 30 μL reactions consist of 15 μL of Phusion High-Fidelity PCR Master Mix (New England Biolabs), 0.2 μM of forward and reverse primers and 10 ng templated DNA sample. The procedure of thermal cycling was as follows: 98℃for 1 min, followed by 30 cycles of denaturation at 98℃for 10 s, annealing at 50℃for 30 s, elongation at 72℃ for 30 s, 72℃ for 5 min. Then, PCR Products Mixing and Purification Mix same volume of 1×loading buffer (contained SYB green) with PCR products was detected on 2% agarose gel for electrophoresis. PCR products were mixed in equidensity ratios and the mixture PCR product was purified with GeneJETTM Gel Extraction Kit (Thermo Scientific). Library preparation and sequencing were generated by Ion Plus Fragment Library Kit 48 rxns

(Thermo Scientific) and the library quality was assessed on the Qubit 2.0 Fluorometer (Thermo Scientific). At last, the library was sequenced on an Ion S5TM XL platform, and 400 bp/600 bp single-end reads were generated. Sequences analyses were performed using Uparse software (Uparse v7.0.1001， http://drive5.com/uparse/) and 97% similarity were considered to the same OTUs. Representative sequence for each OTU was screened for further annotation. The Silva Database (https://www.arb-silva.de/) was used based on Mothur algorithm to annotate taxonomic information. For the difference analysis, both weighted and unweighted of Beta diversity analysis were used to evaluate differences of species complexity, which can be calculated by QIIME software (Version 1.7.0). Anosim and Adonis analysis use anosim function and Adonis function of R vegan package, respectively.

Transcriptomics

Samples from adrenal chromaffin cell were used for transcriptomic signature analysis. The untargeted transcriptomics profiling was performed on the Illumina platform (Novogene, Beijing, China) by Novogene Co., Ltd (Beijing, China). The sample preparation procedures are referred to in the previously published methods with minor modifications (Parkhomchuk et al, 2009). RNA was extracted by a RNA extraction kit (Magen, China). The RNA integrity was assessed by the RNA Nano 6000 Assay Kit of the Bioanalyzer 2100 system (Agilent Technologies, CA, USA). Total RNA (3 μg per sample) was used for the RNA sample preparations. Sequencing libraries were generated using NEBNext® UltraTM RNA Library Prep Kit for Illumina® (NEB, USA) following the manufacturer's recommendations and index codes were added to attribute sequences to each sample.

Briefly, mRNA was fist purified by poly-T oligo-attached magnetic beads. Fragmentation was carried

out using divalent cations under elevated temperature in NEBNext First Strand Synthesis Reaction Buffer (5X). Next, First-strand cDNA was synthesized using random hexamer primer and M-MuLV Reverse Transcriptase (RNase H). And the second strand cDNA synthesis was subsequently performed using DNA Polymerase I, and RNase H. Remaining overhangs were converted into blunt ends via exonuclease/polymerase activities. After adenylation of 3' ends of DNA fragments, NEBNext Adaptor with hairpin loop structure was ligated to prepare for hybridization. The library fragments were purified with AMPure XP system (Beckman Coulter, Beverly, USA) to obtain cDNA fragments of preferentially 250~300 bp in length. Finally, 3 μL USER Enzyme (NEB, USA) was used with size-selected, adaptor-ligated cDNA at 37 °C for 15 min followed by 5 min at 95 °C before PCR. PCR was performed with Phusion High-Fidelity DNA polymerase, Universal PCR primers, and Index (X) Primer. At last, the Agilent Bioanalyzer 2100 system was used for the purify of PCR products and evaluate of library quality.

cBot Cluster Generation System (TruSeq PE Cluster Kit v3-cBot-HS, Illumia) and Illumina Hiseq platform were used for the clustering of the index-coded samples and the library preparations sequenced after cluster generation, and 125 bp/150 bp paired-end reads were generated. Gene networks representing key genes were identified by using Ingenuity Pathways Analysis v7.6 (IPA; Ingenuity Systems).

Endurance exercise training

The method was described as previous (Luo et al, 2012). In brief, the mice engaged in strenuous exercise on a treadmill (47300 TREADMILL, Ugo Basile, Italy) and standard running test to reduce

obesity. 8-week male C57BL/6 male mice were switched to HFD for 12 weeks. At 20 weeks of age, the mice were acclimated to the treadmill with a 5-min run at 10 m/min once daily for 2 days. The endurance test regimen was 10 m/min for the first 20 min, followed by 1 m/min increment increases at about 20-min intervals. The mice were considered exhausted when they were unable to avoid repeated electrical shocks. Exercise endurance capacity was equated with the total running distance achieved before exhaustion. The endurance exercise was conducted for 14 days. Exercise time, distance, body weight and food intake were record every day.

UPLC-Orbitrap-MS/MS analysis for metabolites.

The methods were performed as described previously (Go et al, 2019; Hui et al, 2017; Shi et al, 2016; Xin et al, 2018). After thawed, samples were fully homogenized by vortexing for 2 min. Tissue samples were fully ground and homogenized. One hundred μL of serum or tissue samples were transferred in a 1.5 mL EP microtube, and 500 μL of methanol (mass spectrometry grade) were added to each sample to remove protein. All samples were vortexed for 2 min, centrifuged at 14500 rpm, 4 °C for 15 min. Five hundred μL of the supernatant was taken and dried under nitrogen at normal temperature. After drying, 200 μL of methanol was added to each sample to reconstitute. All samples were vortexed for 2 min, and then centrifuged at 14500 rpm, 4 °C for 15 min. The supernatant was transferredto a sample vial and stored at -80 °C for testing. Serum and tissue extracts were analyzed using LC–MS/MS analysis (Uplc1290-6470A QQQ Liquid chromatography-mass spectrometry instrument, Agilent technologies).

For α-ketoglutarate (AKG), Succinate (SUC) and Malate measurement, the following parameters

were used: Separation column: C18 column, column temperature: 40 °C. Mobile phase: B: 100% acetonitrile, A: Hydrogen peroxide + 0.2% formic acid. Elution gradient: constant elution 99% A, 1% B. Flow velocity: 0.3ml/min. Sample volume: 5uL. Mass Spectrometry Conditions and Parameters: Detector: MS QQQ Mass Spectrometer. Ion source: ESI source; spray voltage 4000 (+), 3500 (-); atomization temperature: 300 degrees; atomizing gas (sheath gas) pressure: 10arb; Scanning mode: negative ion multi-reaction detection (MRM) Compound: MAL parent ion was 133.1 and daughter ion was 115.1 were detected. SUC mother ion was 117.1 and daughter ion was 73.1. AKG mother ion was 145.0 and daughter ion was 57.1 .

For xanthine and hypoxanthine measurement, the following parameters were used: Separation column: C18 column, column temperature: 40 °C. Mobile phase: B: 100% acetonitrile, A: Hydrogen peroxide + 0.2% formic acid. Elution gradient: constant elution 95% A, 5% B. Flow velocity: 0.4ml/min. Sample volume: 5uL. Mass Spectrometry Conditions and Parameters: Detector: MS QQQ Mass Spectrometer. Ion source: ESI source; spray voltage 4000 (+), 3500 (-); atomization temperature: 350 degrees; atomizing gas (sheath gas) pressure: 10arb; Scanning mode: positive ion multi-reaction detection (MRM) Compound: Xanthine parent ion was 153.1 and daughter ion was 110.1 were detected. Hypothine mother ion was 137.1 and daughter ion was 110.1.

Plasma lactate measurement

Serum levels of lactate were measured using commercial available kits according to manufacturer's instructions (Nanjing Jiancheng Bioengineering Institute, Nan Jing, China).

Nuclear protein extraction

For the nuclear or cytoplasmic protein extraction, proteins were isolated according to the procedure of the nuclear extraction kit (Solarbio, SN0020).

Statistics

Statistical analyses were performed using GraphPad Prism 7.0 statistics software (Chicago, IL, USA). Methods of statistical analyses were chosen based on the design of each experiment and indicated in the figure legends. The data were presented as mean ± SEM. $P \leq 0.05$ was considered to be statistically significant.

Study approval

Care of all animals and procedures in South China Agricultural University were confirmed to "The Instructive Notions with Respect to Caring for Laboratory Animals" issued by the Ministry of Science and Technology of the People's Republic of China and were approved by the Animal Subjects Committee of South China Agricultural University.

Author Contributions

Y. Y., P. X. and Q. J. are the main contributors in the conduct of the study, data collection and analysis, data interpretation and manuscript writing; X. C., T. W., W. P., J. S., C. Z., C. Z., D. Y., Z. H., J. Y., Y. Z., M. D., C. Y., F. L., G. X and F. Z contributed to the conduct of the study; S. W., L. W., X. Z., L. I., S. S., Y. J., J. W., J. S., Q. W., P. G., Q. X. and Y. Z. contributed to the manuscript writing and data interpretation; G. S. contributed to the study design, data interpretation, and manuscript writing.

Acknowledgments

This work was supported by grants from National Key Point Research and Invention Program (2016YFD0501205 and 2018YFD0500403 to G. S.), National Natural Science Foundation of China (31790411 to Q. J. and 31572480 to G. S.), Innovation Team Project in Universities of Guangdong Province (2017KCXTD002 to G. S.), National Institute of Diabetes and Digestive and Kidney Diseases from National Institutes of Health (R00DK107008 to P. X., K01DK111771 to Y. J.). We wish to thank Shanghai Model Organisms Center for generating OXGR1KO mouse line, Metabo-Profile Biotechnology for metabolomics analysis and Beijing Novogene Co., Ltd for transcriptomics analysis and 16S rDNA sequencing.

References

Abrigo J, Rivera JC, Aravena J, Cabrera D, Simon F, Ezquer F, Ezquer M, Cabello-Verrugio C (2016) High Fat Diet-Induced Skeletal Muscle Wasting Is Decreased by Mesenchymal Stem Cells Administration: Implications on Oxidative Stress, Ubiquitin Proteasome Pathway Activation, and Myonuclear Apoptosis. *Oxid Med Cell Longev* **2016:** 9047821

Aguer C, Piccolo BD, Fiehn O, Adams SH, Harper ME (2017) A novel amino acid and metabolomics signature in mice overexpressing muscle uncoupling protein 3. *FASEB J* **31:** 814-827

Ait-Ali D, Turquier V, Tanguy Y, Thouennon E, Ghzili H, Mounien L, Derambure C, Jegou S, Salier JP, Vaudry H, Eiden LE, Anouar Y (2008) Tumor necrosis factor (TNF)-alpha persistently activates nuclear factor-kappaB signaling through the type 2 TNF receptor in chromaffin cells: implications for long-term regulation of neuropeptide gene expression in inflammation. *Endocrinology* **149:** 2840-2852

Allen DL, Harrison BC, Maass A, Bell ML, Byrnes WC, Leinwand LA (2001) Cardiac and skeletal muscle adaptations to voluntary wheel running in the mouse. *J Appl Physiol (1985)* **90:** 1900-1908

Ato S, Makanae Y, Kido K, Fujita S (2016) Contraction mode itself does not determine the level of mTORC1 activity in rat skeletal muscle. *Physiological reports* **4**

Bal NC, Singh S, Reis FCG, Maurya SK, Pani S, Rowland LA, Periasamy M (2017) Both brown adipose tissue and skeletal muscle thermogenesis processes are activated during mild to severe cold adaptation in mice. *J Biol Chem* **292:** 16616-16625

Barra NG, Palanivel R, Denou E, Chew MV, Gillgrass A, Walker TD, Kong J, Richards CD, Jordana M, Collins SM, Trigatti BL, Holloway AC, Raha S, Steinberg GR, Ashkar AA (2014) Interleukin-15 modulates adipose tissue by altering mitochondrial mass and activity. *PLoS One* **9:** e114799

Bartelt A, Bruns OT, Reimer R, Hohenberg H, Ittrich H, Peldschus K, Kaul MG, Tromsdorf UI, Weller H, Waurisch C, Eychmuller A, Gordts PL, Rinninger F, Bruegelmann K, Freund B, Nielsen P, Merkel M, Heeren J (2011) Brown adipose tissue activity controls triglyceride clearance. *Nat Med* **17:** 200-205

Bartness TJ, Liu Y, Shrestha YB, Ryu V (2014) Neural innervation of white adipose tissue and the control of lipolysis. *Frontiers in neuroendocrinology* **35:** 473-493

Benito PJ, Bermejo LM, Peinado AB, Lopez-Plaza B, Cupeiro R, Szendrei B, Calderon FJ, Castro EA, Gomez-Candela C, Group PS (2015) Change in weight and body composition in obese subjects following a hypocaloric diet plus different training programs or physical activity recommendations. *J Appl Physiol (1985)* **118:** 1006-1013

Berton R, Conceicao MS, Libardi CA, Canevarolo RR, Gaspari AF, Chacon-Mikahil MP, Zeri AC, Cavaglieri CR (2017) Metabolic time-course response after resistance exercise: A metabolomics approach. *J Sports Sci* **35:** 1211-1218

Bolsoni-Lopes A, Alonso-Vale MI (2015) Lipolysis and lipases in white adipose tissue - An update. *Archives of endocrinology and metabolism* **59:** 335-342

Bookout AL, Mangelsdorf DJ (2003) Quantitative real-time PCR protocol for analysis of nuclear receptor signaling pathways. *Nucl Recept Signal* **1:** e012

Bostrom P, Wu J, Jedrychowski MP, Korde A, Ye L, Lo JC, Rasbach KA, Bostrom EA, Choi JH, Long JZ, Kajimura S, Zingaretti MC, Vind BF, Tu H, Cinti S, Hojlund K, Gygi SP, Spiegelman BM (2012) A PGC1-alpha-dependent myokine that drives brown-fat-like development of white fat and thermogenesis. *Nature* **481:** 463-468

Brosnan ME, Letto J (1991) Interorgan metabolism of valine. *Amino Acids* **1:** 29-35

Bunn SJ, Ait-Ali D, Eiden LE (2012) Immune-neuroendocrine integration at the adrenal gland: cytokine control of the adrenomedullary transcriptome. *J Mol Neurosci* **48:** 413-419

Cai X, Yuan Y, Liao Z, Xing K, Zhu C, Xu Y, Yu L, Wang L, Wang S, Zhu X, Gao P, Zhang Y, Jiang Q, Xu P, Shu G (2018) alpha-Ketoglutarate prevents skeletal muscle protein degradation and muscle atrophy through PHD3/ADRB2 pathway. *FASEB J* **32:** 488-499

Cai X, Zhu C, Xu Y, Jing Y, Yuan Y, Wang L, Wang S, Zhu X, Gao P, Zhang Y, Jiang Q, Shu G (2016) Alpha-ketoglutarate promotes skeletal muscle hypertrophy and protein synthesis through Akt/mTOR signaling pathways. *Sci Rep* **6:** 26802

Chen S, Bin P, Ren W, Gao W, Liu G, Yin J, Duan J, Li Y, Yao K, Huang R, Tan B, Yin Y (2017) Alpha-ketoglutarate (AKG) lowers body weight and affects intestinal innate immunity through influencing intestinal microbiota. *Oncotarget* **8:** 38184-38192

Chin RM, Fu X, Pai MY, Vergnes L, Hwang H, Deng G, Diep S, Lomenick B, Meli VS, Monsalve GC, Hu E, Whelan SA, Wang JX, Jung G, Solis GM, Fazlollahi F, Kaweeteerawat C, Quach A, Nili M, Krall AS, Godwin HA, Chang HR, Faull KF, Guo F, Jiang M, Trauger SA, Saghatelian A, Braas D, Christofk HR, Clarke CF, Teitell MA, Petrascheck M, Reue K, Jung ME, Frand AR, Huang J (2014) The metabolite alpha-ketoglutarate extends lifespan by inhibiting ATP synthase and TOR. *Nature* **510:** 397-401

Chini V, Foka A, Dimitracopoulos G, Spiliopoulou I (2007) Absolute and relative real-time PCR in the quantification of tst gene expression among methicillin-resistant Staphylococcus aureus: evaluation by two mathematical models. *Lett Appl Microbiol* **45:** 479-484

Claustre Y, Leonetti M, Santucci V, Bougault I, Desvignes C, Rouquier L, Aubin N, Keane P, Busch S, Chen Y, Palejwala V, Tocci M, Yamdagni P, Didier M, Avenet P, Le Fur G, Oury-Donat F, Scatton B, Steinberg R (2008) Effects of the beta3-adrenoceptor (Adrb3) agonist SR58611A (amibegron) on serotonergic and noradrenergic transmission in the rodent: relevance to its antidepressant/anxiolytic-like profile. *Neuroscience* **156:** 353-364

1467 Collins S, Yehuda-Shnaidman E, Wang H (2010) Positive and negative control of Ucp1 gene transcription and
1468 the role of beta-adrenergic signaling networks. *Int J Obes (Lond)* **34 Suppl 1:** S28-33
1469
1470 Contreras C, Nogueiras R, Dieguez C, Rahmouni K, Lopez M (2017) Traveling from the hypothalamus to the
1471 adipose tissue: The thermogenic pathway. *Redox Biol* **12:** 854-863
1472
1473 Corkey BE, Shirihai O (2012) Metabolic master regulators: sharing information among multiple systems. *Trends*
1474 *Endocrinol Metab* **23:** 594-601
1475
1476 de Jesus LA, Carvalho SD, Ribeiro MO, Schneider M, Kim SW, Harney JW, Larsen PR, Bianco AC (2001) The
1477 type 2 iodothyronine deiodinase is essential for adaptive thermogenesis in brown adipose tissue. *J Clin Invest*
1478 **108:** 1379-1385
1479
1480 Diehl J, Gries B, Pfeil U, Goldenberg A, Mermer P, Kummer W, Paddenberg R (2016) Expression and
1481 localization of GPR91 and GPR99 in murine organs. *Cell and tissue research* **364:** 245-262
1482
1483 DiPietro L, Stachenfeld NS (2000) Exercise Treatment of Obesity.
1484
1485 Dolezal BA, Potteiger JA (1998) Concurrent resistance and endurance training influence basal metabolic rate in
1486 nondieting individuals. *J Appl Physiol (1985)* **85:** 695-700
1487
1488 Douglas SA, Sreenivasan D, Carman FH, Bunn SJ (2010) Cytokine interactions with adrenal medullary
1489 chromaffin cells. *Cell Mol Neurobiol* **30:** 1467-1475
1490
1491 Duft RG, Castro A, Chacon-Mikahil MPT, Cavaglieri CR (2017) Metabolomics and Exercise: possibilities and
1492 perspectives. *Motriz: Revista de Educação Física* **23**
1493
1494 Finsterer J (2012) Biomarkers of peripheral muscle fatigue during exercise. *BMC musculoskeletal disorders* **13:**
1495 218
1496
1497 Friedberg SJ, Sher PB, Bogdonoff MD, Estes EH, Jr. (1963) The Dynamics of Plasma Free Fatty Acid
1498 Metabolism during Exercise. *J Lipid Res* **4:** 34-38
1499
1500 Go A, Shim G, Park J, Hwang J, Nam M, Jeong H, Chung H (2019) Analysis of hypoxanthine and lactic acid
1501 levels in vitreous humor for the estimation of post-mortem interval (PMI) using LC-MS/MS. *Forensic science*
1502 *international* **299:** 135-141
1503
1504 Gorostiaga EM, Navarro-Amezqueta I, Calbet JA, Sanchez-Medina L, Cusso R, Guerrero M, Granados C,
1505 Gonzalez-Izal M, Ibanez J, Izquierdo M (2014) Blood ammonia and lactate as markers of muscle metabolites
1506 during leg press exercise. *J Strength Cond Res* **28:** 2775-2785
1507
1508 Grassi G, Ram VS (2016) Evidence for a critical role of the sympathetic nervous system in hypertension.
1509 *Journal of the American Society of Hypertension : JASH* **10:** 457-466
1510

1511 Gungor NK (2014) Overweight and obesity in children and adolescents. *Journal of clinical research in pediatric*
1512 *endocrinology* **6:** 129-143
1513
1514 He L, Xu Z, Yao K, Wu G, Yin Y, Nyachoti CM, Kim SW (2015) The Physiological Basis and Nutritional
1515 Function of Alpha-ketoglutarate. *Current protein & peptide science* **16:** 576-581
1516
1517 He W, Miao FJ, Lin DC, Schwandner RT, Wang Z, Gao J, Chen JL, Tian H, Ling L (2004) Citric acid cycle
1518 intermediates as ligands for orphan G-protein-coupled receptors. *Nature* **429:** 188-193
1519
1520 Hou Y, Wang L, Ding B, Liu Y, Zhu H, Liu J, Li Y, Kang P, Yin Y, Wu G (2011) Alpha-Ketoglutarate and
1521 intestinal function. *Frontiers in bioscience (Landmark edition)* **16:** 1186-1196
1522
1523 Hu X, Nesic-Taylor O, Qiu J, Rea HC, Fabian R, Rassin DK, Perez-Polo JR (2005) Activation of nuclear
1524 factor-kappaB signaling pathway by interleukin-1 after hypoxia/ischemia in neonatal rat hippocampus and
1525 cortex. *Journal of neurochemistry* **93:** 26-37
1526
1527 Huffman KM, Koves TR, Hubal MJ, Abouassi H, Beri N, Bateman LA, Stevens RD, Ilkayeva OR, Hoffman EP,
1528 Muoio DM, Kraus WE (2014) Metabolite signatures of exercise training in human skeletal muscle relate to
1529 mitochondrial remodelling and cardiometabolic fitness. *Diabetologia* **57:** 2282-2295
1530
1531 Hui S, Ghergurovich JM, Morscher RJ, Jang C, Teng X, Lu W, Esparza LA, Reya T, Le Z, Yanxiang Guo J,
1532 White E, Rabinowitz JD (2017) Glucose feeds the TCA cycle via circulating lactate. *Nature* **551:** 115-118
1533
1534 Hunter GR, Wetzstein CJ, Fields DA, Brown A, Bamman MM (2000) Resistance training increases total energy
1535 expenditure and free-living physical activity in older adults. *J Appl Physiol (1985)* **89:** 977-984
1536
1537 Ibrahim A, Neinast M, Arany ZP (2017) Myobolites: muscle-derived metabolites with paracrine and systemic
1538 effects. *Current opinion in pharmacology* **34:** 15-20
1539
1540 Jiang Y, Berry DC, Graff JM (2017) Distinct cellular and molecular mechanisms for beta3 adrenergic
1541 receptor-induced beige adipocyte formation. *Elife* **6**
1542
1543 Jocken JW, Blaak EE (2008) Catecholamine-induced lipolysis in adipose tissue and skeletal muscle in obesity.
1544 *Physiol Behav* **94:** 219-230
1545
1546 Jung TW, Hwang HJ, Hong HC, Yoo HJ, Baik SH, Choi KM (2015) BAIBA attenuates insulin resistance and
1547 inflammation induced by palmitate or a high fat diet via an AMPK-PPARdelta-dependent pathway in mice.
1548 *Diabetologia* **58:** 2096-2105
1549
1550 Karin M, Yamamoto Y, Wang QM (2004) The IKK NF-kappa B system: a treasure trove for drug development.
1551 *Nature reviews Drug discovery* **3:** 17-26
1552
1553 Kerschner JE, Hong W, Taylor SR, Kerschner JA, Khampang P, Wrege KC, North PE (2013) A novel model of
1554 spontaneous otitis media with effusion (OME) in the Oxgr1 knock-out mouse. *International journal of pediatric*

otorhinolaryngology **77:** 79-84

Kilani H (2010) *The Effect of Aerobic vs. Anaerobic Exercises on Weight Reduction*.

Kim JS, Yoon DH, Kim HJ, Choi MJ, Song W (2016) Resistance exercise reduced the expression of fibroblast growth factor-2 in skeletal muscle of aged mice. *Integrative medicine research* **5:** 230-235

Leibowitz A, Klin Y, Gruenbaum BF, Gruenbaum SE, Kuts R, Dubilet M, Ohayon S, Boyko M, Sheiner E, Shapira Y, Zlotnik A (2012) Effects of strong physical exercise on blood glutamate and its metabolite 2-ketoglutarate levels in healthy volunteers. *Acta Neurobiol Exp (Wars)* **72:** 385-396

Lewis GD, Farrell L, Wood MJ, Martinovic M, Arany Z, Rowe GC, Souza A, Cheng S, McCabe EL, Yang E, Shi X, Deo R, Roth FP, Asnani A, Rhee EP, Systrom DM, Semigran MJ, Vasan RS, Carr SA, Wang TJ, Sabatine MS, Clish CB, Gerszten RE (2010) Metabolic signatures of exercise in human plasma. *Sci Transl Med* **2:** 33ra37

Li T, Zhang Z, Kolwicz SC, Jr., Abell L, Roe ND, Kim M, Zhou B, Cao Y, Ritterhoff J, Gu H, Raftery D, Sun H, Tian R (2017) Defective Branched-Chain Amino Acid Catabolism Disrupts Glucose Metabolism and Sensitizes the Heart to Ischemia-Reperfusion Injury. *Cell metabolism* **25:** 374-385

Li X, Hansen J, Zhao X, Lu X, Weigert C, Haring HU, Pedersen BK, Plomgaard P, Lehmann R, Xu G (2012) Independent component analysis in non-hypothesis driven metabolomics: improvement of pattern discovery and simplification of biological data interpretation demonstrated with plasma samples of exercising humans. *J Chromatogr B Analyt Technol Biomed Life Sci* **910:** 156-162

Liu PS, Wang H, Li X, Chao T, Teav T, Christen S, Di Conza G, Cheng WC, Chou CH, Vavakova M, Muret C, Debackere K, Mazzone M, Huang HD, Fendt SM, Ivanisevic J, Ho PC (2017) alpha-ketoglutarate orchestrates macrophage activation through metabolic and epigenetic reprogramming. *Nat Immunol* **18:** 985-994

Luo Z, Ma L, Zhao Z, He H, Yang D, Feng X, Ma S, Chen X, Zhu T, Cao T, Liu D, Nilius B, Huang Y, Yan Z, Zhu Z (2012) TRPV1 activation improves exercise endurance and energy metabolism through PGC-1alpha upregulation in mice. *Cell research* **22:** 551-564

Maillard F, Pereira B, Boisseau N (2018) Effect of High-Intensity Interval Training on Total, Abdominal and Visceral Fat Mass: A Meta-Analysis. *Sports medicine (Auckland, NZ)* **48:** 269-288

Makimura H, Mizuno TM, Beasley J, Silverstein JH, Mobbs CV (2003) Adrenalectomy stimulates hypothalamic proopiomelanocortin expression but does not correct diet-induced obesity. *BMC Physiol* **3:** 4

Makimura H, Mizuno TM, Roberts J, Silverstein J, Beasley J, Mobbs CV (2000) Adrenalectomy reverses obese phenotype and restores hypothalamic melanocortin tone in leptin-deficient ob/ob mice. *Diabetes* **49:** 1917-1923

Mills EL, Pierce KA, Jedrychowski MP, Garrity R, Winther S, Vidoni S, Yoneshiro T, Spinelli JB, Lu GZ, Kazak L, Banks AS, Haigis MC, Kajimura S, Murphy MP, Gygi SP, Clish CB, Chouchani ET (2018) Accumulation of succinate controls activation of adipose tissue thermogenesis. *Nature* **560:** 102-106

Mullen AR, Hu Z, Shi X, Jiang L, Boroughs LK, Kovacs Z, Boriack R, Rakheja D, Sullivan LB, Linehan WM, Chandel NS, DeBerardinis RJ (2014) Oxidation of alpha-ketoglutarate is required for reductive carboxylation in cancer cells with mitochondrial defects. *Cell reports* **7:** 1679-1690

Mullur R, Liu YY, Brent GA (2014) Thyroid hormone regulation of metabolism. *Physiological reviews* **94:** 355-382

Nair KS, Short KR (2005) Hormonal and signaling role of branched-chain amino acids. *J Nutr* **135:** 1547S-1552S

Ni Y, Su M, Qiu Y, Jia W, Du X (2016) ADAP-GC 3.0: Improved Peak Detection and Deconvolution of Co-eluting Metabolites from GC/TOF-MS Data for Metabolomics Studies. *Analytical chemistry* **88:** 8802-8811

Omede A, Zi M, Prehar S, Maqsood A, Stafford N, Mamas M, Cartwright E, Oceandy D (2016) The oxoglutarate receptor 1 (OXGR1) modulates pressure overload-induced cardiac hypertrophy in mice. *Biochemical and biophysical research communications* **479:** 708-714

Park KH, Brotto L, Lehoang O, Brotto M, Ma J, Zhao X (2012) Ex vivo assessment of contractility, fatigability and alternans in isolated skeletal muscles. *Journal of visualized experiments : JoVE***:** e4198

Parkhomchuk D, Borodina T, Amstislavskiy V, Banaru M, Hallen L, Krobitsch S, Lehrach H, Soldatov A (2009) Transcriptome analysis by strand-specific sequencing of complementary DNA. *Nucleic acids research* **37:** e123

Patel H, Alkhawam H, Madanieh R, Shah N, Kosmas CE, Vittorio TJ (2017) Aerobic vs anaerobic exercise training effects on the cardiovascular system. *World J Cardiol* **9:** 134-138

Pechlivanis A, Kostidis S, Saraslanidis P, Petridou A, Tsalis G, Mougios V, Gika HG, Mikros E, Theodoridis GA (2010) (1)H NMR-based metabonomic investigation of the effect of two different exercise sessions on the metabolic fingerprint of human urine. *J Proteome Res* **9:** 6405-6416

Poehlman ET, Denino WF, Beckett T, Kinaman KA, Dionne IJ, Dvorak R, Ades PA (2002) Effects of endurance and resistance training on total daily energy expenditure in young women: a controlled randomized trial. *J Clin Endocrinol Metab* **87:** 1004-1009

Poehlman ET, Melby CL, Goran MI (1991) The impact of exercise and diet restriction on daily energy expenditure. *Sports Med* **11:** 78-101

Qiu Y, Cai G, Su M, Chen T, Zheng X, Xu Y, Ni Y, Zhao A, Xu LX, Cai S, Jia W (2009) Serum metabolite profiling of human colorectal cancer using GC-TOFMS and UPLC-QTOFMS. *Journal of proteome research* **8:** 4844-4850

Qun Z, Xinkai Y, Jing W (2014) Effects of eccentric exercise on branched-chain amino acid profiles in rat serum and skeletal muscle. *Journal of animal physiology and animal nutrition* **98:** 215-222

Rai M, Demontis F (2016) Systemic Nutrient and Stress Signaling via Myokines and Myometabolites. *Annu Rev Physiol* **78:** 85-107

Rao RR, Long JZ, White JP, Svensson KJ, Lou J, Lokurkar I, Jedrychowski MP, Ruas JL, Wrann CD, Lo JC, Camera DM, Lachey J, Gygi S, Seehra J, Hawley JA, Spiegelman BM (2014) Meteorin-like is a hormone that regulates immune-adipose interactions to increase beige fat thermogenesis. *Cell* **157:** 1279-1291

Roberts LD, Bostrom P, O'Sullivan JF, Schinzel RT, Lewis GD, Dejam A, Lee YK, Palma MJ, Calhoun S, Georgiadi A, Chen MH, Ramachandran VS, Larson MG, Bouchard C, Rankinen T, Souza AL, Clish CB, Wang TJ, Estall JL, Soukas AA, Cowan CA, Spiegelman BM, Gerszten RE (2014) beta-Aminoisobutyric acid induces browning of white fat and hepatic beta-oxidation and is inversely correlated with cardiometabolic risk factors. *Cell metabolism* **19:** 96-108

Roberts RE (2012) The extracellular signal-regulated kinase (ERK) pathway: a potential therapeutic target in hypertension. *J Exp Pharmacol* **4:** 77-83

Salgueiro RB, Peliciari-Garcia RA, do Carmo Buonfiglio D, Peroni CN, Nunes MT (2014) Lactate activates the somatotropic axis in rats. *Growth hormone & IGF research : official journal of the Growth Hormone Research Society and the International IGF Research Society* **24:** 268-270

Sato S, Basse AL, Schonke M, Chen S, Samad M, Altintas A, Laker RC, Dalbram E, Barres R, Baldi P, Treebak JT, Zierath JR, Sassone-Corsi P (2019) Time of Exercise Specifies the Impact on Muscle Metabolic Pathways and Systemic Energy Homeostasis. *Cell Metab*

Schnyder S, Handschin C (2015) Skeletal muscle as an endocrine organ: PGC-1alpha, myokines and exercise. *Bone* **80:** 115-125

Sharara-Chami RI, Joachim M, Mulcahey M, Ebert S, Majzoub JA (2010) Effect of epinephrine deficiency on cold tolerance and on brown adipose tissue. *Molecular and cellular endocrinology* **328:** 34-39

Shi Y, Tse S, Rago B, Yapa U, Li F, Fast DM (2016) Quantification of fumarate and investigation of endogenous and exogenous fumarate stability in rat plasma by LC-MS/MS. *Bioanalysis* **8:** 661-675

Shimomura Y, Murakami T, Nakai N, Nagasaki M, Harris RA (2004) Exercise promotes BCAA catabolism: effects of BCAA supplementation on skeletal muscle during exercise. *The Journal of nutrition* **134:** 1583S-1587S

Stanford KI, Goodyear LJ (2016) Exercise regulation of adipose tissue. *Adipocyte* **5:** 153-162

Starnes JW, Parry TL, O'Neal SK, Bain JR, Muehlbauer MJ, Honcoop A, Ilaiwy A, Christopher PM, Patterson C, Willis MS (2017) Exercise-Induced Alterations in Skeletal Muscle, Heart, Liver, and Serum Metabolome Identified by Non-Targeted Metabolomics Analysis. *Metabolites* **7**

1687 Strasser B (2013) Physical activity in obesity and metabolic syndrome. *Ann N Y Acad Sci* **1281:** 141-159
1688
1689 Tank AW, Lee Wong D (2015) Peripheral and central effects of circulating catecholamines. *Compr Physiol* **5:**
1690 1-15
1691
1692 Tekwe CD, Lei J, Yao K, Li X, Rezaei R, Dahanayaka S, Meininger C, Carroll RJ, Bazer FW, Wu G (2012) Oral
1693 administration of α-ketoglutarate or interferon-τ reduces adiposity in diet-induced obese rats. *FASEB J* **26:** 45
1694
1695 Tokonami N, Morla L, Centeno G, Mordasini D, Ramakrishnan SK, Nikolaeva S, Wagner CA, Bonny O,
1696 Houillier P, Doucet A, Firsov D (2013) alpha-Ketoglutarate regulates acid-base balance through an intrarenal
1697 paracrine mechanism. *J Clin Invest* **123:** 3166-3171
1698
1699 Wang L, Hou Y, Yi D, Li Y, Ding B, Zhu H, Liu J, Xiao H, Wu G (2015) Dietary supplementation with
1700 glutamate precursor alpha-ketoglutarate attenuates lipopolysaccharide-induced liver injury in young pigs. *Amino*
1701 *acids* **47:** 1309-1318
1702
1703 Wittenberger T, Hellebrand S, Munck A, Kreienkamp HJ, Schaller HC, Hampe W (2002) GPR99, a new G
1704 protein-coupled receptor with homology to a new subgroup of nucleotide receptors. *BMC Genomics* **3:** 17
1705
1706 Wu N, Yang M, Gaur U, Xu H, Yao Y, Li D (2016) Alpha-Ketoglutarate: Physiological Functions and
1707 Applications. *Biomol Ther (Seoul)* **24:** 1-8
1708
1709 Xiao D, Zeng L, Yao K, Kong X, Wu G, Yin Y (2016) The glutamine-alpha-ketoglutarate (AKG) metabolism
1710 and its nutritional implications. *Amino acids* **48:** 2067-2080
1711
1712 Xin Z, Ma S, Ren D, Liu W, Han B, Zhang Y, Xiao J, Yi L, Deng B (2018) UPLC-Orbitrap-MS/MS combined
1713 with chemometrics establishes variations in chemical components in green tea from Yunnan and Hunan origins.
1714 *Food chemistry* **266:** 534-544
1715
1716 Xu J, Zhu C, Zhang M, Tong Q, Wan X, Liao Z, Cai X, Xu Y, Yuan Y, Wang L, Zhu X, Wang S, Gao P, Xi Q,
1717 Xu Y, Jiang Q, Shu G (2018) Arginine reverses growth hormone resistance through the inhibition of toll-like
1718 receptor 4-mediated inflammatory pathway. *Metabolism: clinical and experimental* **79:** 10-23
1719
1720 Yang Q, Liang X, Sun X, Zhang L, Fu X, Rogers CJ, Berim A, Zhang S, Wang S, Wang B, Foretz M, Viollet B,
1721 Gang DR, Rodgers BD, Zhu MJ, Du M (2016) AMPK/alpha-Ketoglutarate Axis Dynamically Mediates DNA
1722 Demethylation in the Prdm16 Promoter and Brown Adipogenesis. *Cell metabolism* **24:** 542-554
1723
1724 Yde CC, Ditlev DB, Reitelseder S, Bertram HC (2013) Metabonomic Response to Milk Proteins after a Single
1725 Bout of Heavy Resistance Exercise Elucidated by 1H Nuclear Magnetic Resonance Spectroscopy. *Metabolites* **3:**
1726 33-46
1727
1728 Zdzisinska B, Zurek A, Kandefer-Szerszen M (2017) Alpha-Ketoglutarate as a Molecule with Pleiotropic
1729 Activity: Well-Known and Novel Possibilities of Therapeutic Use. *Arch Immunol Ther Exp (Warsz)* **65:** 21-36
1730

Zhu C, Xu P, He Y, Yuan Y, Wang T, Cai X, Yu L, Yang L, Wu J, Wang L, Zhu X, Wang S, Gao P, Xi Q, Zhang Y, Xu Y, Jiang Q, Shu G (2017) Heparin Increases Food Intake through AgRP Neurons. *Cell Rep* **20:** 2455-2467

1775 **Figures**

1776 **Fig. 1**

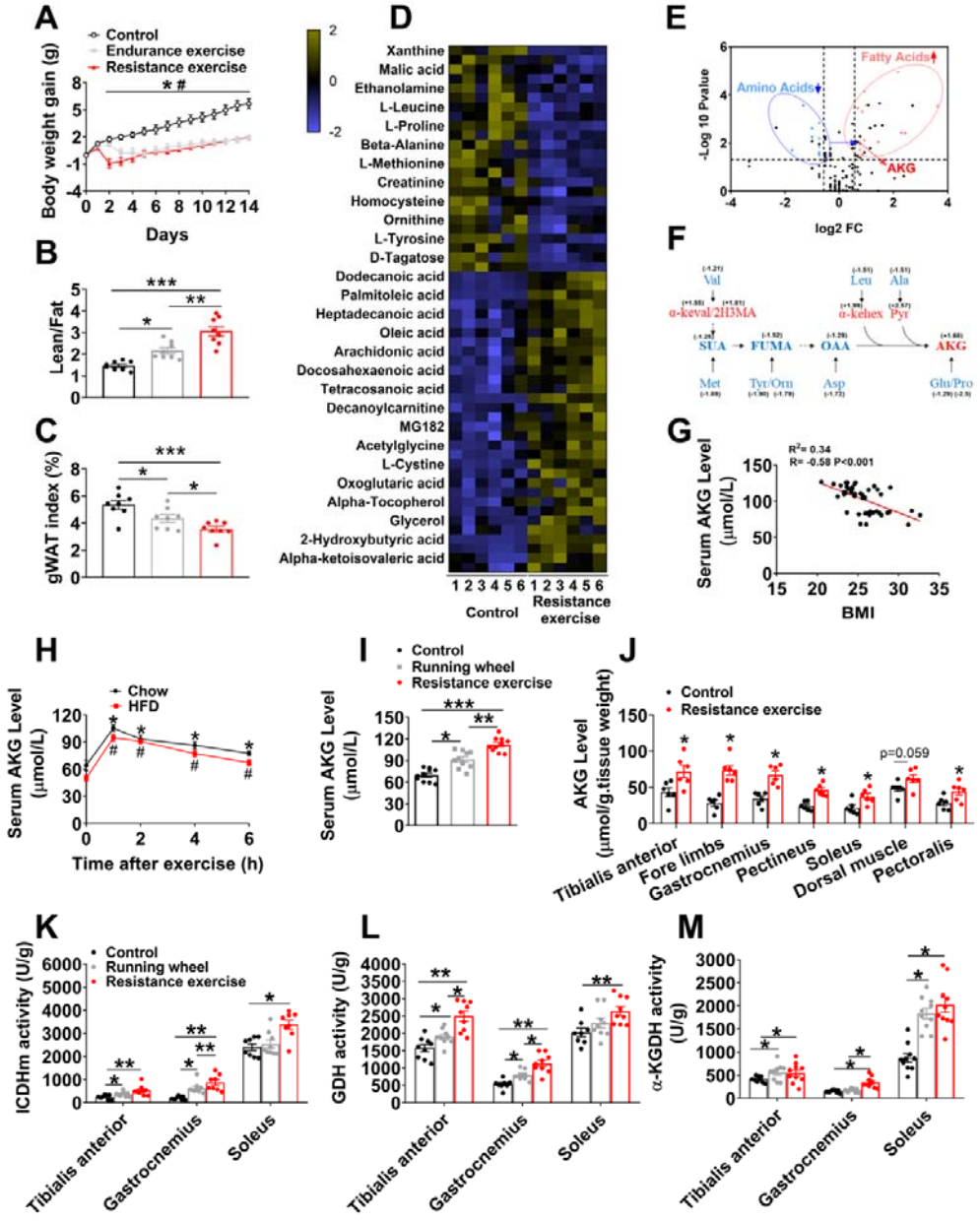

1777

1778 **Figure 1. AKG synthesis is induced by exercises**

1779 (A-C). Mice body weight gain (A), the lean-to-fat ratio (B) and gWAT index (C). At 8 weeks of age, male
1780 C57BL/6 mice were switched to HFD. After 12 weeks of HFD feeding, mice were divided into three
1781 groups receiving non-exercise, endurance exercise or resistance exercise for 14 days. (n = 8 per group).
1782 (D). Relative changes in metabolites in response to resistance exercise. Heat maps show changes of
1783 metabolites in the serums from mice receiving resistance exercise or non-exercise. Male C57BL/6 mice
1784 (10 weeks) fed with normal chow were divided into two groups receiving either non-exercise or resistance
1785 exercise for 40 min (n = 6 per group). Shades of yellow and blue represent fold increase and fold decrease
1786 of a metabolite, respectively (see color scale).

(E). A volcano plot of metabolome. Metabolites with $\log_2$FC ≥ 0.58 and $-\log_{10}$P value ≥ 1.3 were considered significant. Fatty acids (red dots) and amino acids (blue dots) metabolites were found to be significantly different between groups (n = 6 per group).

(F). Enrichment of tricarboxylic acid cycle (TCA cycle) intermediates/AKG metabolites in serum during resistance exercise. Blue color indicates significant decreases, while red color indicates significant increases by the volcano plot analysis between groups in serum metabolite levels. (Val: Valine; Leu: Leucine; Ala: Alanine; Met: Methionine; Tyr: Tyrosine; Orn: Ornithine; Asp: Aspartic acid; Glu: Glutamic acid; Pro: Proline; SUA: Succinic acid; FUMA: Fumaric acid; OAA: oxaloacetic acid; AKG: Oxoglutaric acid; α-keval: Alpha-ketoisovaleric acid; 2H3MA: 2-Hydroxy-3-methylbutyric acid; α-kehex: α-ketoleucine; Pyr: Pyruvic acid).

(G). Two tailed Pearson's correlation coefficient analysis of plasma AKG level and body mass index (BMI) in Chinese adults (10 males and 35 females).

(H). Serum AKG concentration-time profile obtained before and after 40-min resistant exercise. At 8 weeks of age, male C57BL/6 mice were switched to HFD and continuously fed with HFD for 12 weeks. At 20 weeks of age, mice received resistance exercise for 40 min. Another group of chow fed male C57BL/6 mice (10 weeks) received resistance exercise for 40 min. The serum AKG level were tested at 0, 1, 2, 4 and 6 hrs after exercise (n = 8-10 per group).

(I). Serum AKG levels after exercise. Male C57BL/6 mice (10 weeks) fed with normal chow were divided into three groups receiving non-exercise, running wheel free access for 1 day or resistance exercise for 40 min.(n = 8-10 per group).

(J). Muscles AKG levels after exercise. Male C57BL/6 mice (10 weeks) fed with normal chow were divided into two groups receiving either non-exercise or resistance exercise for 40 min (n = 6 per group).

(K-M). Muscle ICDHm (K), GDH (L), and α-KGDH (M) enzyme activity after exercise. Male C57BL/6 mice (10 weeks) fed with normal chow were divided into three groups receiving non-exercise, running wheel free access for 1day or resistance exercise for 40 min (n = 8-9 per group).

Results are presented as mean ± SEM. In (A), *p≤0.05 (Control vs. Endurance exercise), $^{\#}$p≤0.05 (Control vs. Resistance exercise) by two-way ANOVA followed by post hoc Bonferroni tests. In (B-C), and (I-M), *p≤0.05, **p≤0.01, and ***p≤0.001 by one-way ANOVA followed by post hoc Tukey's tests. In (H), *p≤0.05 (Chow), $^{\#}$p≤0.05 (HFD) by non-paired Student's t test compared with before exercise.

Fig. 2

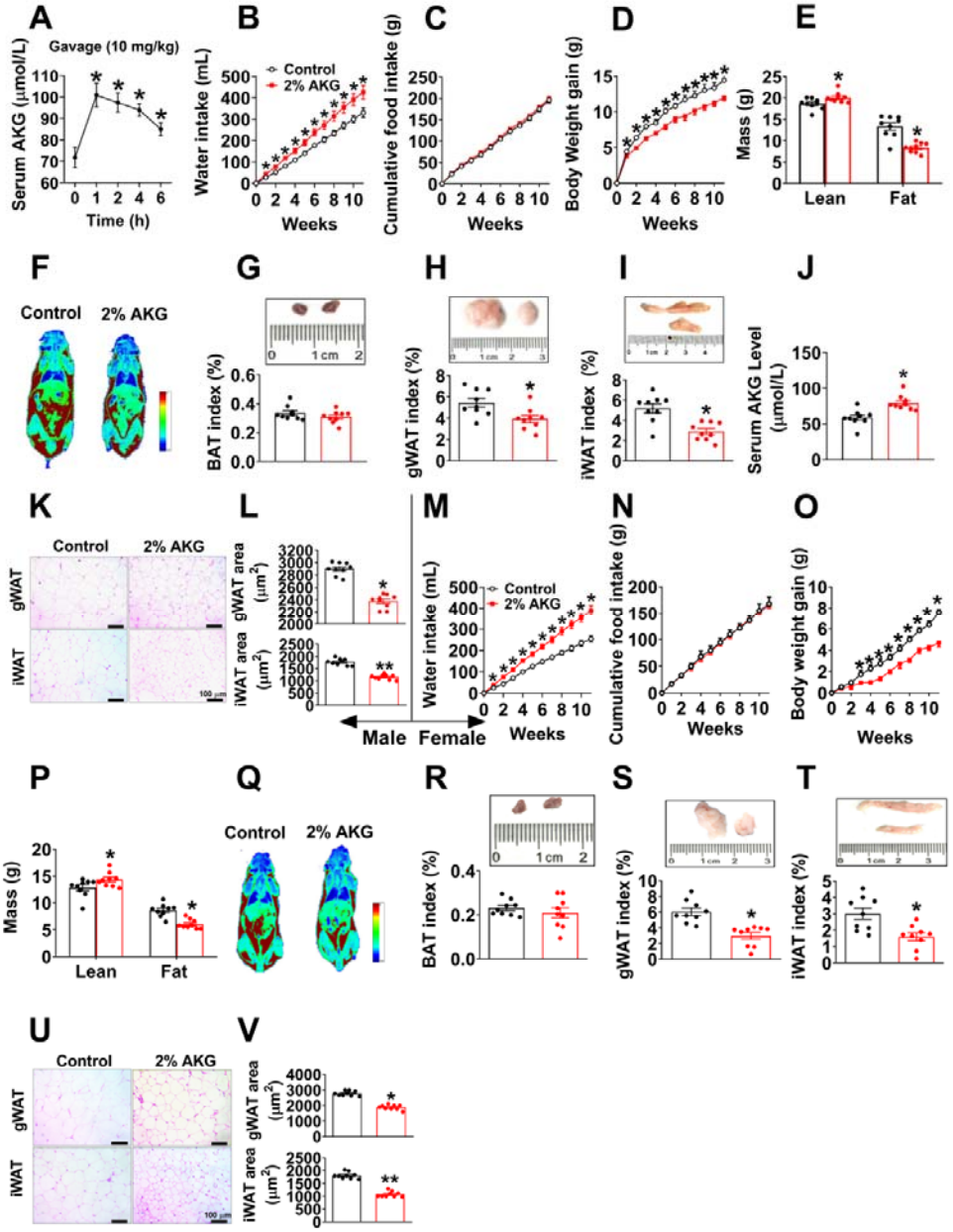

Figure 2. AKG prevents diet-induced obesity

(A). Serum AKG concentration-time profile obtained from male C57BL/6 mice (10 weeks) fed with normal chow before or after AKG gavage (10 mg/kg). The serum AKG level were tested at 0, 1, 2, 4 and 6 hrs after gavage (n = 8 per group).

(B-D). Water intake (B), cumulative food intake (C) and body weight gain (D) of male C57BL/6 mice. At 12 weeks of age, mice were switched to HFD and received tap water or water supplemented with 2% AKG for 11 weeks (n = 9 per group).

(E-F). Fat and lean mass (E) and representative images (F) of body composition from male mice after 11 weeks of AKG supplementation (n = 9 per group).

(G-I). Weight index of BAT (G), gWAT (H) and iWAT (I) from male mice after 11 weeks of AKG supplementation (n = 9 per group).
(J). Serum AKG level of male mice after 11 weeks of AKG supplementation (n = 9 per group).
(K-L). Representative images (K) and quantification (L) of gWAT and iWAT HE staining from male mice after 11 weeks of AKG supplementation (n = 9 per group).
(M-O). Water intake (M), cumulative food intake (N) and body weight gain (O) of female C57BL/6 mice. At 12 weeks of age, mice were switched to HFD and received tap water or water supplemented with 2% AKG for 11 weeks (n = 9 per group).
(P-Q). Fat and lean mass index (P) and representative image (Q) of body composition from female mice after 11 weeks of AKG supplementation (n = 9 per group).
(R-T). Weight index of BAT (R), gWAT (S) and iWAT (T) from female mice after 11 weeks of AKG supplementation (n = 9 per group).
(U-V). Representative images (U) and quantification (V) of gWAT and iWAT HE staining from female mice after 11 weeks of AKG supplementation (n = 9 per group).
Results are presented as mean ± SEM. In (A), *$p \leq 0.05$ by non-paired Student's t test compared with before gavage. In (B-D) and (M-O), $*p \leq 0.05$ by two-way ANOVA followed by post hoc Bonferroni tests. In (E), (G-J), (L), (P), (R-T) and (V), $*p \leq 0.05$ and $**p \leq 0.01$ by non-paired Student's t test.

Fig. 3

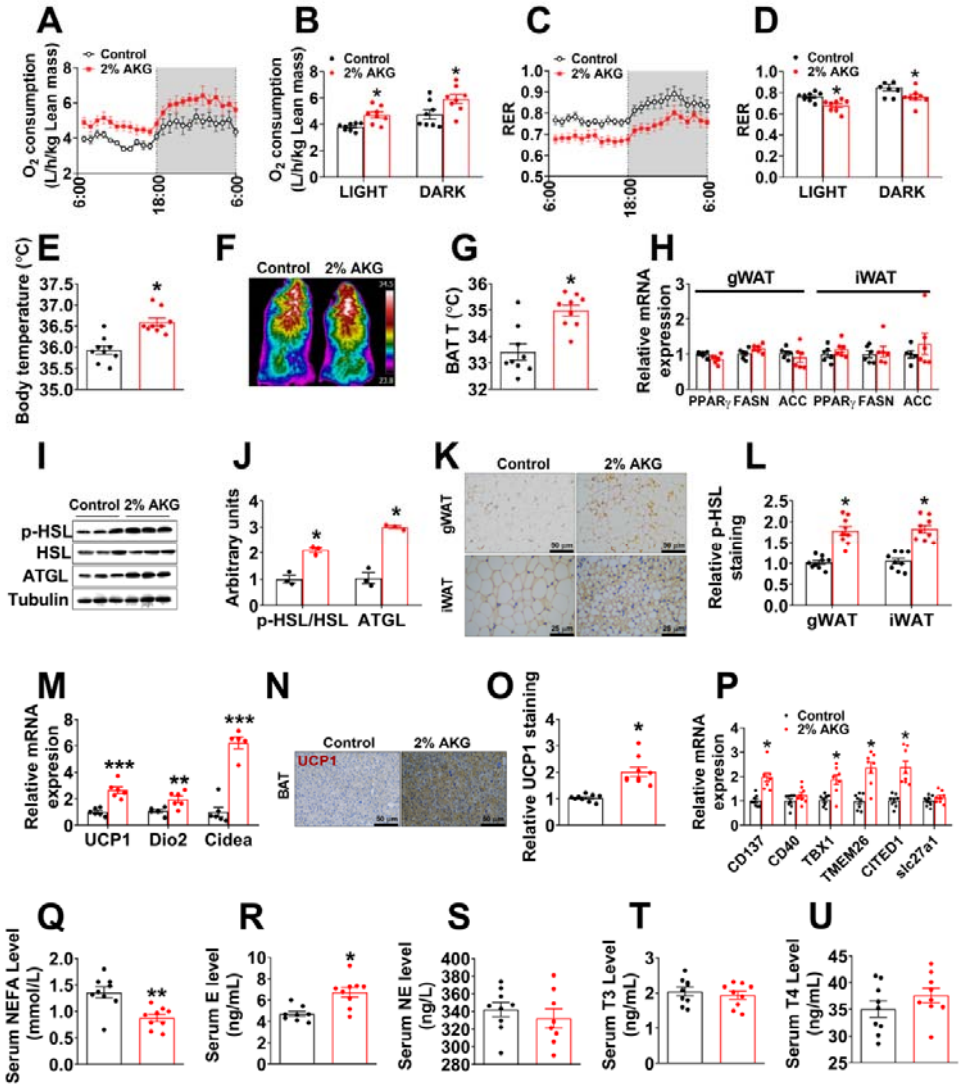

Figure 3. AKG increases fat thermogenesis and lipolysis

(A-D). Oxygen consumption (A-B) and respiratory exchange ratio (RER, C-D) in male C57BL/6 mice after 11 weeks of AKG supplementation (n = 8 per group).

(E). Body temperature of male mice after 11 weeks of AKG supplementation (n = 9 per group).

(F-G). Representative images (F) and quantification (G) of BAT thermogenesis induced by 6 hr cold exposure at 4°C in male mice supplemented with AKG for 11 weeks (n = 9 per group).

(H). The mRNA expression of PPARγ, FASN and ACC in the gWAT and iWAT from male mice supplemented with AKG for 11 weeks (n = 6 per group).

(I-J). Immunoblots (I) and quantification (J) of p-HSL and ATGL protein in gWAT of male mice after 11 weeks of AKG supplementation (n = 3 per group).

(K-L). DAB staining (K) and quantification (L) of p-HSL in gWAT and iWAT of male mice after 11 weeks of AKG supplementation (n = 9 per group).

(M–O). The mRNA expression of thermogenic genes (M) and DAB staining (N) and quantification (O) of UCP1 in BAT of male mice supplemented with AKG for 11 weeks (n = 6-8 per group).

(P). The mRNA expression of CD137, CD40, TBX1, TMEM26, CITED1 and slc27a1 in iWAT of male mice supplemented with AKG for 11 weeks (n = 8 per group).

(Q–U). Serum levels of NEFA (Q), E (R), NE (S), T3 (T), and T4 (U) in male mice supplemented with AKG for 11 weeks (n = 8-9 per group).

Results are presented as mean ± SEM. In (B), (D-E), (G-H), (J), (L-M), and (O-U), *p≤0.05, **p≤0.01, and ***p≤0.001 by non-paired Student's t test.

1870 **Fig. 4**

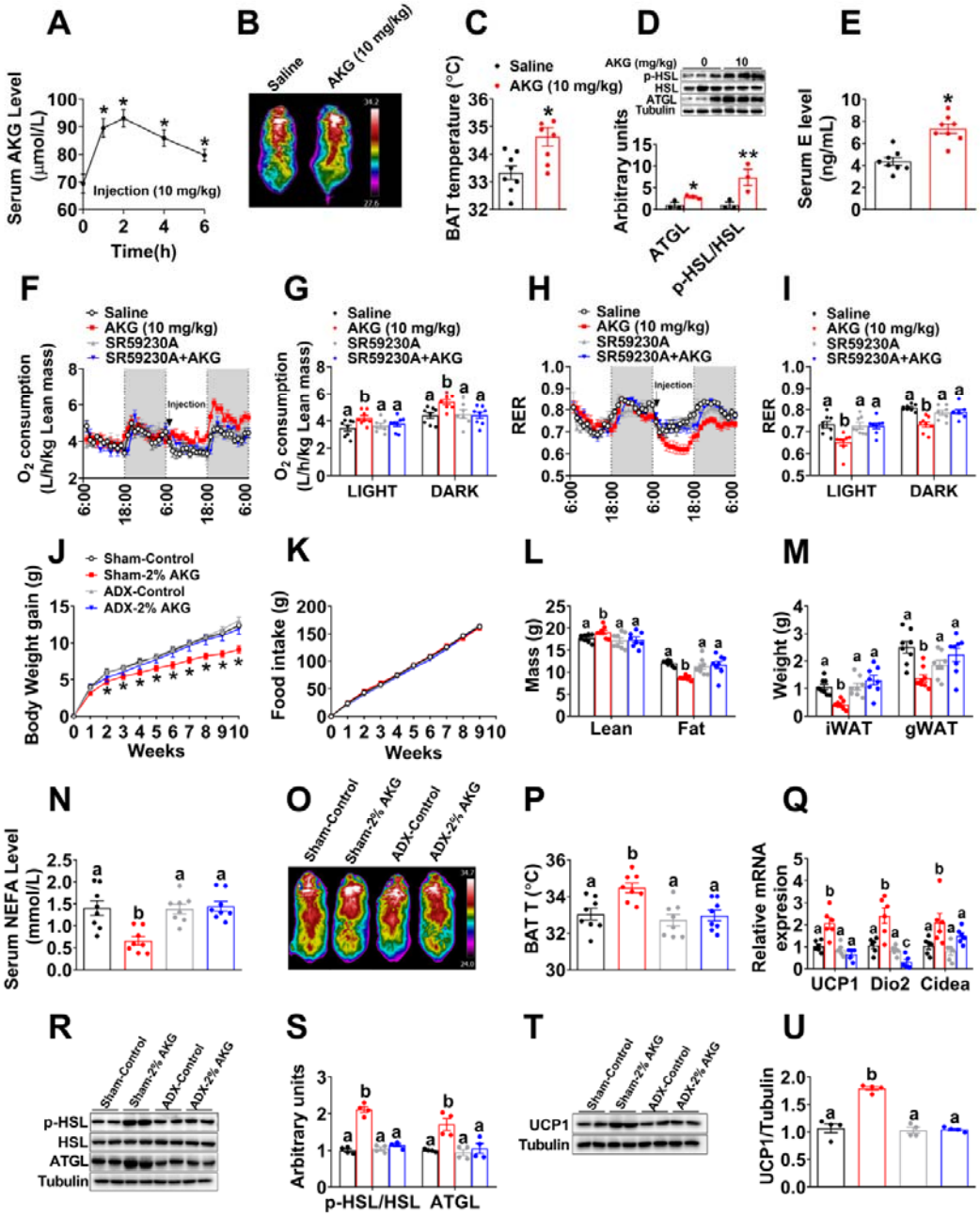

1871

1872 **Figure 4. Metabolic effects of AKG is mediated by adrenergic stimulation of thermogenesis and**
1873 **lipolysis**

1874 (A). Serum AKG concentration-time profile obtained from male C57BL/6 mice (10 weeks) fed with
1875 normal chow before or after i.p AKG (10 mg/kg body weight). The serum AKG level were tested at 0, 1, 2,
1876 4 and 6 hrs after injection (n = 8 per group).

1877 (B-C). Representative images (B) and quantification (C) of BAT thermogenesis after 6 hr cold exposure at
1878 4°C. Male C57BL/6 mice (10 weeks) were i.p. injected with 10 mg/kg AKG or saline and immediately
1879 exposed to cold stress at 4°C (n = 8 per group).

(D). Immunoblots and quantification of p-HSL and ATGL in the gWAT of male C57BL/6 mice (10 weeks) 3 hrs after i.p. injection of 10 mg/kg AKG or saline (n = 3 per group).
(E). Serum E level in AKG treated male mice 3 hrs after i.p. injection (n = 8 per group).
(F-I). Oxygen consumption (F-G) and RER (H-I) in male C57BL/6 mice (10 weeks) i.p. injected with saline, 10 mg/kg AKG, 1 mg/kg SR59230A (ADRB3 inhibitor) or AKG + SR59230A (n = 8 per group). All injections were performed at 7:00 am of second day. Data was summarized in bar graph (G and I) by light or dark cycle of second day.
(J-N). Body weight gain (J), cumulative food intake (K), body composition (L), fat weight (M) and serum NEFA (N) of shame or adrenalectomized male C57BL/6 mice. Male mice were adrenalectomized at 8 weeks of age. Two weeks after surgeries, male mice were switched to HFD and given free access to tap water or 2% AKG for 9 weeks (n = 8 per group).
(O-P). Representative images (O) and quantification (P) of BAT thermogenesis after 6h cold exposure at 4℃ in shame or adrenalectomized male mice treated with AKG for 9 weeks (n = 8 per group).
(Q). The mRNA expression of themogenic genes in the BAT of shame or adrenalectomized male mice treated with AKG for 9 weeks (n = 6 per group).
(R-S) Immunoblots (R) and quantification (S) of p-HSL and ATGL protein in the gWAT of shame or adrenalectomized male mice treated with AKG for 9 weeks (n = 4 per group).
(T-U). Immunoblots (T) and quantification (U) of UCP1 protein in the BAT of shame or adrenalectomized male mice treated with AKG for 9 weeks (n = 4 per group).
Results are presented as mean ± SEM. In (A), *$p \leq 0.05$ by non-paired Student's t test compared with before injection. In (C-E), *$p \leq 0.05$, **$p \leq 0.01$ by non-paired Student's t test. In (J-K), *$p \leq 0.05$ by two-way ANOVA followed by post hoc Bonferroni tests. In (G), (I), (L-N), (P-Q), (S) and (U), different letters between bars indicate $p \leq 0.05$ by one-way ANOVA followed by post hoc Tukey's tests .

1905 **Fig. 5**

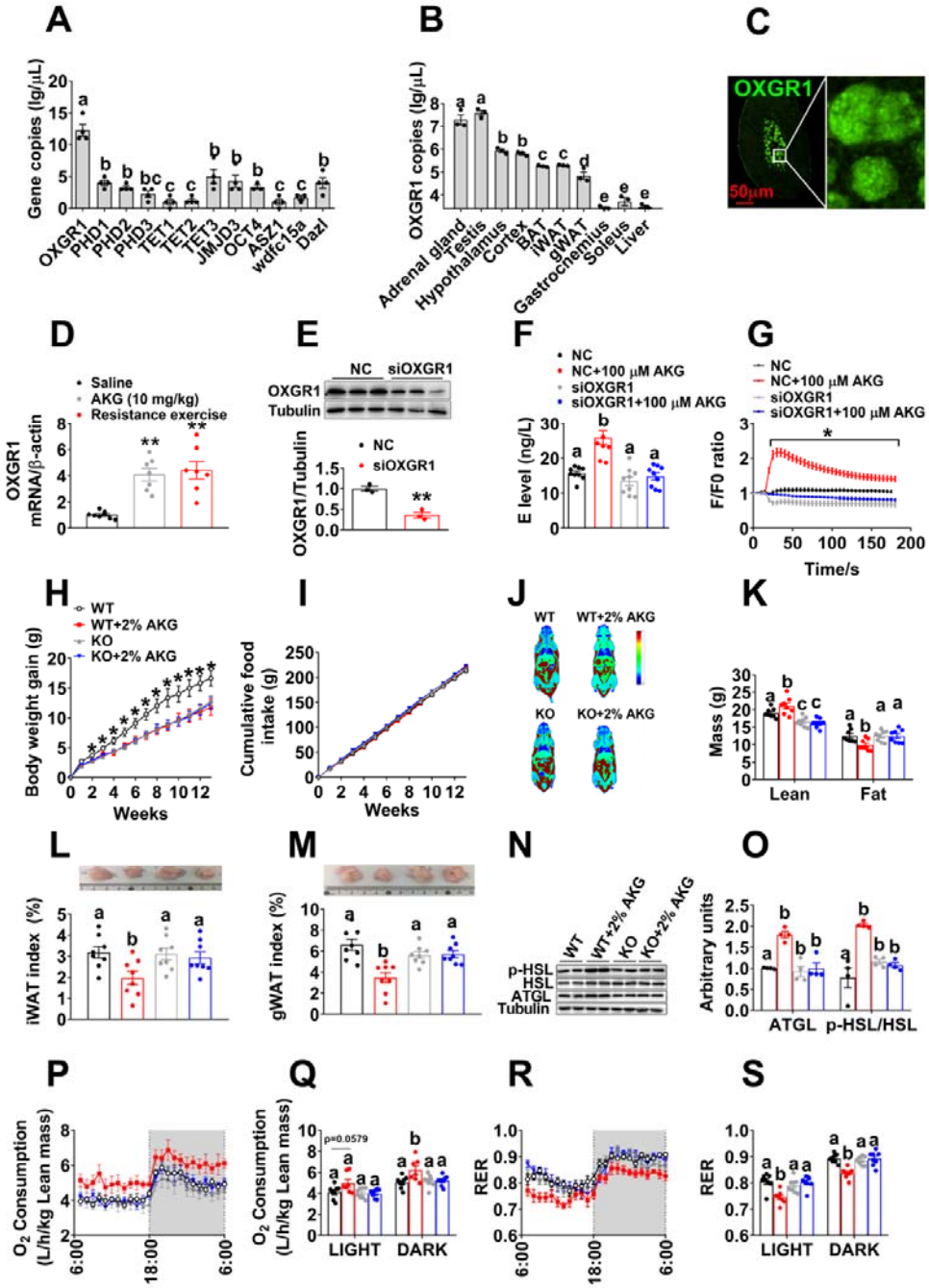

1906

1907 **Figure 5. OXGR1 is required for the stimulatory effects of AKG on thermogenesis and lipolysis**

1908 (A). The mRNA expression of AKG-sensing genes in the adrenal gland tissue of 12-weeks male C57BL/6

1909 mice (n = 4 per group).

1910 (B). The mRNA expression of OXGR1 in different tissues of 12-weeks male C57BL/6 mice (n = 3 per

1911 group).

1912 (C). OXGR1 localization in adrenal gland medulla indicated by fluorescent staining of OXGR1 (green).

1913 (D). The mRNA expression of OXGR1 in the adrenal gland of male mice 3 hrs after i.p. injection of saline

or 10 mg/kg AKG, or immediately after 40-mins resistance exercise (n=8 per group).
(E). Immunoblots and quantification of OXGR1 protein expression in adrenal chromaffin cells treated with negative control (NC) siRNA or siOXGR1 (n = 3 per group).
(F). E level in the medium from adrenal chromaffin cell cultured with vehicle + NC, vehicle + siOXGR1, AKG (100 μM) + NC or AKG + siOXGR1 for 30 mins (n = 8 per group).
(G). Intracellular calcium ion [Ca^{2+}] changes in adrenal medulla cell cultured with vehicle + NC, vehicle + siOXGR1, AKG (100 μM) + NC or AKG + siOXGR1 (n = 30 per group).
(H-I). Body weight gain (H) and cumulative food intake (I) of male WT control (littermates) or OXGR1 global knock out (OXGR1KO) mice. At 12 weeks of age, both control and KO mice were switched to HFD and further divided into two groups, receiving tap water or water supplemented with 2% AKG for 13 weeks (n = 8 per group).
(J-K). Representative images of body composition (J) and fat and lean mass index (K) of male WT or OXGR1KO mice treated with AKG for 13 weeks (n = 8 per group).
(L-M). Weight index of iWAT (L) and gWAT (M) in male WT or OXGR1KO mice treated with AKG for 13 weeks (n = 8 per group).
(N-O). Immunoblots (N) and quantification (O) of p-HSL and ATGL protein in gWAT of male WT or OXGR1KO mice treated with AKG for 13 weeks (n = 4 per group).
(P-S). Oxygen consumption (P-Q) and RER (R-S) of male WT or OXGR1KO mice treated with AKG for 13 weeks (n = 8 per group).
Results are presented as mean ± SEM. In (A-B), (F), (K-M), (O), (Q) and (S), different letters between bars indicate $p \leq 0.05$ by one-way ANOVA followed by post hoc Tukey's tests. In (D), $^{**}p \leq 0.01$ by one-way ANOVA followed by post hoc Dunnett's tests. In (E), $^{**}p \leq 0.01$ by non-paired Student's t test. In (G), (H-I), $^{*}p \leq 0.05$ by two-way ANOVA followed by post hoc Bonferroni tests.

Fig. 6

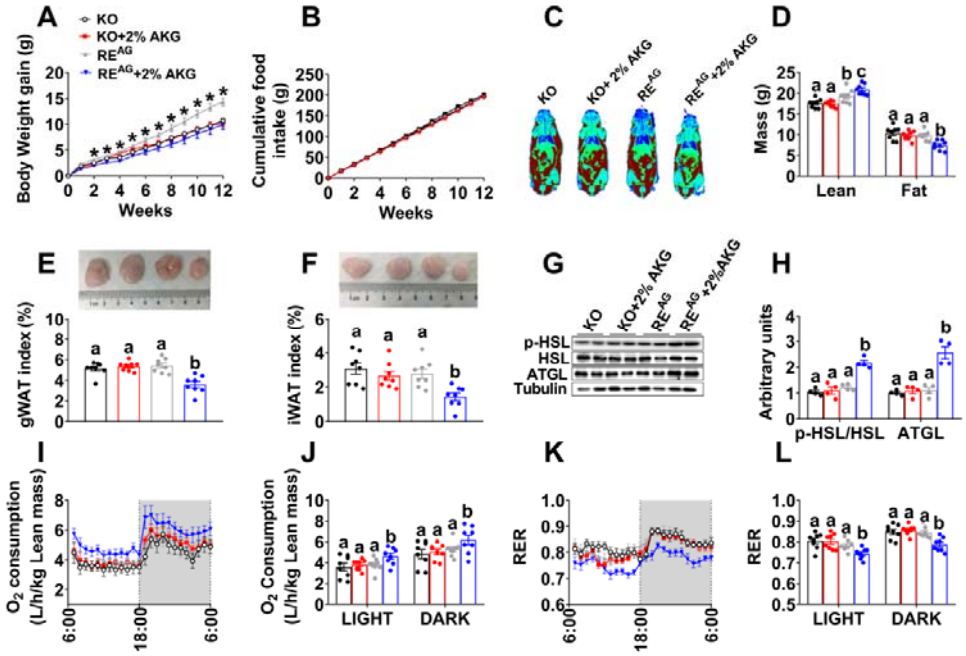

Figure 6. OXGR1 expressed by adrenal gland mediates the stimulatory effects of AKG on thermogenesis and lipolysis

(A-B). Body weight gain (A) and cumulative food intake (B) of male OXGR1 adrenal-specific reexpression mice (OXGR1RE^{AG}). Male OXGR1KO mice (8 weeks) were adrenal-specifically injected with control HBAAV2/9-GFP (OXGR1KO control) or HBAAV2/9-OXGR1 (OXGR1RE^{AG}). Two weeks after injections, mice were switched to HFD and further divided into two groups, receiving tap water or water supplemented with 2% AKG for 12 weeks (n = 8 per group).

(C-D). Representative image of body composition (C) and fat and lean mass index (D) of male OXGR1RE^{AG} mice treated with AKG for 12 weeks (n = 8 per group).

(E-F). Weight index of gWAT (E) and iWAT (F) in male OXGR1RE^{AG} mice treated with AKG for 12 weeks (n = 8 per group).

(G-H). Immunoblots (G) and quantification (H) of p-HSL and ATGL protein in gWAT of male OXGR1RE^{AG} mice treated with AKG for 12 weeks (n = 8 per group).

(I-J). Oxygen consumption (I-J) and RER (K-L) of male OXGR1RE^{AG} mice treated with AKG for 12 weeks (n = 8 per group).

Results are presented as mean ± SEM. In (A-B), *p≤0.05 by two-way ANOVA followed by post hoc Bonferroni tests. In (D-F), (H), (J) and (L), different letters between bars indicate p≤0.05 by one-way ANOVA followed by post hoc Tukey's tests.

Fig. 7

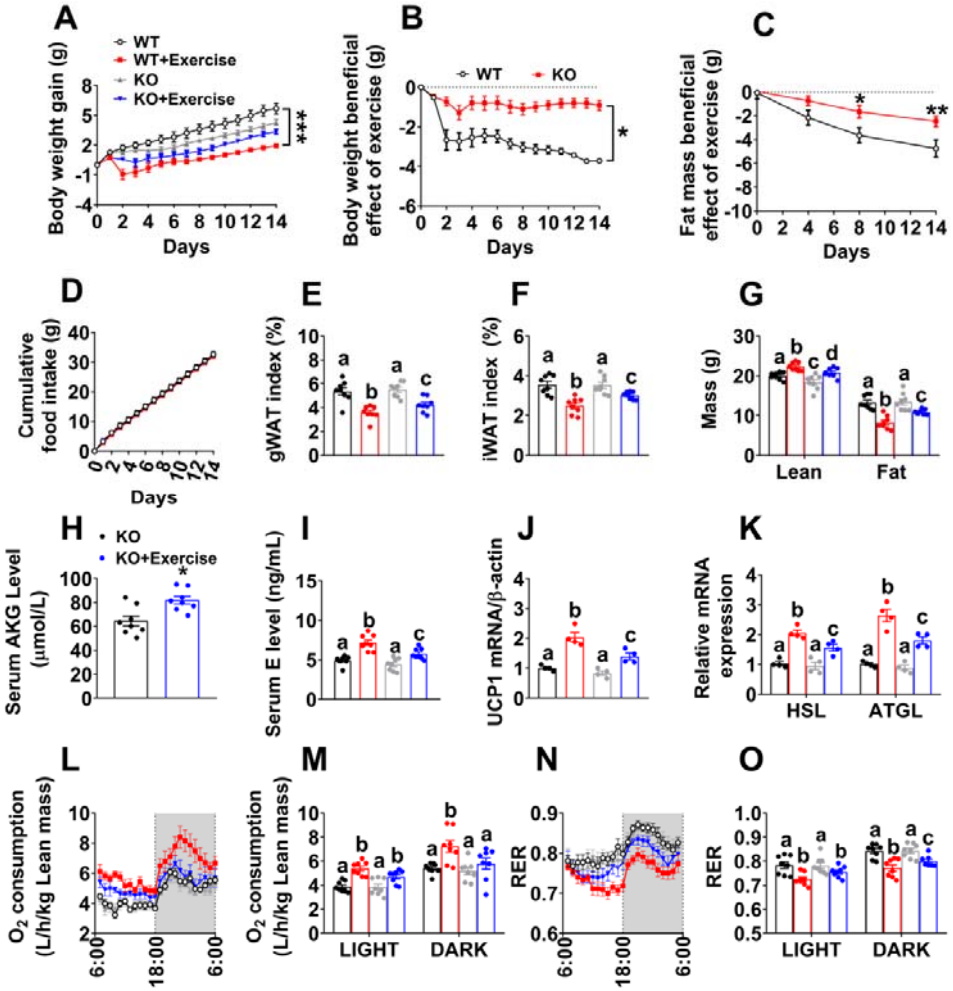

Figure 7. OXGR1 is required for metabolic beneficial effects of resistance exercise

(A). Body weight gain in male WT littermates and OXGR1KO mice. At 8 weeks of age, male C57BL/6 WT control or OXGR1KO mice were switched to HFD. After 12 weeks of HFD feeding, mice were further divided into two groups, receiving non-exercise or resistance exercise for 14 days. (n = 8 per group).

(B). Exercise-induced body weight loss in male WT littermates and OXGR1KO mice. Body weights from exercise mice were subtracted by the average body weight of non-exercise control group for each genotype (n = 8 per group).

(C). Exercise-induced fat mass loss in male WT littermates and OXGR1KO mice. Fat mass from exercise mice were subtracted by the average fat mass of non-exercise control group for each genotype (n = 8 per group).

(D). Cumulative food intake of male WT littermates and OXGR1KO mice after 14-day resistance exercise (n = 8 per group).

(E-F). Weight index of gWAT (E) and iWAT (F) of male OXGR1KO mice after 14-days resistance exercise (n = 8 per group).

(G). Body composition of male OXGR1KO mice after 14-days resistance exercise (n = 8 per group).

(H). Serum AKG levels of male OXGR1KO mice after resistance exercise. Male OXGR1KO mice (10 weeks) fed with normal chow were receiving resistance exercise for 40 min (n = 8 per group). The serum AKG levels were tested before and immediately after exercise.

(I). Serum E level in male OXGR1KO mice after 14-day resistance exercise (n = 8 per group).

(J-K). The mRNA expression of UCP1 (J) in the BAT or HSL and ATGL (K) in the gWAT of male OXGR1KO mice after 14-day resistance exercise (n = 4 per group).

(L-O). Oxygen consumption (L-M) and RER (N-O) in male OXGR1KO mice after 14-day resistance exercise (n = 8 per group).

Results are presented as mean ± SEM. In (A-D) *$p \leq 0.05$, ** $p \leq 0.01$ by two-way ANOVA followed by post hoc Bonferroni tests. In (H), *$p \leq 0.05$ by non-paired Student's t test. In (E-G), (I-K), (M) and (O), different letters between bars indicate $p \leq 0.05$ by one-way ANOVA followed by post hoc Tukey's tests.

1990 **Fig. 8**

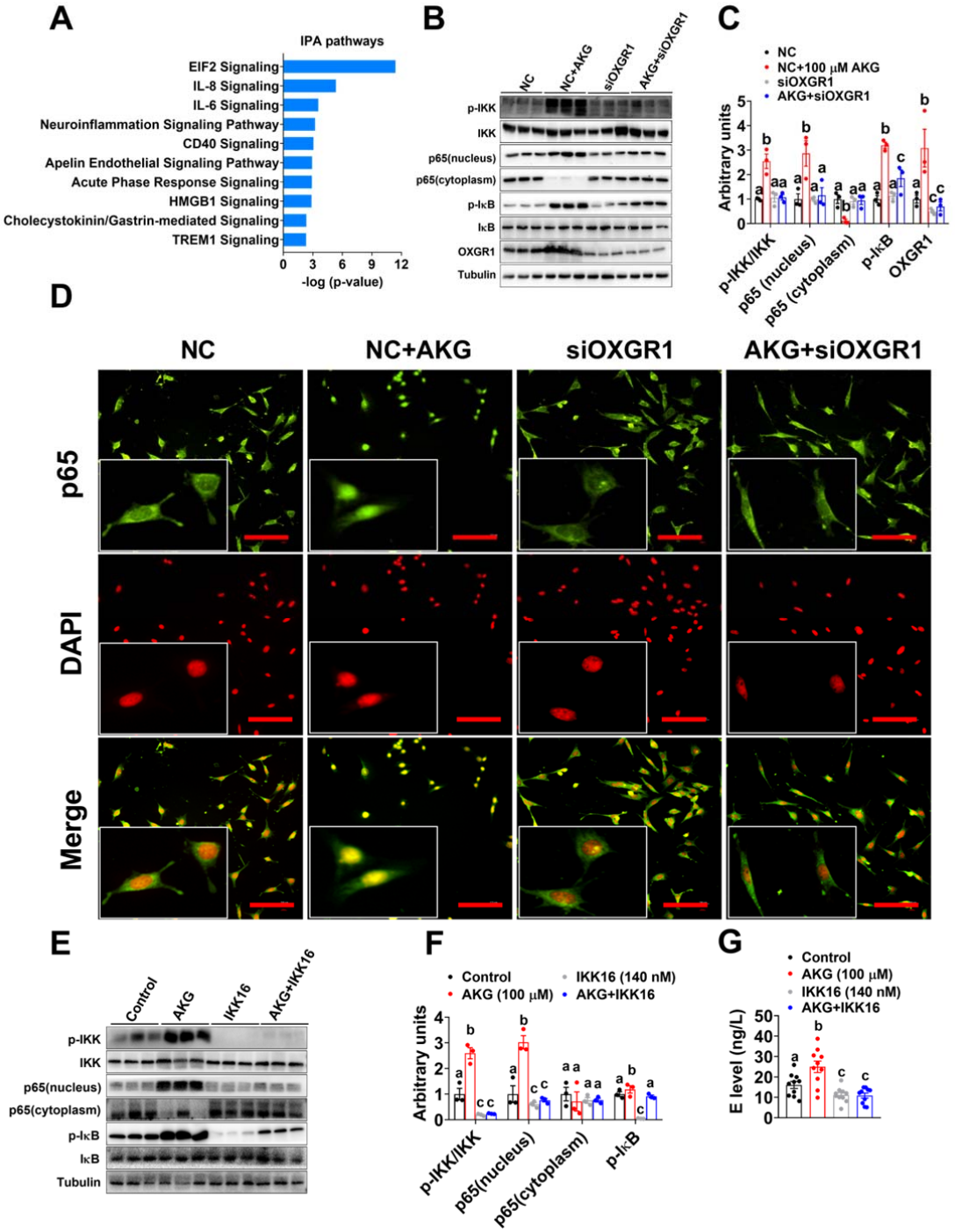

1991

1992

1993 **Figure 8. p65/NF-κB inflammatory pathway is required for the stimulatory effects of AKG on E**
1994 **release of adrenal chromaffin cell *in vitro*.**
1995 (A). Ingenuity Pathway Analysis (IPA) of AKG-induced transcriptome signature in adrenal chromaffin cell
1996 treated with AKG. The mRAN was extracted from adrenal chromaffin cells after 3-hrs incubation ofvehicle

1997 or AKG (100 μM). (n = 6 per group).
1998 (B-C). Immunoblots (B) and quantification (C) of p-IKK/IKK, p65, p-IκB/IκB and OXGR1 protein in
1999 adrenal chromaffin cells cultured with vehicle + NC, vehicle + siOXGR1, AKG (100 μM) + NC or AKG +
2000 siOXGR1 for 3 hrs (n = 3 per group).
2001 (D). p65 translocation in adrenal chromaffin cells cultured with vehicle + NC, vehicle + siOXGR1, AKG
2002 (100 μM) + NC or AKG + siOXGR1 for 3 hrs (n = 3 per group). Scale bars, 100 μm.
2003 (E-F). Immunoblots (E) and quantification (F) of p-IKK/IKK, p65 and p-IκB/IκB protein in adrenal
2004 chromaffin cells cultured with vehicle, AKG (100 μM), IKK inhibitor IKK16 or AKG + IKK16 for 3 hrs.
2005 (G). E level in the medium from adrenal chromaffin cell cultured with vehicle, AKG (100 μM), IKK16 or
2006 AKG + IKK16 for 3 hrs (n = 10 per group).
2007 Results are presented as mean ± SEM. In (C), (F) and (G), different letters between bars indicate $p \leq 0.05$ by
2008 one-way ANOVA followed by post hoc Tukey's tests.
2009

Fig. EV1

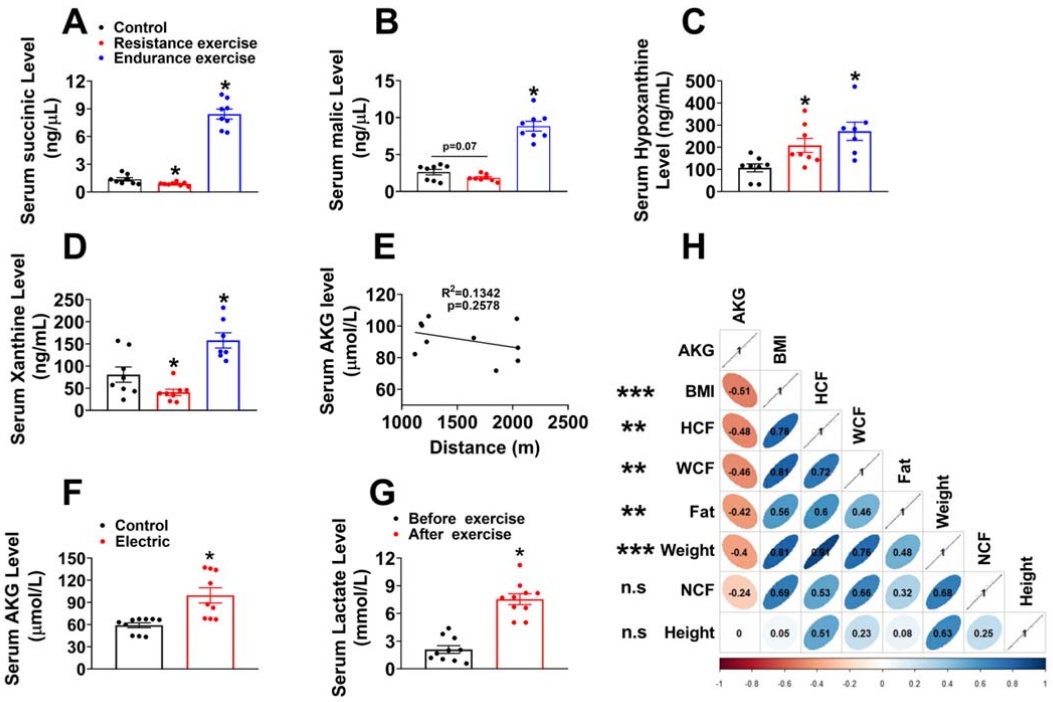

Figure EV1. Physiological relevance of AKG

(A-D). The serum concentration of succinic acid (A), malic (B), hypoxanthine (C) and xanthine (D) in mice. Chow fed male C57BL/6 mice (10 weeks) were divided into three groups receiving non-exercise, endurance exercise (treadmill, 10 meters/minute, increased by 2 meters/minute every two minutes to exhaustion) or resistance exercise (ladder climbing for 40 min) (n = 8 per group).

(E). Two tailed Pearson's correlation coefficient analysis of plasma AKG level and the running distance of wheels. Chow fed male C57BL/6 mice (10 weeks) received one-day free access to running wheel. (n = 10 per group).

(F). Two tailed Pearson's correlation coefficient analysis of plasma AKG level and the ladder climbing time. Chow fed male C57BL/6 mice (10 weeks) received resistance exercise (ladder climbing for 40 min). (n = 10 per group).

(F). Serum AKG level after electric stimulation. Electric stimulation was performed in unilateral gastrocnemius for 40 min (1 ms width/50 Hz, 10 times, each time for 4 min, resting for 2 min between stimulates) *in vivo* in 10 weeks male C57BL/6 mice fed with chow diet (n = 8-9 per group).

(G). Serum lactate concentration. Chow fed male C57BL/6 mice (10 weeks) received resistance exercise for 40 min. The serum lactate concentration was test before and immediately after exercise. (n = 10 per group).

(H). Two tailed Pearson's correlation coefficient analysis of human plasma AKG level and BMI, hip circumference (HCF), waist circumference (WCF), fat mass, body weight, neck circumference (NCF), and height. *p≤0.05, ** p≤0.01, *** p≤0.001 indicate significant correlation between human plasma AKG level and BMI, HCF, WCF, fat mass and body weight.

Results are presented as mean ± SEM. In (A-D) and (G-H), ∗p≤0.05 by one-way ANOVA followed by post hoc Turkey's tests.

Fig. EV2

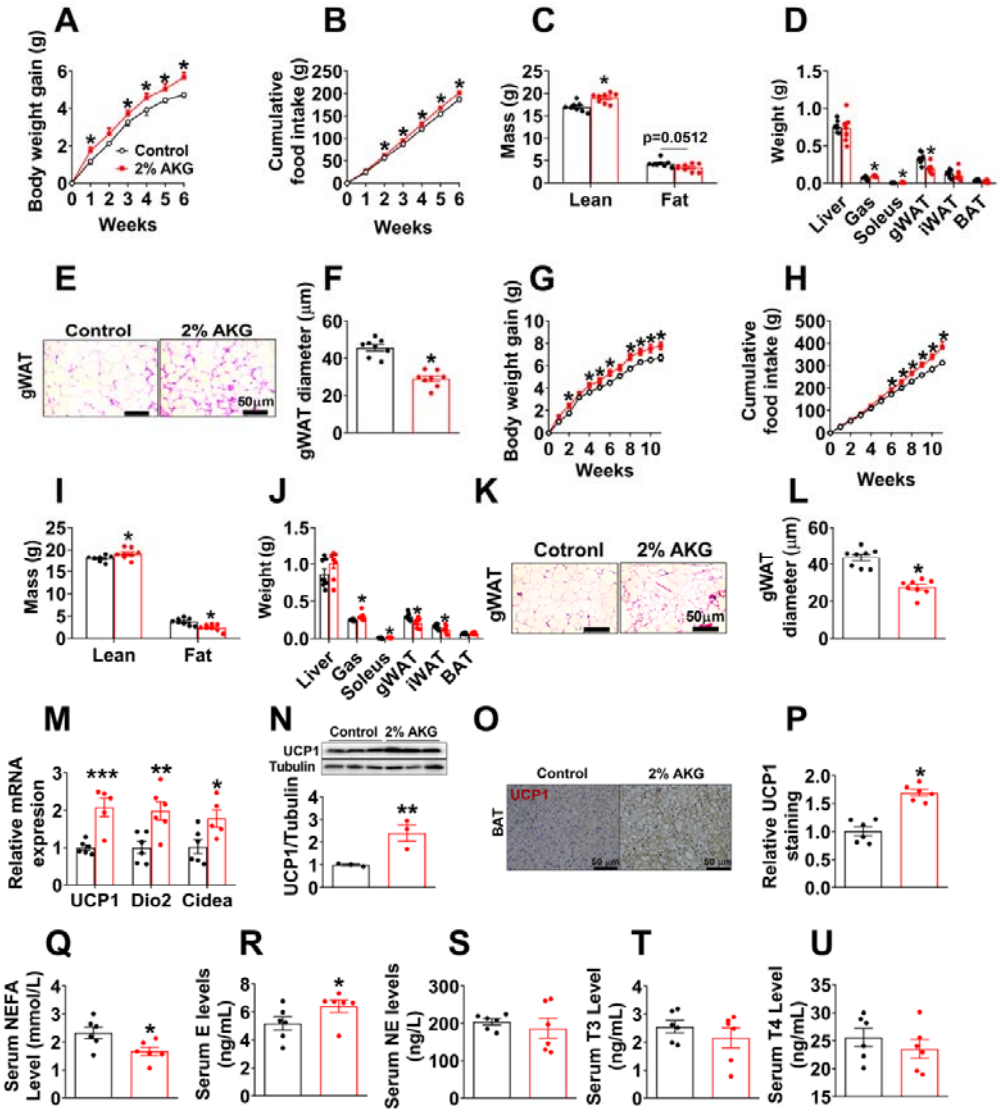

Figure EV2. Metabolic effects of AKG in mice fed on chow.

(A-B). Body weight gain (A) and cumulative food intake (B) of male C57BL/6 mice. At 12 weeks of age, chow-fed male mice were divided into two groups, receiving tap water or water supplemented with 2% AKG for 6 weeks (n = 8 per group).

(C-D). Body composition (C) and tissue weight (D) of male mice treated with AKG for 6 weeks (n = 7-8 per group).

(E-F). Representative images (E) and quantification (F) of gWAT HE staining from male mice treated with AKG for 6 weeks (n = 8 per group).

(G-H). Body weight gain (G) and cumulative food intake (H) of female C57BL/6 mice. At 12 weeks of age, chow-fed female mice were divided into two groups, receiving tap water or water supplemented with 2% AKG for 11 weeks (n = 8 per group).

(I-J). Body composition (C) and tissue weight (D) of female mice treated with AKG for 11 weeks (n = 8 per group).

(K-L). Representative images (K) and quantification (L) of gWAT HE staining from female mice treated with AKG for 11 weeks (n = 8 per group).

(M). The mRNA expression of thermogenic genes in BAT of male C57BL/6 mice supplemented with AKG for 6 weeks (n = 6 per group).

(N-P). Immunoblots and quantification of UCP1 (N) and representative images of DAB staining (O) and quantification (P) of UCP1 in BAT of male mice supplemented with AKG for 6 weeks (n = 3-6 per group).

(Q-U). Serum levels of NEFA (Q), E (R), NE (S), T3 (T), and T4 (U) in male mice supplemented with AKG for 6 weeks (n = 6 per group).

Results are presented as mean ± SEM. In (A-B) and (G-H), *p≤0.05 by two-way ANOVA followed by post hoc Bonferroni tests. In (C-D), (F), (I-J), (L-N) and (P-U), *p≤0.05, **p≤0.01, ***p≤0.01 by non-paired Student's t-test.

2094 **Fig. EV3**

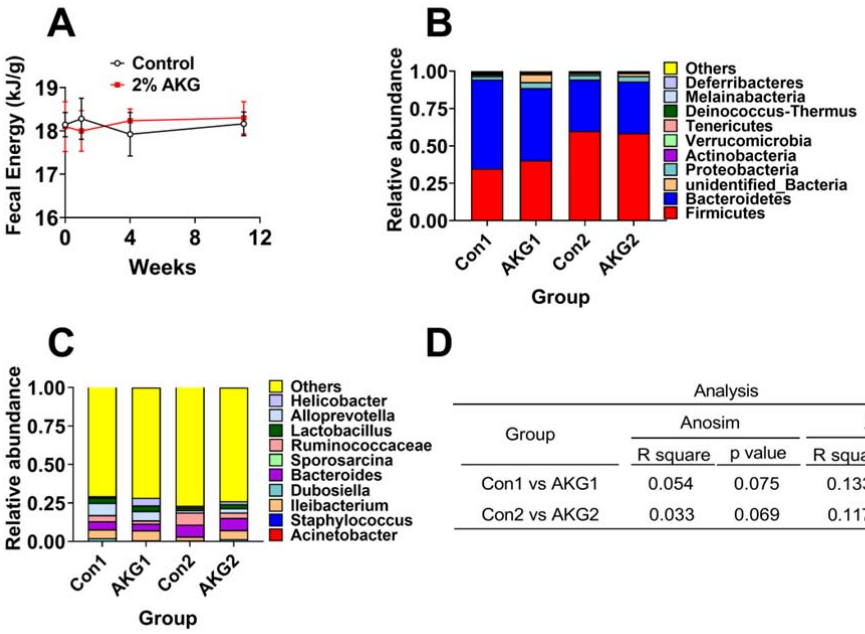

Group	Analysis			
	Anosim		Adonis	
	R square	p value	R square	p value
Con1 vs AKG1	0.054	0.075	0.133	0.105
Con2 vs AKG2	0.033	0.069	0.117	0.093

2095

2096 **Figure EV3. The effects of AKG supplementation on fecal microbiota composition in mice.**

2097 (A). Fecal energy of male C57BL/6 mice after 1, 4 and 11 weeks of AKG supplementation. At 12 weeks of
2098 age, male C57BL/6 mice were switched to HFD and received tap water or water supplemented with 2%
2099 AKG for 11 weeks (n = 9 per group).

2100 (B-C). The fecal microbial composition in the phylum (B) and genus (C) in male C57BL/6 mice receiving
2101 2% AKG water supplementation for 1 weeks (AKG1) or 4 weeks (AKG2) (n = 5 per group).

2102 (D). Community structure test by Anosim and Adonis analysis of beta diversity in genus between groups. .
2103 Results are presented as mean ± SEM. In (A), data was analyzed by two-way ANOVA followed by post
2104 hoc Bonferroni tests.

2105

Fig. EV4

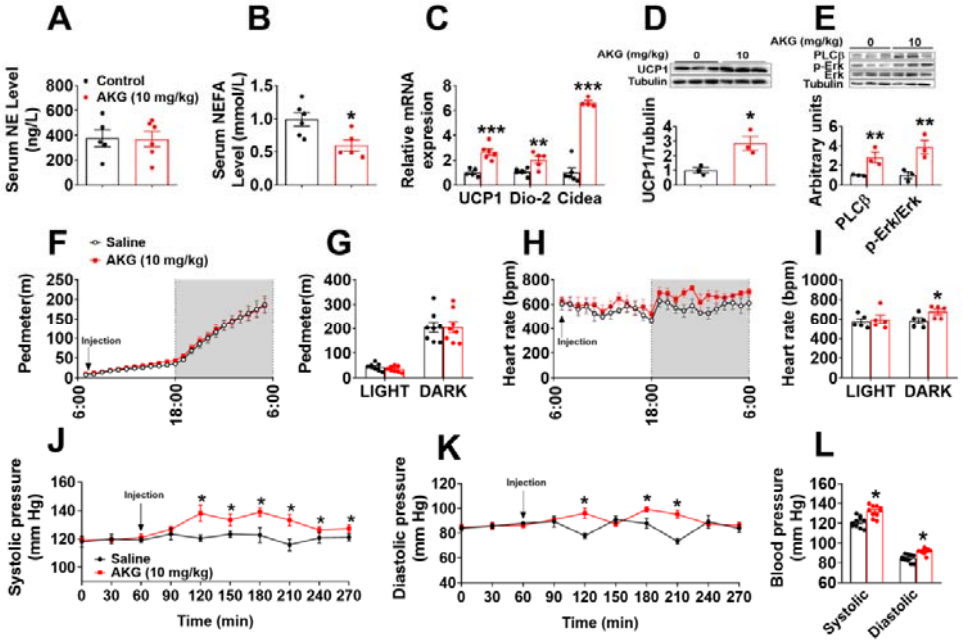

Figure EV4. Acute *in vivo* effects of AKG

(A-B). Serum levels of NE (A) and NEFA (B) in male C57BL/6 mice (10 weeks) 3 hrs after i.p. injection of saline or AKG (10 mg/kg) (n = 5-6 per group).

(C). The mRNA expression of thermogenic genes in male C57BL/6 mice (10 weeks) 3 hrs after i.p. injection of saline or AKG (10 mg/kg) (n = 5-6 per group).

(D). Immunoblots and quantification of UCP1 in BAT of male C57BL/6 mice (10 weeks) 3 hrs after i.p. injection of saline or AKG (10 mg/kg) (n = 3 per group).

(E). Immunoblots and quantification of PLCβ and pErk in the adrenal glands of male C57BL/6 mice (10 weeks) 3 hrs after i.p. injection of saline or AKG (10 mg/kg) (n = 3 per group).

(F-I). Physical activity (pedometer, F-G) and heart rate (H-I) of male mice i.p. injected with 10 mg/kg AKG or saline at 7:00 am (n = 8 per group).

(J-L). Blood pressure of male mice i.p. injected with 10 mg/kg AKG or saline (n = 8 per group).

Results are presented as mean ± SEM. In (A-E), (G), (I), (L), *p≤0.05, **p≤0.01, ***p≤0.01 by non-paired Student's t-test. In (F), (H) and (J-K), *p≤0.05 by two-way ANOVA followed by post hoc Bonferroni tests.

Fig. EV5

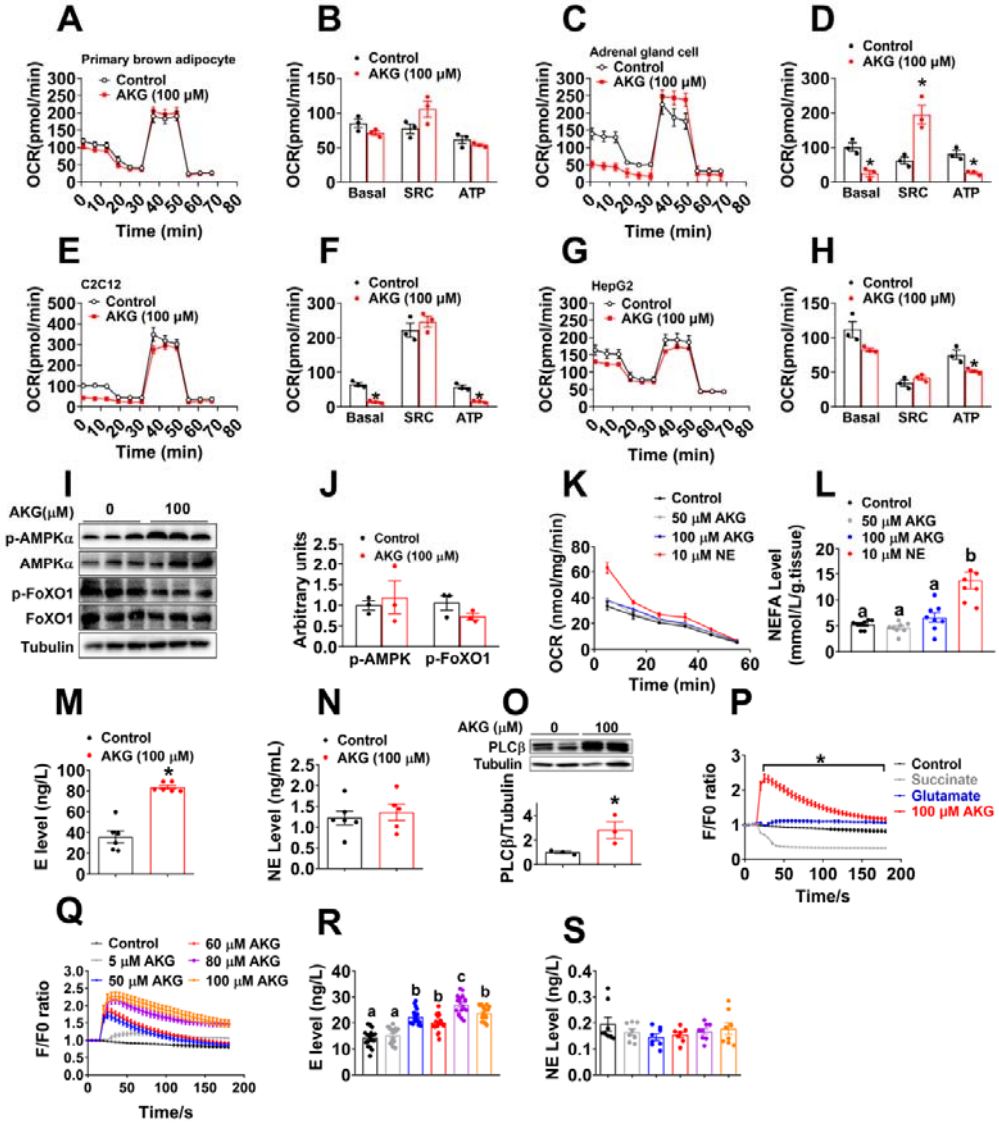

Figure EV5. Metabolic effects of AKG in *in vitro* and *ex vivo* models of BAT and adrenal gland.

(A-H). Oxygen consumption rate (OCR) of primary brown adipocyte (A-B), adrenal chromaffin cell line (C-D), C2C12 cell line (E-F) and HepG2 cell line (G-H) treated with vehicle or 100 μM AKG for 3 hrs (n=3 per group). OCR was monited using the Agilent Seahorse XFp analyzer with the sequential injection of oligomycin, FCCP, and rotenone/antimycin.

(I-J). Immunoblots (I) and quantification (J) of p-AMPKα and p-FoxO1 in primary brown adipocyte treated with vehicle or 100 μM AKG (n = 3 per group).

(K). Oxygen consumption rate (OCR) of *ex vivo* BAT cultured with vehicle, 50 μM AKG, 100 μM AKG or 10 μM NE for 5, 15, 25, 25, 45, and 55 min (n = 3 per group).

(L). Medium NEFA level from *ex vivo* BAT treated with vehicle, 50 μM AKG, 100 μM AKG or 10 μM NE for 30 min (n = 6 per group).

(M-N). Medium E (M) and NE (N) level from *ex vivo* adrenal gland treated with vehicle or 100 μM AKG for 30 min *in vitro* (n = 5-6 per group).

(O). Immunoblots and quantification of PLCβ in *ex vivo* adrenal gland treated with vehicle or 100 μM AKG for 30 min *in vitro* (n = 3 per group).

(P). Intracellular calcium ion [Ca^{2+}] changes in *in vitro* adrenal chromaffin cells treated with vehicle, 100 μM AKG, 100 μM succinate or 100 μM glutamine (n=30 per group).

(Q). Intracellular calcium ion [Ca^{2+}] changes in *in vitro* adrenal chromaffin cells treated with vehicle, 5, 50, 60, 80, 100 μM AKG (n=30 per group).

(R-S). Medium E (R) or NE (S) level from *in vitro* adrenal chromaffin cells treated with vehicle, 5, 50, 60, 80, 100 μM AKG for 30 min (n=8-18 per group).

Results are presented as mean ± SEM. In (B), (D), (F), (H), (J) and (M-O) *p≤0.05 by non-paired Student's t-test. In (K) and (P-Q), *p≤0.05 by two-way ANOVA followed by post hoc Bonferroni tests. In (L) and (R-S), different letters indicate significant differences between groups by one-way ANOVA followed by post hoc Turkey's tests.

2152 **Fig. EV6**

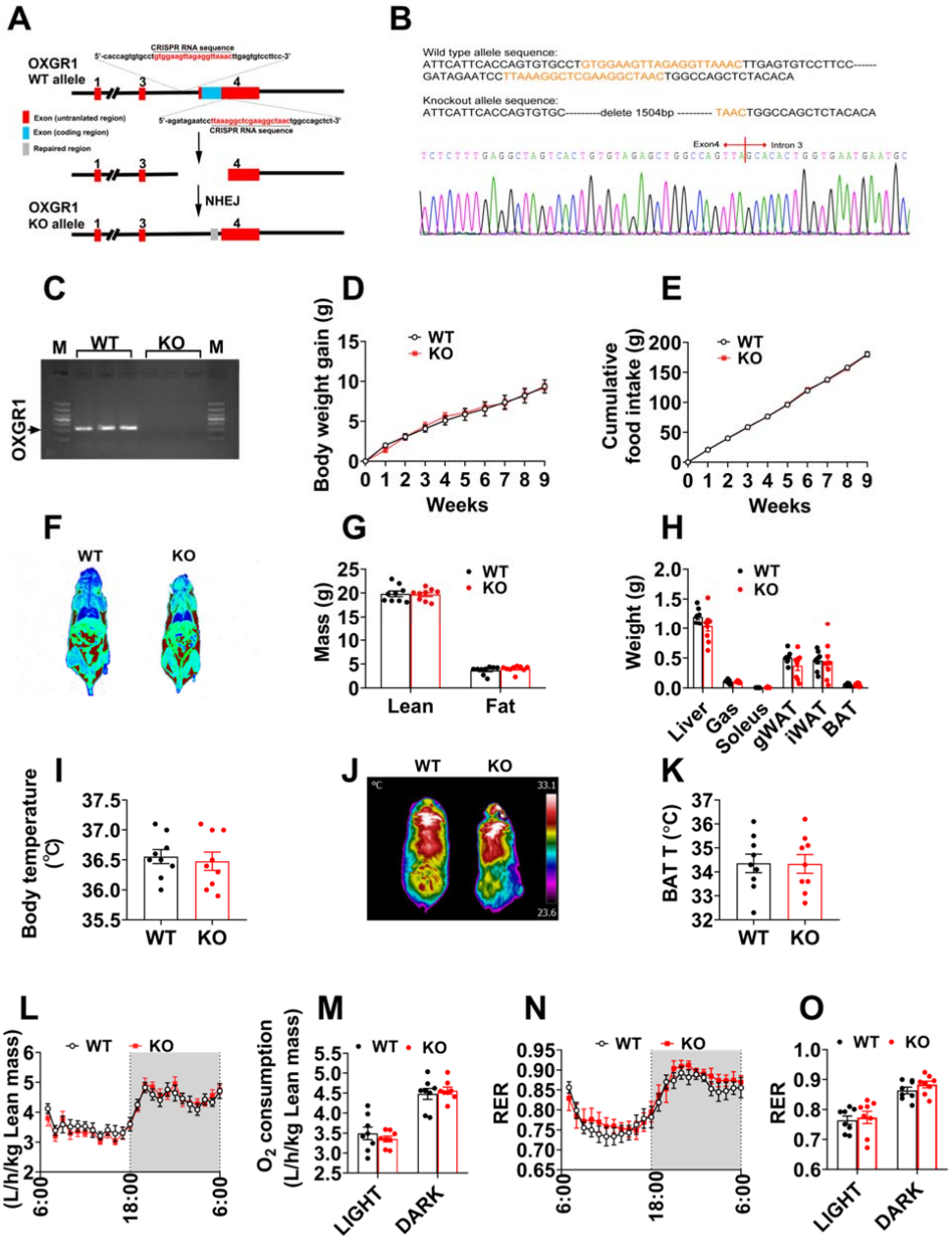

2153

2154 **Figure EV6. The metabolic phenotype of OXGR1 KO mouse on normal chow**

2155 (A). Schematic representation of OXGR1KO mouse line generation by Clustered Regularly Interspaced
2156 Short Palindromic Repeats (CRISPR) strategy. The sgRNA sites were located in intron 3 and exon 4 of the
2157 OXGR1 gene. The DNA sequences contained sgRNA-binding regions are labeled with red.
2158 (B). The genomic sequencing of sgRNA target sites in wild-type and OXGR1KO mice. The orange letter is
2159 the sgRNA target sequence.
2160 (C). The validation of OXGR1KO mice. The mRNA expression of OXGR1 was determined in the adrenal
2161 glands from male WT control (littermates) or OXGR1KO mice.
2162 (D-E). Body weight gain (D) and cumulative food intake (E) of male OXGR1 KO mice and littlermates.

Chow fed male mice (8 weeks of age) were monitored for 9 weeks (n = 8 per group).
(F-H). Representative images (F) of body composition and fat and lean mass (G) and tissue weight (H) of male OXGR1KO mice after 9-weeks of monitoring (n = 8 per group).
(I) The body temperature of male OXGR1KO mice after 9-weeks of monitoring (n = 8 per group).
(J-K). Representative images (J) and quantification (K) of BAT thermogenesis induced by 6-hrs cold exposure at 4°C in male OXGR1KO mice after 9-weeks of monitoring (n = 8 per group).
(L-O). Oxygen consumption (L-M) and RER (N-O) in male OXGR1KO mice after 9-weeks of monitoring (n = 8 per group).
Results are presented as mean ± SEM. In (D-E), (L) and (N) data was analyzed by two-way ANOVA followed by post hoc Bonferroni tests. In (G-I), (K), (M) and (O), data was analyzed by non-paired Student's t-test.

Fig. EV7

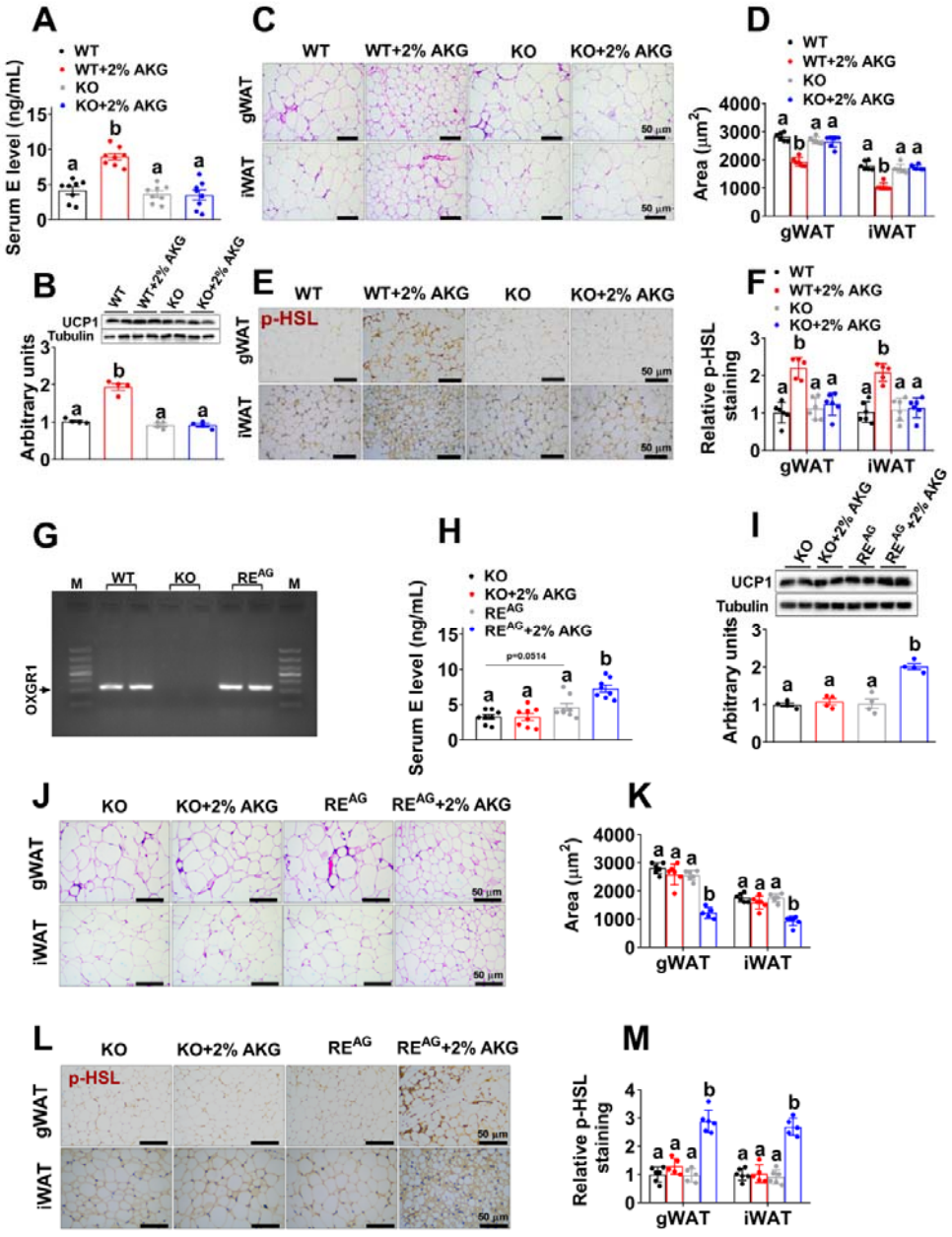

Figure EV7. Adrenal specific reexpression of OXGR1 rescues the stimulatory effects of AKG on thermogenesis and lipolysis

(A). Serum E level in male OXGR1KO mice. At 12 weeks of age, male control or OXGR1KO mice were switched to HFD and received tap water or water supplemented with 2% AKG for 13 weeks (n = 8 per group).

(B). Immunoblots and quantification of UCP1 protein expression in the BAT of male OXGR1KO mice treated with AKG for 13 weeks (n = 4 per group).

(C-D). Representative images (C) and quantification (D) of iWAT and gWAT HE staining from male OXGR1KO mice treated with AKG for 13 weeks (n = 6 per group).

(E-F). Representative images (E) and quantification (F) of p-HSL DAB staining from male OXGR1KO mice treated with AKG for 13 weeks (n = 6 per group).

(G). The validation of OXGR1 reexpression. The mRNA expression of OXGR1 was determined in the adrenal glands from male WT control, OXGR1KO injected with HBAAV2/9-GFP, and OXGR1KO injected with HBAAV2/9-OXGR1 (OXGR1RE^{AG}) mice.

(H). Serum E level in male OXGR1RE^{AG}. Male OXGR1KO mice (8 weeks) were adrenal-specifically injected with control HBAAV2/9-GFP or HBAAV2/9-OXGR1. Two weeks after injections, mice were switched to HFD and further divided into two groups, receiving tap water or 2% AKG for 13 weeks. (n = 6 per group).

(I). Immunoblots and quantification of UCP1 protein expression in the BAT of OXGR1RE^{AG} mice treated with AKG for 13 weeks (n = 4 per group).

(J-K). Representative images (J) and quantification (K) of iWAT and gWAT HE staining from OXGR1RE^{AG} mice treated with AKG for 13 weeks (n = 6 per group).

(L-M). Representative images (L) and quantification (M) of p-HSL DAB staining from OXGR1RE^{AG} mice treated with AKG for 13 weeks (n = 6 per group).

Results are presented as mean ± SEM. In (A-B), (D), (F), (H-I), (K) and (M), different letters between bars indicate $p \leq 0.05$ by one-way ANOVA followed by post hoc Turkey's tests.

2204 **Fig. EV8**

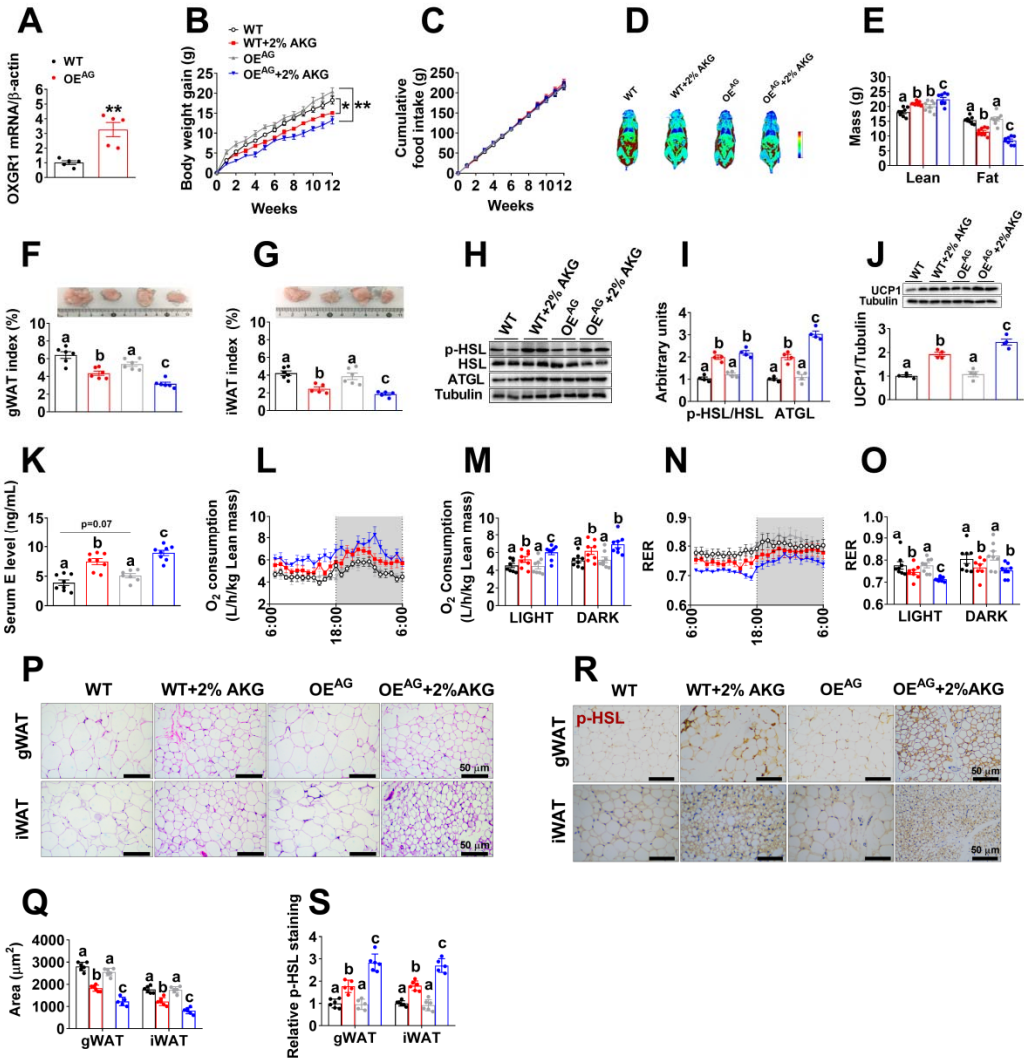

2205

2206 **Figure EV8. Adrenal specific overexpression of OXGR1 enhances stimulatory effects of AKG on**
2207 **thermogenesis and lipolysis**

2208 (A). The validation of OXGR1 overexpression. The mRNA expression of OXGR1 was determined in the
2209 adrenal glands from male WT control, WT injected with HBAAV2/9-GFP, and WT injected with
2210 HBAAV2/9-OXGR1 (OXGR1OE^{AG}) mice (n=5 per group).

2211 (B-C). Body weight gain (B) and cumulative food intake (C) of OXGR1OE^{AG}. Male C57BL/6 mice (8
2212 weeks) were adrenal-specifically injected with control HBAAV2/9-GFP or HBAAV2/9-OXGR1. Two
2213 weeks after injections, mice were switched to HFD and further divided into two groups, receiving tap
2214 water or water supplemented with 2% AKG for 12 weeks (n = 8 per group).

2215 (D-E). Representative image of body composition (D) and fat and lean mass index (E) of male
2216 OXGR1OE^{AG} mice treated with AKG for 12 weeks (n = 8 per group).

2217 (F-G). Weight index of gWAT (F) and iWAT (G) in male OXGR1OE^{AG} mice treated with AKG for 12
2218 weeks (n = 6 per group).

2219 (H-I). Immunoblots (H) and quantification (I) of p-HSL and ATGL protein in the gWAT of male

OXGR1OE^{AG} mice treated with AKG for 12 weeks (n = 4 per group).
(J). Immunoblots and quantification of UCP1 protein in the BAT of male OXGR1OE^{AG} mice treated with AKG for 12 weeks (n = 4 per group).
(K) Serum E level in male OXGR1OE^{AG} mice treated with AKG for 12 weeks (n= 8 per group).
(L-O). Oxygen consumption (L-M) and RER (N-O) of male OXGR1OE^{AG} mice treated with AKG for 12 weeks (n = 8 per group).
(P-Q). Representative images (P) and quantification (Q) of gWAT and iWAT HE staining from male OXGR1OE^{AG} mice treated with AKG for 12 weeks (n = 6 per group).
(R-S). Representative images (R) and quantification (S) of p-HSL DAB staining from male OXGR1OE^{AG} mice treated with AKG for 12 weeks (n = 6 per group).
Results are presented as mean ± SEM. In (A), ** $p \leq 0.01$ by non-paired Student's t test. In (B-C), *$p \leq 0.05$, **$p \leq 0.01$ by two-way ANOVA followed by post hoc Bonferroni tests. In (E-G), (I-K), (M), (O), (Q) and (S), different letters between bars indicate $p \leq 0.05$ by one-way ANOVA followed by post hoc Turkey's tests.

NO.	Gender	Age	Height (cm)	Weight (kg)	BMI (kg/m^2)	Fat mass (%)	VFA (cm^2)	NCF (cm)	WCF (cm)	HCF (cm)	Blood pressure (mmHg)
1	F	48	154	61.7	26.02	37.7	111.8	33.9	85.9	99.3	113.5/91
2	F	44	159.5	58.2	22.88	31.6	80.6	33.4	78.5	87.4	106/76
3	F	47	160.5	63.4	24.61	35.3	98.6	36	80	95	114/82
4	F	42	165.5	64.7	23.62	35.3	96.1	33.5	83.5	98.5	113.5/88
5	F	40	176.5	75.3	24.17	38.9	101.4	33	83.5	104.5	113/78
6	F	42	161	66.2	25.54	38.9	105.2	32.5	87	100.9	117/74
7	F	36	168.5	89.8	31.63	41.5	140.5	37	96	113.5	159/107
8	F	32	157.8	66	26.51	37	89.1	35.5	79	100	95/67
9	F	35	168	71.5	25.33	32.1	87.8	36.5	84.5	102	118/87
10	F	36	164.7	75.5	27.83	40.4	110.7	34	84.5	109	112/74
11	F	32	163	65.3	24.58	30.1	74.8	33.5	85	99.5	132/90.5
12	F	28	160	66.2	25.86	30.7	72.3	34	86.5	97	109/71
13	F	31	155.5	63.6	26.3	40.1	97.9	33.9	94	100	101/69
14	F	29	170.5	71.6	24.63	42.1	102.2	34	80	105.5	105/75
15	F	30	161.5	64	24.54	34.4	74.8	32.8	82.5	94	106/75
16	F	31	161.3	71.9	27.64	39.4	100	34	92	106	/
17	F	30	162.5	72.1	27.3	36.8	98.9	36.5	95	103.5	112/69
18	F	27	164.5	70.1	25.91	36.5	91.8	33	86	105	126/82
19	F	31	159	63.5	25.12	36.8	76.1	33.8	79.5	97.9	/
20	F	29	174.8	87.5	28.64	38.4	126.2	38	99.5	112.5	/
21	F	30	162.5	76.3	28.89	41.5	108.6	36	93.9	105	110/78
22	F	27	161.7	61.8	23.64	36.9	78.2	33	76.2	96	123/82
23	F	51	162	62.2	23.7	34.7	98.4	34	81.5	96.5	117/79
24	F	49	160.5	63.6	24.69	34	96.2	33	83.5	98.2	130/82
25	F	43	161.5	61.4	23.54	35.2	100.1	34	78.5	96	104/78
26	F	49	163.5	69.9	26.15	38.1	115.3	33.9	86	103.5	115/78
27	F	29	160	68.8	26.88	42.7	98	34.5	88	102.9	108/65
28	F	46	162.2	69.5	26.42	43.4	126.8	35.5	92.5	104.5	120/80
29	F	29	169.5	80.1	27.88	36.2	106.5	34.9	93.5	106	114/66
30	F	38	158	81.5	32.65	40.6	144.7	37	99.5	110.5	124/87
31	F	46	167.8	77.2	27.42	35.5	123.6	37.5	91	106.5	116/77
32	F	47	156.2	59.3	24.3	33.2	90.5	31	72.5	98.7	88/61
33	F	43	156.3	70.8	28.98	41.4	126.1	37	87.5	100	123/88
34	M	43	170	78	27	/	/	/	/	/	/
35	F	57	150	50	22	/	/	/	/	/	/
36	M	61	168	58	20.5	/	/	/	/	/	/
37	M	44	163	62	23.3	/	/	/	/	/	/
38	M	52	145	49.5	23.5	/	/	/	/	/	/
39	M	24	160	61	23.8	/	/	/	/	/	/
40	M	45	160	65	25.3	/	/	/	/	/	/
41	M	71	161	81	31.2	/	/	/	/	/	/
42	M	57	174	77.5	25.6	/	/	/	/	/	/
43	M	76	167	65	23.3	/	/	/	/	/	/
44	M	37	151	51.3	22.5	/	/	/	/	/	/
45	F	82	157	60	24.3	/	/	/	/	/	/

Table 1. Clinical characteristics of all human subjects. BMI: body mass index as the body mass divided by the square of the body height; VFA: visceral fat area; NCF: neck circumference; WCF: waist circumference; HCF: hip circumference.